Title

A15 SUPERCONDUCTORS THROUGH DIRECT ""SOLID-STATE"" PRECIPITATION: V3Ga AND N63AI

Author

Hong, Minghwei

Publication Date

1980-09-01

Lawrence Berkeley Laboratory
UNIVERSITY OF CALIFORNIA

Materials & Molecular
Research Division

A15 SUPERCONDUCTORS THROUGH DIRECT "SOLID-STATE" PRECIPITATION: V_3Ga and Nb_3Al

MINGHWEI HONG
(Ph.D. thesis)

September 1980

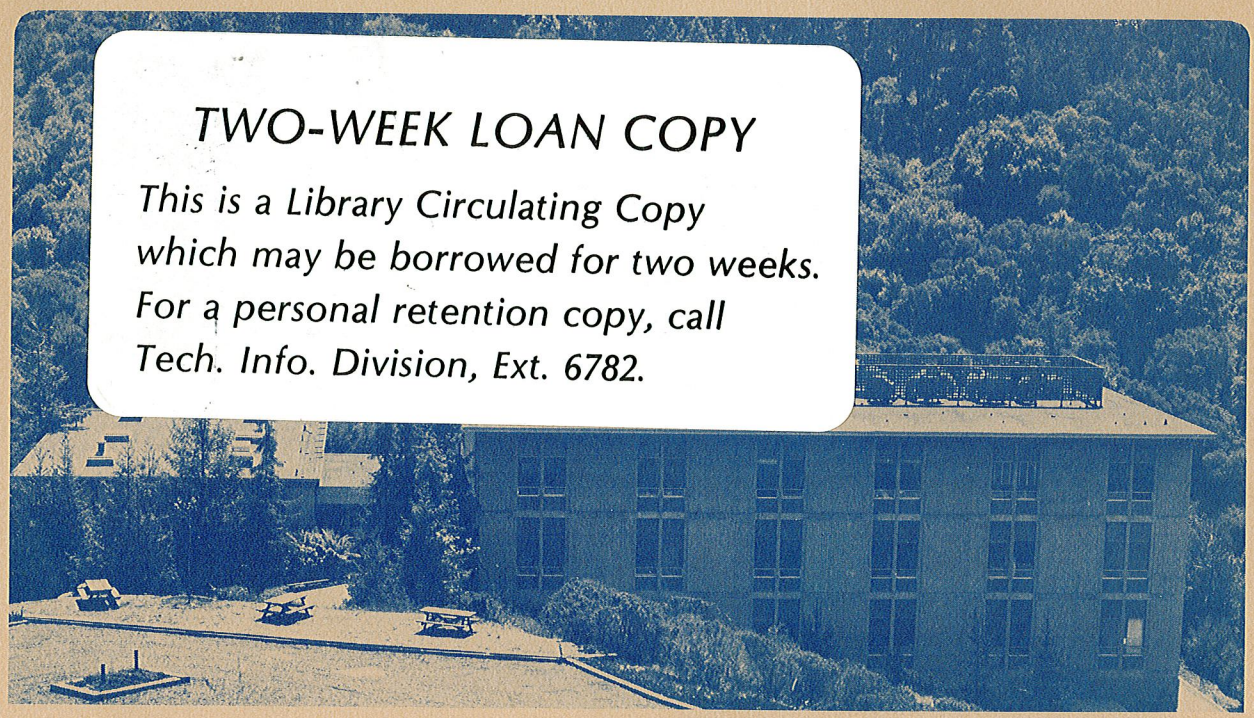

Prepared for the U.S. Department of Energy under Contract W-7405-ENG-48

A15 SUPERCONDUCTORS THROUGH DIRECT "SOLID-STATE" PRECIPITATION: V_3Ga and Nb_3Al

MINGHWEI HONG

Materials and Molecular Research Division
Lawrence Berkeley Laboratory
University of California
Berkeley, California

ABSTRACT

A "solid-state precipitation" process was used to prepare superconducting tapes containing an A15 phase, V_3Ga or Nb_3Al, in a ductile niobium or vanadium containing BCC matrix. Ingots weighing as large as 30~50 gms of V-(14~19 at.%) Ga and Nb-(13~22 at.%) Al were prepared by arc-melting, homogenized, quenched, warm-rolled over 99% into tape, and aged at temperatures in the range 600°C-1000°C to precipitate the superconducting A15 phase. The features demonstrated by the process are very attractive for practical applications.

In the V-Ga system, transmission electron microscopy (TEM) studies revealed the A15 precipitates in an elongated form. However, for the Nb-Al samples, deformed and aged at 750°C, TEM studies revealed A15 precipitation in fine equi-axed particles which formed as a semi-continuous network over sub-grain boundaries formed by the recovery of deformation-induced dislocations.

In the V-Ga system, the maximum critical transition temperature (~15 K) was found in materials aged at temperatures of 750°C or below. At these aging temperatures the T_c initially increased with aging time and passed through a distinct maximum. The source of the exceptionally high T_c is discussed. In the Nb-Al system, the aging response of the T_c of the

tested samples was somewhat different; the T_c increased with aging time to a plateau, and then increased again to a second plateau. The maximum T_c measured was ~17 K. Promising high-field overall critical currents were obtained in the Nb-Al system (overall J_c ~10^4 A/cm^2 in a magnetic field of 140 KG at 4.2 K).

A15 SUPERCONDUCTORS THROUGH DIRECT "SOLID-STATE" PRECIPITATION: V_3Ga and Nb_3Al

Table of Contents

ACKNOWLEDGMENTS

It is a very stimulating experience of me to be a member of such an active materials science research group under the leadership of Professor J. W. Morris, Jr. I thank Bill who initially introduced me with new and exciting research ideas and later offered me with opportunities to be exposed to challenges throughout the course of my graduate study. It is from these challenges that I have leatned to be a problem-solving physical metallurgist both theoretically and experimentally. The courage possessed by Bill in coping with difficult situations sets a good example of my research career.

Special thanks for reviewing this manuscript are extended to Professors M. L. Cohen and J. Washburn.

I am indebted to John L. F. Wang and John T. Holthuis for very fruitful discussions about the A15 superconducting materials and the processes of making these brittle materials.

I am grateful to S. Foner and E. J. McNiff, Jr. of the National Magnet Laboratory at M.I.T. for helpful discussions and assistance. It was Dr. Foner who urged me to go to the National Magnet Laboratory to measure $J_c(H)$ values. Larry Rubin and Bruce Brandt also provided a great deal of experimental assistance in obtaining the $J_c(H)$ data.

My special thanks go to Dan Dietderich with whom I started this project three years ago. His assistance and collaboration on the V-Ga system was most helpful. The other sub-group members, including I-Wei Wu, Joe Barrett, Chuck Gibson, and Verna Manty, are enthusiastic and dedicated to their work which is strongly related to this study.

Acknowledgment is also due for the assistance provided by the support staff of the Materials and Molecular Research Division, Lawrence Berkeley Laboratory. In particular, I would like to thank Donald Krieger (materials preparation), Sandy Stewart (purchasing), Gloria Peltowski (line drawing), Weyland Wong (machining), and Kenneth Gaugler (SEM).

I would like to thank all the group members over the past five years for their enthusiastic discussions, valuable advice and sincere friendship, especially Gene Wedge, Kim W. Mahin, and Keh-Minn Chang.

I would also like to thank Jeanne Shull, Madeline Penton, Melanie Lutz, and Verna Manty for their help in preparing this manuscript.

I wish to thank my parents and sisters and brother for their encouragement through all these years.

Finally, and most importantly, I would like to thank Jueinai Kwo, my dear fiancée and a condensed-matter physicist, who shares happiness, hardship, and learning experiences with me throughout my graduate years. I would also like to thank for her deep concern about this thesis work and many helpful discussions about superconductivity.

This work was supported by the Division of Materials Sciences, Office of Basic Energy Sciences and by the Division of Magnetic Fusion Energy, U.S. Department of Energy under Contract No. W-7405-Eng-48. The $J_c(H)$ data was obtained at the Francis Bitter National Magnet Laboratory which is supported at M.I.T. by the National Science Foundation.

INTRODUCTION

The research on the high-field superconducting materials has been intensified for the past two decades due to a great demand for these materials in the areas of high energy physics, magnetic thermonuclear fusion, magnetohydrodynamics (MHD), power transmission lines, and other areas. Superconductors are employed in large-scale electrical devices mainly because they can be constructed to carry extremely high overall current densities. The critical current density of the superconductor itself lies in the range of $10^5 \sim 10^7$ A/cm^2. In the construction of the practical conductors, these values can be reduced by a factor of 10 due to the required stabilizers, such as aluminum and copper, and the required reinforcement materials, such as stainless steels for the mechanical strength. Still, these overall current densities of the conductors compare very superiorly with the maximum current densities of 10^2 A/cm^2 and 10^3 A/cm^2 of the copper in the uncooled and forced-cooled conditions, respectively.

These high current densities allow the construction of more compact machines. The lack of energy dissipation (into heat) due to the absence of electrical resistance reduces the necessity for internal cooling. It is the reduction in size that largely accounts for the economical attractiveness of superconducting materials in lowering capital, installation, maintenance, and running costs. This concept has been applied in many areas; a good example of one application is the Energy Doubler/Saver in high-energy physics. The term, "Energy Doubler", implies that the energy of accelerated particles should be increased while the "Energy Saver" infers that the total expense of the experiments should be decreased. It should be noted, however, that for using superconductors the reduced power requirements must be balanced against the cost consumed by refrigeration.

Superconductivity, long a fascinating subject studied by solid-state physicists, has recently become an area of growing interest to physical metallurgists. The development and the demand of the practical high-field superconductors have stimulated much of the metallurgical research.

To fabricate the superconductors with high critical transition temperatures (T_c), high critical magnetic fields (H_c), and high critical current densities (J_c) for real applications, encounters various metallurgical difficulties. For example, most of the high-field superconductors are intermetallic compounds, and thus are intrinsically brittle. How to convert them into a useful form, and furthermore to control and improve their superconducting properties become the first essential problem. Second, research-scale superconducting materials are usually difficult to be scaled up to commercial quantities. Third, superconducting properties such as J_c are subject to deterioration due to mechanical strain. How to improve the metallurgical parameters in order to subdue the strain effects is therefore of great importance. There are some other problems, including the enhancement of J_c and H_c, which can be solved or improved by either using a new approach or modifying the existing method.

In this work we have used a direct "solid-state precipitation" process to fabricate the brittle A15 superconducting materials which have high values of T_c, H_c, and J_c. The "solid-state precipitation" approach is a monolithic method which includes arc-casting, high temperature homogenization, quenching, conventional mechanical-deformation, and aging to precipitate the superconducting A15 phase. The A15 precipitates thus formed are embedded in the relatively ductile BCC parent matrix. Furthermore, the morphology and the grain size of the A15 precipitates can be controlled

by the prior deformation and the final aging treatment. This is important since it is known that the superconducting and mechanical properties of the practical high-field superconductors are strongly influenced by metallurgical microstructures. We have successfully applied this method to the V-Ga and Nb-Al A15 systems in obtaining high T_c's of 15K in the V-Ga system and 17K in the Nb-Al system, and high overall J_c's in the Nb-Al system of $\sim 10^4$ A/cm^2 at 140 Kilogauss and 4.2K.

In the next chapter, the basic phenomena of superconductivity and the properties relevant to the development of high-field superconductors are briefly described. In chapter III, current high-field superconductors are described, their properties and potential are discussed, and the processes used to fabricate them are also presented. For most large-scale applications, superconductors should exhibit not only suitable dc critical properties such as high H_c and J_c, but also high mechanical load tolerance and low ac losses. Thus, one should be aware of all the practical superconductors discovered and all the methods developed to fabricate them in order to choose a proper material and process to fulfill the requirements of a particular application. In chapter IV, the monolithic direct "solid-state precipitation" is described in more detail. The experimental procedure and the apparatus employed are also presented in this chapter. The results of the V-Ga and the Nb-Al systems are described and discussed in Chapters V and VI respectively. The summary and conclusion of this work are presented in the last chapter.

II. SUPERCONDUCTIVITY, SUPERCONDUCTORS, AND FUNDAMENTAL PHENOMENA

A. Critical States of Superconductors

Superconductivity is the complete loss of dc electrical resistance at some finite, but low, temperature[1]. This phenomenon is not peculiar to a few metals. More than twenty metallic elements can become superconductors. Even certain semiconductors can be made superconducting under suitable conditions, such as application of high pressure, or preparation of the specimen in thin films. Thousands of alloys and intermetallic compounds have been proved to be superconductors[2]. The number of superconducting materials is increasing continuously as research advances.

The temperature below which superconductivity occurs is called the critical transition temperature (T_c), which is an intrinsic characteristic of each superconductor. Above T_c the properties of the metal are completely normal, e.g., the resistivity has the form[3]

$$\rho(T) = \rho_o + \alpha T^5, \qquad \text{(II.1)}$$

where the constant term comes from impurity and defect scattering, and the second term arises from phonon scattering. At T_c the resistance drops sharply to zero and remains zero at all temperatures below T_c*. Measured critical temperatures range from 0.01 K for some semiconductors up to 23.2 K for the intermetallic compound Nb_3Ge[6].

---

* Two compounds, $ErRh_4B_4$[4] and $Ho_{1.2}Mo_6S_8$[5], were recently discovered to become superconducting at critical temperatures T_{c1}'s followed by a return to the normal state at second critical temperatures T_{c2}'s. The coexistance of superconductivity and magnetism was found in these compounds.

Superconductivity can be destroyed by the application of an external magnetic field greater than a critical value (H_c). The critical field is also a characteristic of the superconductor. Superconductivity can also be destroyed by the passage of a transport current greater than a certain critical value (I_c).

T_c, H_c, and I_c are three parameters below which superconductivity appears. These three parameters depend on each other, and the relationship is schematically illustrated in Fig. II.1.

B. Type I, Type II, and "True Hard" Superconductors

All superconductors which contain inhomogeneities no larger than atomic dimensions can be separated into two groups: Type I superconductors, which include all pure metals except niobium (Nb) and vanadium (V); and Type II superconductors, which include Nb, V, and all superconducting alloys and intermetallic compounds.

$$\frac{H_c(T)}{H_c(0)} \approx 1 - \left(\frac{T}{T_c}\right)^2, \qquad \text{(II.2)}$$

which is one of the elementary BCS[7] (Bardeen-Cooper-Schrieffer) predictions. Typical critical fields in Type I superconductors are about 10^2G (G $\equiv$ Gauss) at temperatures well below T_c. Such low fields make Type I superconductors useless in real applications. For Type I superconductors, the current flows along the surface of the specimen and at some depth.

The transition from the normal state into the superconducting state in the presence of a magnetic field is a first-order phase transformation for Type I materials. However, in the absence of a magnetic field, such a transition is a second order one, in which no latent heat is involved and thus no

jump takes place in specific heat.

The Meissner-Ochsenfeld effect is a very important property of the Type I superconductors: When a specimen is placed in a magnetic field (provided that it is not too strong) and is then cooled below T_c, the magnetic flux originally present is abruptly expelled from the specimen. The transition from the normal to the superconducting state, when it occurs in a magnetic field, is accompanied by the appearance of whatever surface currents are required to cancel the magnetic field in the interior of the specimen. The magnetic behavior of Type I superconductors is illustrated in Fig. II.2. Below a critical field H_c, the entire specimen reverts to the normal state and the field penetrates perfectly.

The special feature of Type II superconductors as compared with that of Type I is the existence of two critical fields which are illustrated in Fig. II.3 for the magnetic behavior of Type II materials. Below a lower critical field H_{c1}, there is no penetration of flux. When the applied field exceeds an upper one, H_{c2}, the entire specimen becomes normal and the field penetrates perfectly. When the applied field is between H_{c1} and H_{c2}, there is partial penetration of flux, and the specimen develops a complicated microscopic structure of the coexistence of both normal and superconducting regions, known as the "mixed state"[8] or "vortex state". In the mixed state, Type II superconductors have no Meissner-Ochsenfeld effect. As far as the magnetic behaviors are concerned, the ideal homogeneous Type I and Type II materials are all magnetically reversible (See Figs. II.2 and II.3).

When reversible Type II superconductors are placed in a magnetic field which is greater than H_{c1}, less than H_{c2}, and perpendicular to the transport

current, the critical current is practically zero[9]. Whenever a current flows in the Type II superconductor, flux lines in the mixed state experience a Lorentz force F, given by

$$\underset{\sim}{F} = \underset{\sim}{J} \times \underset{\sim}{B} \qquad (II.3)$$

where $\underset{\sim}{J}$ is the current density, and $\underset{\sim}{B}$ is the flux density. Unless otherwise stopped, the flux lines will move in the direction of this force. Under such a condition, an induced electric field ($\underset{\sim}{E} = \underset{\sim}{V} \times \underset{\sim}{B}$, where $\underset{\sim}{V}$ is the velocity of the flux lines) appears. Thus, the superconductor now shows an induced resistance, and the heat caused by the induced resistance drives the whole specimen into a normal state.

Since the critical current is the current at which a detectable voltage across the specimen is first produced, it is the current which initializes movement of the flux lines. If there is no hindrance to the motion of flux lines, the critical current above H_{c1} is zero. Although for Type II superconductors the upper critical magnetic fields (H_{c2}) can be as high as 10^5G or more, their inability to carry transport currents in the mixed state makes these reversible Type II materials practically useless.

Nevertheless, there are other superconductors called "irreversible" (magnetic behavior) or "true hard" Type II superconductors which have physical and/or chemical inhomogeneities exceeding atomic dimensions. In practice, all Type II superconductors prepared by ordinary metallurgical methods are "true hard" superconductors. These superconductors have all the characteristics of the reversible type, i.e., an upper critical field H_{c2} and a lower one H_{c1}, a mixed state, and an absence of the Meissner-Ochsenfeld effect.

In addition to these properties, irreversible superconductors have some unique properties. In the mixed state they are able to pass a current more uniformly throughout the whole specimen in the presence of a perpendicular magnetic field. The critical current I_c of the superconductor is proportional to the cross section of the specimen. For these superconductors, it is possible to pin flux lines and prevent them from moving by interaction with heterogeneities in the microstructure of the material[10,11]. In other words, a pinning force F_p is exerted on the flux lines, and the pinning force opposes the Lorentz force $\underset{\sim}{F}$ given by Eq. (II.3). Therefore the critical current density J_c is determined by the magnitude of the pinning force $\underset{\sim}{F}_p$. Pinning is due to the heterogeneities[12-30] which may take the form of grain boundaries, second phase precipitates, radiation-induced damages, impurities, non-superconducting phases, dislocation lines, dislocation cell structures, or structural imperfections introduced by phase transformations such as coherent strains. Strong pinning materials are usually metallurgically "dirty" and are called "true hard" superconductors since they are analogous with magnetically hard or mechanically strong materials. The magnetic behavior of "true hard" materials is hysteretic (irreversible), retaining trapped flux after removal of the externally applied field. The behavior is shown in Fig. II.4.

The ability of carrying high current inside the specimen and the very high upper critical field ($> 10^5$G) have made "true hard" superconductors of considerable practical importance in the design of high-field magnets. Different kinds of high-T_c or high-field superconductors will be described in the next chapter.

C. Conclusion

Having introduced the fundamental phenomena of superconductivity and the different types of superconductors, it is important to review and discuss the basic mechanisms behind the superconductive properties such as T_c, H_c, and J_c. These mechanisms have been postulated on the basis of either pure theory or empirical rules. The detailed discussion of the fundamental theories is beyond the scope of this work. Nevertheless, for clarity, some brief comments are necessary: When predicting T_c for certain materials or explaining why some class of materials have high T_c's, the BCS theory[7] has been used to deal with weak-coupling superconductors and it has also been extended[31,32] to handle strong-coupling superconductors to a limited extent. Since the metals or the intermetallic compounds which have high T_c's are least understood in the normal state, it is very difficult for these theories to accurately predict T_c's or to explain why certain materials, e.g., the A15 class, have high T_c's.

The existing theories of superconductivity are insufficient to predict the properties of certain materials. As yet, we cannot say in advance what element and what proportions should be used to create superconducting materials with specified critical parameters. In studying the superconductivity of materials, experimental investigations must therefore play an important role as in other branches of solid-state physics. After examining all the available experimental data, Matthias[33] systematized the occurrence of superconductivity and formulated some important empirical rules. These rules could be used to predict a value for T_c of a new member of an already well-known class of materials.

However, it is almost impossible even with the existing empirical rules to make any prediction about the superconductive properties of an entirely new class of materials.

Experimental efforts to improve the upper critical fields of existing superconductors, e.g., Nb_3Sn (one of the commercially interesting A15 materials), are now being carried out under guidance of theoretical work. For example, it is known from Abrikosov[8] that

$$H_{c_2}(T) = \sqrt{2}\,\kappa H_c(T) \tag{II.4}$$

where κ is the dimensionless Ginzberg-Landau parameter[34]. κ is related to ρ_n, the normal-state resistivity by[35]

$$\kappa = \kappa_o + 7.5 \times 10^{-3}\,\gamma^{1/2}\,\rho_n, \tag{II.5}$$

where κ_o is an intrinsic material constant, and γ is the temperature coefficient of the electronic specific heat. Substituting Ta at the Nb site makes the Nb_3Sn material "dirtier" and increases ρ_n. Consequently, as indicated by Eqs. (II.4) and (II.5), the upper critical field could be increased substantially provided that the "dirtying" effects do not decrease the T_c value too much. This idea has been applied to the "Bronze" processed Nb_3Sn with very successful results[36].

We know that high values of the critical current result from strong interactions between the flux lines and the lattice imperfections. Thus, the third element addition can also increase the critical current density by increasing pinning effects as discussed previously. However, due to the complicated situations such as various types of pinning centers in a given system and dependence of the interaction (between flux lines and

pinning centers) on temperature, magnetic field, etc., theories worked out for some model systems[37] may not be applicable to the real systems of practical materials.

From the experimental work that has been carried out in relating the microstructure to the flux pinning, some empirical rules may be established. It should, however, be noted that there is no single rule which can be applicable to all the systems. For example, the dislocation density and the size of the dislocation cell structure play a dominant role in the flux pinning effect for the superconducting Nb-Ti bcc alloy[24], while the pinning in the A15 compounds is produced by the fine grain size and by the precipitates[25].

It is true that there is no single theory which can satisfactorily explain every aspect of superconductivity. It is also true that in the search of high T_c and/or high-field superconductors, the experimental efforts have always been in advance of the theoretical predictions[38]. However, it is important and essential for the physical metallurgists to be aware of the correlations among the metallurgical parameters, the superconductive phenomena, the existing theories, and the empirical rules. An understanding of the related parameters will certainly enable the metallurgists to improve existing manufacturing processes and to develop new processes for the fabrication of advanced superconductors which cannot now be handled by existing processes.

II. REFERENCES

1. H. K. Onnes, Akad. van Wetenschappen (Amsterdan) 14, 113, 818 (1911).
2. B. W. Roberts, J. Phys. Chem. Ref. Data 5, 581 (1976).
3. C. Kittel, Intro. to Solid State Phys. 4th Edition, John Wiley & Sons, Inc., New York, N. Y., 261 (1971).
4. W. A. Fertig, D. C. Johnston, L. E. DeLong, R. W. McCallum, M. B. Maple, and B. T. Matthias, Phys. Rev. Lett. 38, 987 (1977).
5. M. Ishikawa and ϕ. Fischer, Solid State Commu. 23, 37 (1977).
6. J. R. Gavaler, Appl. Phys. Lett. 23, 480 (1973).
7. J. Bardeen, L. N. Cooper, and J. R. Schrieffer, Phys. Rev. 106, 162 (1957); 108, 1175 (1957).
8. A. A. Abrikosov, Sov. Phys. JETP 5, 1174 (1957).
9. C. J. Gorter, Phys. Lett. 1, 69 (1962); 2, 26 (1962).
10. P. W. Anderson, Phys. Rev. Lett. 9, 309 (1963).
11. Y. B. Kim, C. F. Hempstead, and A. R. Strand, Phys. Rev. Lett. 9, 306 (1962); Phys. Rev. 129, 528 (1963).
12. W. W. Webb, Phys. Rev. Lett. 11, 191 (1963).
13. R. L. Fleischer, Phys. Lett. 3, 111 (1962).
14. A. V. Narlikar and D. Dew-Hughes, Phys. Stat. Sol. 6, 383 (1964).
15. D. Kramer and C. G. Rhodes, Trans. TMS-AIME 233, 192 (1965).
16. E. J. Kramer and C. L. Bauer, Philos. Mag. 15, 1189 (1967).
17. A. M. Campell, J. E. Evetts, and D. Dew-Hughes, Phil. Mag. 10, 333 (1964); ibid 18, 313 (1968).
18. J. Silcox and R. W. Rollins, Rev. Mod. Phys. 36, 52 (1964).
19. J. D. Livingston, Rev. Mod. Phys. 36, 54 (1964).
20. G. W. Culler, Appl. Phys. Lett. 4, 147 (1964).
21. J. P. McEvoy, Jr., R. F. Decell, and R. L. Novak, Appl. Phys. Lett. 4, 43 (1964).

22. R. Mailfert, B. W. Batterman, and J. J. Hanak, Phys. Lett. 24A, 315 (1967).

23. D. Dew-Hughes, Rep. Prog. Phys. 34, 821 (1971).

24. D. F. Neal, A. C. Barber, A. Woolcock, and J. A. Gidley, Acta Metall. 19, 143 (1971).

25. J. D. Livingston, Phys. Status Solidi (a) 44, 295 (1977).

26. E. Nembach and K. Tachikawa, J. Less-Common Met. 19, 359 (1969).

27. M. G. Benz, Trans. Metall. Soc. AIME 242, 1067 (1968).

28. R. V. Carlson, R. J. Barlett, L. R. Newkirk, and F. A. Valencia, IEEE Trans. on Magn. MAG-13, 648 (1977).

29. A. I. Braginski, J. R. Gavaler, G. W. Roland, M. R. Daniel, M. A. Janocko, and A. I. Santhanam, IEEE Trans. on Magn. MAG-13, 300 (1977).

30. E. J. Kramer, J. Nucl. Mater. 72, 5 (1978).

31. W. L. McMillan, Phys. Rev. 167, 331 (1968).

32. P. B. Allen and R. C. Dynes, PHys. Rev. B12, 905 (1975).

33. B. T. Matthias, Progress in Low Temp. Phys., Vol. II, edited by C. J. Gorter, North Holland Publishing Co., Amsterdam, p. 138 (1957).

34. V. L. Ginzburg and L. D. Landau, JETP USSR 20, 1064 (1950).

35. B. B. Goodman, IBM J. Res. Dev. 6, 63 (1962).

36. J. D. Livingston, to be published in Trans of IEEE.

37. A. M. Campbell and J. E. Evetts, Adv. Phys. 21, 199 (1972).

38. B. T. Matthias, Superconductivity in d- and f-Band Metals, La Jolla, California, June 21-23, 1979.

FIGURE CAPTIONS

Fig. II-1. A schematic diagram showing the superconducting state, the normal state, and the relationship between the three critical parameters: T_c, H_c, and J_c.

Fig. II-2. Magnetic (B vs. H) behavior of reversible Type I superconductors.

Fig. II-3. Magnetic (B vs. H) behavior of reversible Type II superconductors.

Fig. II-4. The irreversible (hysteretic) magnetic behavior of the "true hard" superconductors.

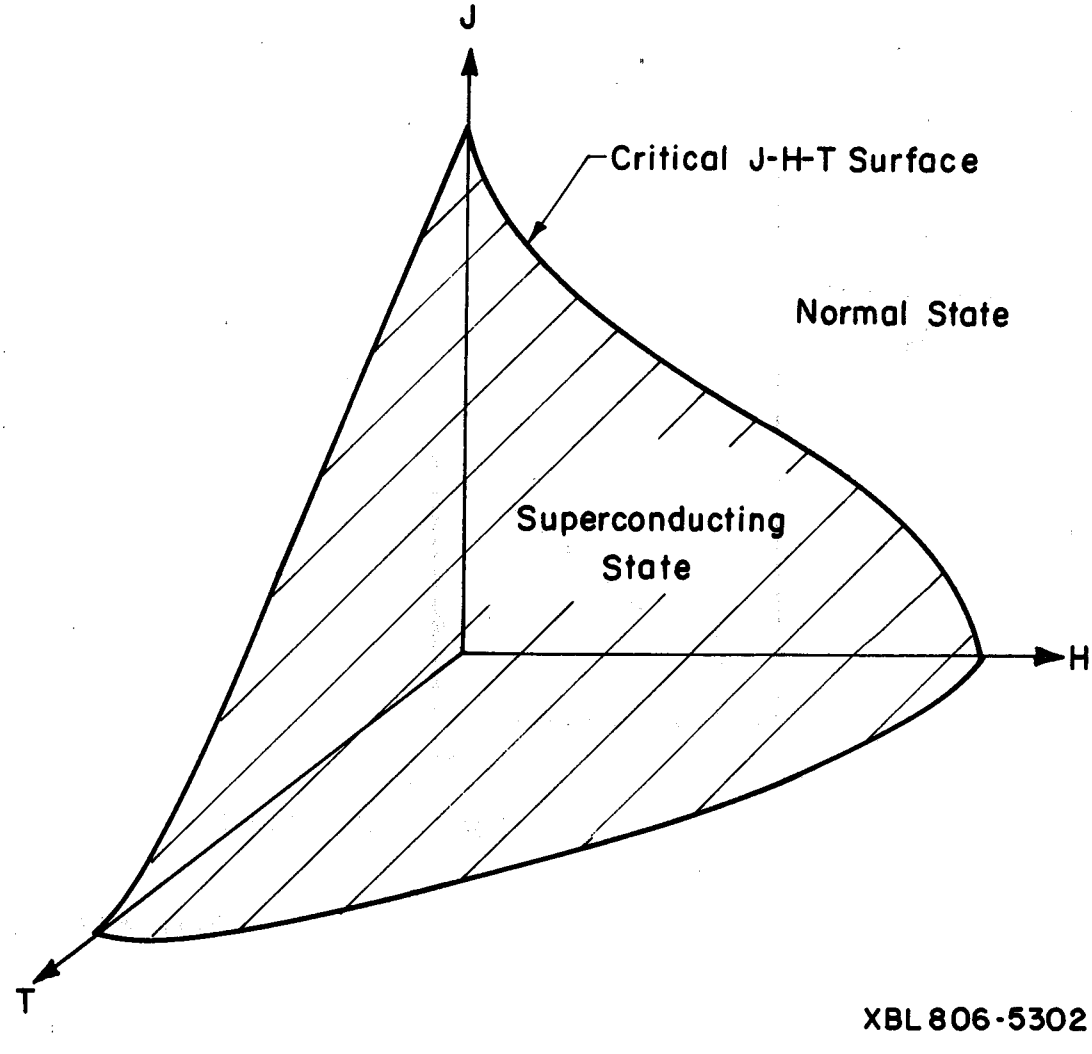
J
Critical J-H-T Surface
Normal State
Superconducting
State
H
T
XBL 806-5302

Fig. II-1

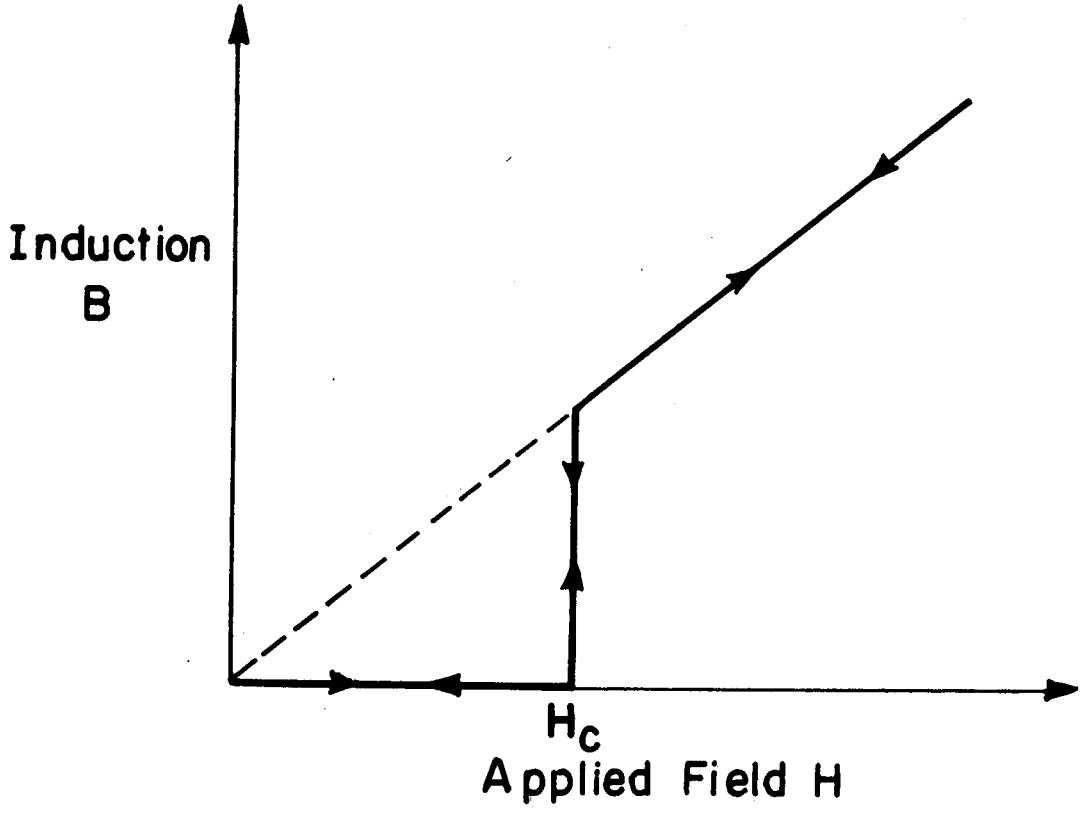

Fig. II-2

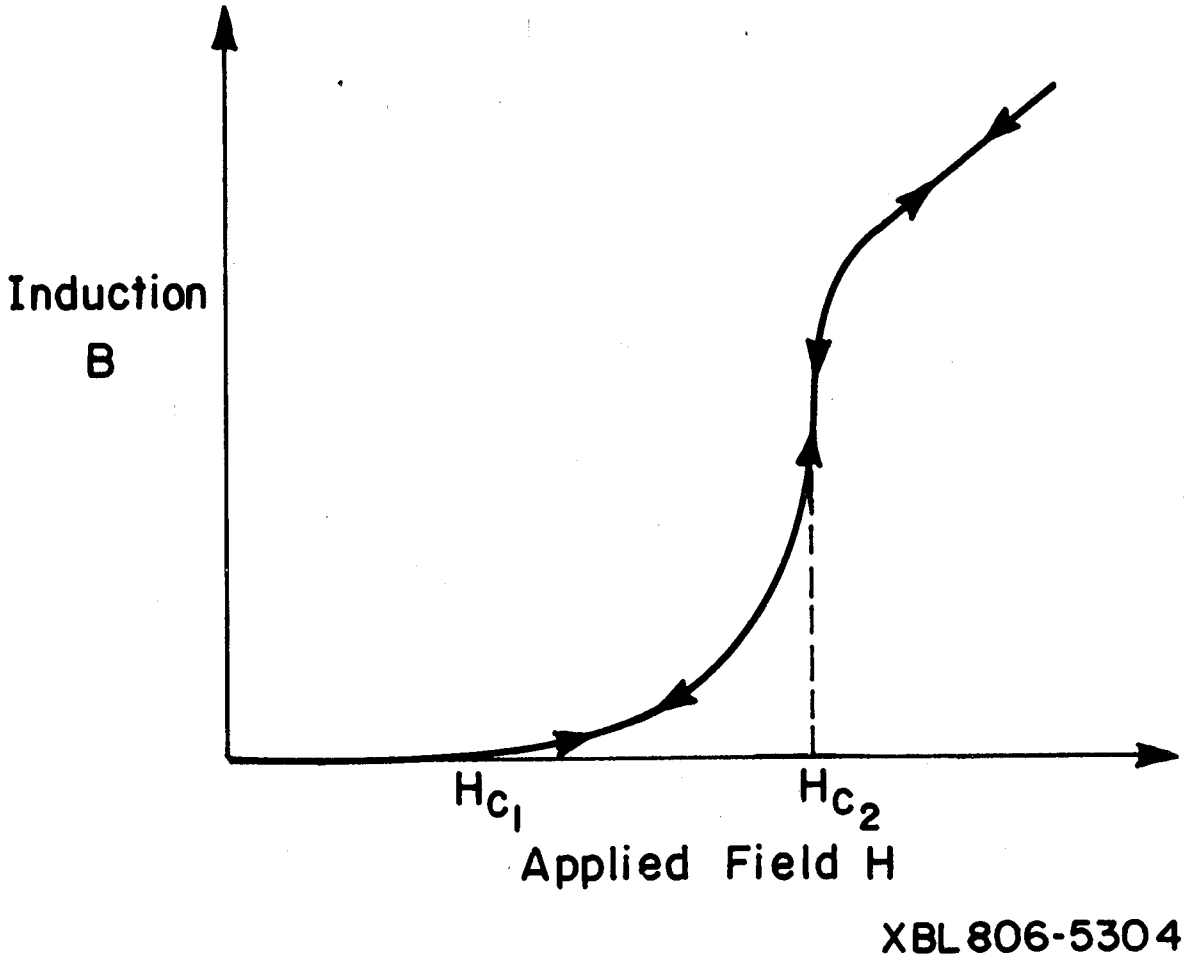

Fig. II-3

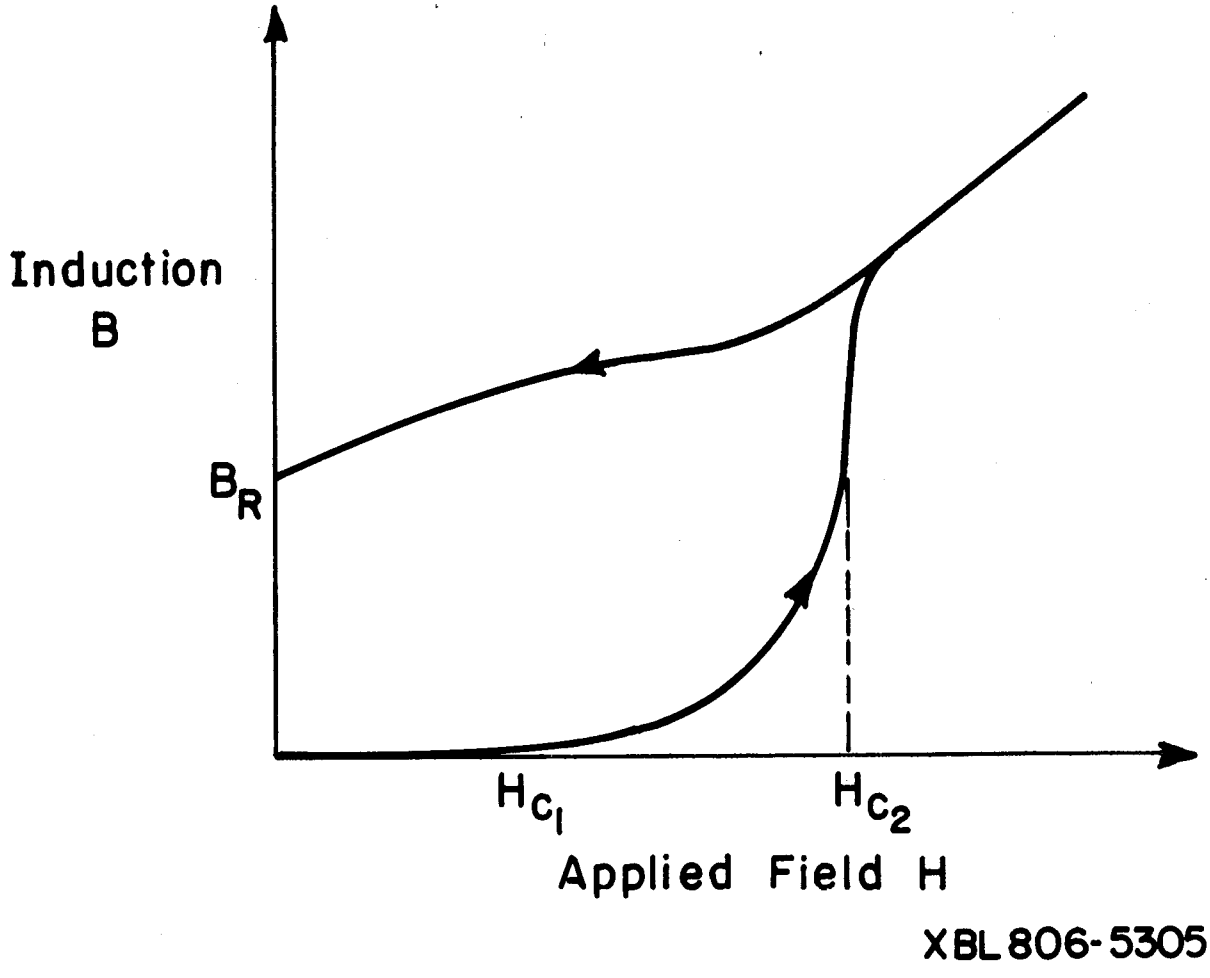

Fig. II-4

III. HIGH-T_c OR HIGH-FIELD SUPERCONDUCTORS

A. Discoveries of High-T_c or HIgh-Field Superconductors

Immediately after the discovery of superconductivity, its possible use in creating strong magnetic fields was investigated. It was found, however, that a magnetic field of a few gauss destroyed the superconductivity of mercury, tin, and lead. In the early 1930's it was discovered that a lead-bismuth alloy remained superconductive in moderate fields. On this basis, the possibility of making superconducting magnets with a strength of twenty kilogauss was proposed. However, the idea was finally rejected due to a very low critical current density. In 1941 NbN, the first high-T_c and high-field superconductor was found[1]. The T_c and H_{c_2} of NbN are 15K and 150 KG, respectively. In 1953 the first A15 compound, V_3Si, with a T_c of 17.1 K, was discovered by Hardy and Hulm[2]. In the same year, a ductile Nb-Zr BCC alloy, with a T_c of 11 K and a H_{c_2} of 100 KG was found[3]. During the following year Matthias et al. obtained a T_c of 18 K in Nb_3Sn[4], another A15 compound. The intermetallic compound V_3Ga, which also has an A15 crystal structure, joined the ranks of the high-T_c superconductors in 1960[5]. Nb_3Sn and V_3Ga later became of commercial interest in the 1970's due to the extensive development of the "Bronze" process. A ductile BCC alloy of nominal composition, Mo_3Re, whose superconductivity was reported by Hulm[6], was produced in a wire form in sufficient quantity to construct a solenoid in 1961[7]. Nb-Ti, another ductile BCC alloy, was also discovered during this period. Since 1964 Nb-Ti alloys have been extensively studied and developed. They are now marketed by several industrial companies. One interesting superconducting phase (Laves phase) with a C15 crystal structure was found by Matthias et al.

in V_2Zr[8] and Sadagopan et al. in V_2Hf[9]. The first material with T_c greater than 20 K is the ternary compound $Nb_3(Al_{0.8}Ge_{0.2})$ which was found by Matthias and his co-workers in 1967[10]. The highest T_c ever reported is 23 K for Nb_3Ge[11,12]. So far the record for high T_c has remained within the A15 family: V_3Ga (15.7 K), V_3Si (17.1 K), Nb_3Sn (18.3 K), Nb_3Al (18.8 K), Nb_3Ga (20.3 K), $Nb_3(Al_{0.8}Ge_{0.2})$ (20.7 K), and Nb_3Ge (23 K). A new class of ternary compounds based on molybdenum sulfide (Chevrel Phase) have been synthesized as recently as 1971[13], and many of them have been shown to be superconductors[14]. Among these ternary compounds was $PbMo_5S_6$, the most interesting superconductor on the basis of its H_{c2} of 500~600 KG which is the highest ever measured[15].

In this chapter some useful high-T_c and/or high-field superconductors are briefly reviewed. Their properties and potentials are discussed.

B. Ductile BCC Alloys Based on Niobium

BCC alloys of Nb-Ti, Nb-Zr, and their ternary systems are much more ductile than the brittle intermetallic compounds of A15 and Chevrel phases. For applications with magnetic fields less than 80 KG and temperatures less than 5 K,* the ductile superconducting Nb-base BCC materials, especially Nb-Ti alloys, are used almost exclusively due to their ease of fabrication and excellent mechanical properties.

Since the early 1960's Nb-Ti and its ternary systems have been extensively studied[17-23] with respect to conductor design, which includes consideration of its cryogenic and enthalpy properties, as well as the dynamic

---

* For constructing magnets of 80 KG or below, Nb-Ti alloys are used at 4.2 K. For magnets of 80-100 KG, Nb-Ti or Nb-Ti-Ta might be used at temperatures below 3 K[16].

stabilization, conductor fabrication, the relationship between critical current density and microstructures, and the theories of flux-pinning. For brevity, only the correlations between J_c and metallurgical parameters will be discussed in this section.

Since there is more than one competing mechanism for flux-pinning, no correlation can be drawn between superconducting properties and metallurgical structures with the single exception of the relationship between critical current densities and dislocation substructure sizes. On the basis of this correlation and other experimental data, however, the following conclusions can be drawn: (1) Critical current density is enhanced by deformation. This is due to the refinement of the size of the dislocation substructure and the high density of dislocations within the cell structure. (2) Critical current density is enhanced by a precipitation heat treatment. The α (HCP)-phase precipitation followed by a cold deformation has two advantages: First, α-phase precipitate itself can be an effective pinning center. Second, with the presence of α-phase precipitate, the dislocation substructure can be further refined. (3) The addition of a ternary element such as Zr results in very fine grain structures, which enhances the critical current density. (4) The addition of Ta provides a potentially greater high-field performance due to an enhanced H_{c2} at 1.8 K.

In developing the superconducting Nb-Ti and its ternary alloys, thermomechanical treatments (TMT) have not yet been optimized. High resolution transmission electron microscopy should be used in order to characterize microstructures and improve the TMT process. It is believed that with an optimal TMT process, the present $J_c(H)$ data and the associated mechanical properties can be enhanced substantially.

C. V_2Hf-Base C15 Type Laves Compounds

Many of the compounds which form in the hexagonal structure, C14 ($MgZn_2$ type), C15 ($MgCu_2$ type), and C36 ($MgNi_2$ type), known as Laves phases, are superconductors. Of these, the V_2Hf-base C15 type (Laves phase) compounds have the best superconducting properties. These compounds include the V-Hf, V-Hf-Zr, V-Nb-Hf, V-Ta-Hf, V-Cr-Hf, and V-Nb-Ti-Hf systems. Superconducting tapes have been fabricated in the V-Hf-Zr, V-Nb-Hf, and V-Nb-Ti-Hf systems. For the V-Hf-Zr system[24], tapes containing a $V_2(Hr,Zr)$ compound were made by a diffusion process in which a composite of vanadium sheath and Hf-Zr alloy core is rolled and then heat treated. For V-Nb-Hf and V-Nb-Ti-Hf[25], tapes were fabricated directly by plastic deformation with final heat treatments introduced after cold work. The ingots containing V, Hf, Nb and/or Ti were prepared by arc-melting in an argon atmosphere. The ingots were then rolled into tapes with intermediate annealings at high temperatures (1300-1500° C), and subjected to a final heat treatment at temperatures ranging from 600° C to 1500° C.

From the experimental data, it is clear that the C15 compounds are slightly superior to Nb-Ti and its ternary alloys in critical temperatures; for critical magnetic fields, C15 materials are much higher than the BCC Nb-base alloys. In addition, these high-field C15 compounds have better mechanical properties than the A15 type materials and are highly resistive to neutron irradiation[26].

The best overall J_c ever obtained in these C15 compounds is 10^4 A/cm^2 at 120 KG and 4.2 K, which is comparable with those of the A15 compounds fabricated by the "Bronze" or Tsuei's process.

The V_2Hf-base C15 type Laves phase compounds have gained much interest

as high-field superconductors due to their high upper critical fields (> 200 KG), better mechanical properties and higher resistivity to radiation damages as compared to the A15 and Chevrel phases. The ac losses and the effects of mechanical stress on the superconducting properties, however, have not been reported.

D. Ternary Molybdenum Sulfides

As mentioned in Section III.A, the highest critical fields ever reported for any superconductor belong to $PbMo_5S_6$, one of the Chevrel phase ternary compounds.

Attempts to make useful forms of these materials such as Pb-Mo-S and Cu-Mo-S, have been very disappointing[27-30]. For the Pb-Mo-S system, wires or tapes have been fabricated using a modified Kunzler technique (powder metallurgy), chemical vapor deposition, and sputtering. Although the critical field H_{c2} (4.2 K) is still very high, the critical current densities, J_c (4.2 K, 40 KG), are in the range of 10^3-10^4 A/cm^2. For Cu-Mo-S, the results obtained by the sputtering technique are also disappointingly low.

Furthermore, the Chevrel phase materials are intrinsically brittle and are sensitive to neutron irradiation. Nevertheless, due to their very high critical fields, more effort should be directed towards the development of these materials.

E. A15 Compounds

Intermetallic compounds of the A_3B type, which form in the A15 crystal structure, are currently the best superconducting materials with very high T_c, H_c, and J_c. It is meaningful to group the known high-T_c A15 compounds into two classes[31]. The first class includes those with commercial

potential; Nb_3Sn, V_3Ga, and V_3Si. They are characterized by very high electronic coefficients of heat capacity and temperature-dependent magnetic susceptibilities and resonances. They can easily be made with the correct stoichiometric ratio of 3:1. The second class includes all those with T_c > 18 K such as Nb_3Al, Nb_3Ga, $Nb_3(Al,Ge)$, and Nb_3Ge. They have electronic heat capacity coefficients about the same as the element niobium, which is a factor of two or more lower than those of the first class. Perhaps related, but even more significant, is the fact that the compounds of the second class are always A-site rich, frequently having a composition close to Nb_4X when prepared from the melt, or by equilibrium solid-state reactions.

One of the early attempts to develop A15 conductors was the work done by Kunzler and co-workers[32] at Bell Laboratories in 1961. This process was not commercially accepted since they suffered from severe flux jumping and damage during quench and burnout.

In 1966, Tachikawa and Tanaka[33] developed a solid state diffusion technique which was applied to the V-Ga system. Their work eventually led to the commercial production of fine-filament A15 conductors. This technique, referred to as the "Bronze" process[34], takes advantage of the fact that Nb_3Sn and V_3Ga are formed by an equilibrium solid state reaction at an interface between the Nb(V) and Cu-Sn(Ga) bronze. Final wires or tapes could be produced by drawing the composite of Nb(V) rod and Cu-Sn(Ga) bronze sheath. A15 filaments of 1-10 μm size could then be formed by solid-state reactions during the final heat treatments. The "Bronze" process has been extensively studied and developed, and is the only commercialized process employed today.

In order to enhance $J_c(H)$, increase H_{c2}, improve mechanical properties, and increase the kinetics of A15 layer formation, many methods have been used. Among these are the addition of Ta(Zr) into the Nb(V) core[35,36], Al or Mg to Cu-Ga bronze[37,38], small amounts of Ga in the V core[39], etc. The concepts of those attempts include (1) making the A15 phase "dirtier", e.g., by substituting Ta into a Nb-site; (2) changing the columnar A15 grain size to a more equi-axed structure and further refining it, e.g., by increasing the A15-formation kinetics or by introducing Zr or Al. Zr and Al have a high affinity for oxygen. During the processing these oxides are distributed along grain boundaries and play important roles in the refinement and equi-axed tendency of these grains. A "dirtier" A15 phase can increase the H_{c2} and a smaller grain size can increase the pinning effects, thus enhancing $J_c(H)$ data.

In 1971, a powder metallurgical process named "liquid infiltration" was developed at the Lawrence Berkeley Laboratory[40,41]. Later, the Nb_3Sn wires were fabricated by this process[42,43]; the $J_c(H)$ data obtained for the material fabricated by this process is comparable with those obtained by the "Bronze" process. Other properties such as ac losses and mechanical properties have not yet been reported.

In 1973, Tsuei[44] invented a new approach to fabricate Nb_3Sn and V_3Ga. Later, this process was extensively developed by groups at M.I.T.[45], Harvard[46], and Ames Laboratory[47] and is now called the "In-Situ" process.

The "In-Situ" process starts with Cu-Nb (V) alloys melted at high temperatures. When the melt is chill-cast by rapid cooling, small uniform precipitates of Nb(V) are condensed out of the Cu-Nb(V) alloys. After casting, the ingots are then processed with large area reductions, external

plating diffusion and finally reaction to form Nb_3Sn (V_3Ga) filaments in the bronze matrix. Because the initial particle sizes are quite small, the sizes of the final Nb(V) filaments after the large areal reductions could be in the range of several hundred to several thousand Å's. The A15 fibers thus formed are sub-micron in size, and are considerably smaller in cross section than the A15 layers produced by the "Bronze" process. The fine fibers lead to improved mechanical properties. Increase of Nb(V) in the initial Cu-Nb(V) alloy enhances the $J_c(H)$ values. However, the mechanical properties deteriorate. Therefore, an appropriate amount of Nb(V) must be chosen in order to reach optimal conditions.

It should be noted that both the "Bronze" process and the "In-Situ" method can only be applied to the fabrication of the stable first class A15 compounds, namely, Nb_3Sn, V_3Ga, and V_3Si. Second class A15 materials, e.g., Nb_3Al and Nb_3Ge, fail in manufacturing due to thermodynamic reasons[48]. The earlier attempts to fabricate second class A15 materials[49-51], especially the Nb-Al system, will be discussed in Chapter VI.

Recently, processes associated with powder metallurgy have gained much attention. Under equilibrium conditions, powder metallurgy (P/M) can be applied to the first class A15 materials[52,53]. Moreover, under non-equilibrium situations, this process might be applicable to the second class A15 compounds[54,55].

It was mentioned in the previous chapter that the pinning in the A15 compounds is produced by the fine grain size and the precipitates. After examining the processes which are used to fabricate the A15 compounds, it is difficult to distinguish between the two effects since the presence of precipitates will cause the refinement of the grain size. Grain boundaries

in A15 compounds are expected to be more efficient than those in other alloys as flux pinning centers since they represent an interruption in the high degree of order necessary for superconductivity in the intermetallic compounds. Much experimental work using the "Bronze" process has demonstrated the effect of refinement of grain size in increasing J_c[56-58]; for Nb_3Sn, V_3Ga, and V_3Si, the current density increases with decreasing grain size, reaching a maximum value at a grain diameter around 800 Å, and then decreases. However, using Tsuei's method to produce the Nb_3Sn, Bevk et al.[59] were able to obtain an average grain size of ~ 400 Å to ensure an effective flux pinning. An average A15 grain size of ~300 Å in the Nb-Al system was obtained by using the "solid-state precipitation" process[60]. Moreover, the grain size of $Nb_3(Al,Si)$ and $Nb_3(Al,Ge)$ samples prepared by the liquid-quenched method is less than 100 Å, and the J_c's of the tested samples are ~ 10^6 A/cm^2 at 42 K and 150 KG[62]. Therefore, it is still an open argument: What is the minimum grain size of the A15 compounds necessary to reach the optimal flux pinning and, thus, maximal critical current density?

In this work, we are mainly concerned with the bulk materials, particularly A15 compounds, and the associated processes which are applied to fabricate the conductors or cables for constructing magnets. These can be used in the areas of high-energy physics accelerators, thermonuclear fusion reactors, etc. Thin-film synthesizing techniques, such as sputtering and electron-beam coevaporation have been omitted.

III. REFERENCES

1. G. Ascherman, E. Frederik, E. Just, and J. Kramer, Phys. Z. 42, 349 (1941).

2. G. F. Hardy and J. K. Hulm, Phys. Rev. 87, 884 (1953).

3. B. T. Matthias, Phys. Rev. 92, 874 (1953).

4. B. T. Matthias, T. H. Geballe, S. Geller, and E. Corenzwit, Phys. Rev. 95, 1435 (1954).

5. W. E. Blumberg, J. Eisinger, V. Jaccarino, and B. T. Matthias, Phys. Rev. Lett. 5, 149 (1960).

6. J. K. Hulm, Phys. Rev. 98, 1539 (1955).

7. J. E. Kunzler, E. Buehler, F. S. L. Hsu, B. T. Matthias, and C. Wahl, J. Appl. Phys. 32, 325 (1961).

8. B. T. Matthias, V. B. Compton, and E. Corenzwit, J. Phys. Chem. Solids 19, 139 (1961).

9. V. Sadagopan, E. Pollard, and H. C. Gatos, Solid State Commun. 3, 97 (1965).

10. B. T. Matthias, T. H. Geballe, L. D. Longinotti, E. Corenzwit, G. W. Hull, R. H. Willens, and J. P. Maita, Science 156, 645 (1967).

11. J. R. Gavaler, Appl. Phys. Lett. 23, 480 (1973).

12. L. R. Testardi, J. H. Wernick, and W. A. Royer, Solid State Commun. 15, 1 (1974).

13. R. Chevrel, M. Sergent, and J. Prigent, J. Solid State Chem. 3, 515 (1971).

14. B. T. Matthias, M. Marezio, E. Corenzwit, A. S. Cooper, and H. E. Barz, Science 175, 1465 (1972).

15. S. Foner, E. J. McNiff, Jr., and E. J. Alexander, Phys. Lett. 49A, 269 (1974).

16. C. D. Henning, IEEE Trans. on Magn. MAG-13, 15 (1977).

17. T. G. Gerlincourt and R. R. Hake, Phys. Rev. Lett. 9, 293 (1962).

18. J. B. Vetrano and R. W. Boom, J. Appl. Phys. 36, 1179 (1965).

19. D. Kramer and C. G. Rhodes, IEEE Trans. Magn. 239, 1612 (1967).

20. A. D. McInturff and G. G. Chase, J. Appl. Phys. 44, 2378 (1973).

21. P. R. Critchlow, E. Gregory, and B. Zeitlin, Cryogenics 11, 3 (1971).

22. D. F. Neal, A. C. Barber, A. Woodcock, and J. S. F. Grindley, Acta Metall. 19, 143 (1971).

23. M. Suenaga and K. M. Ralls, J. Appl. Phys. 40, 4457 (1969).

24. K. Inoue and K. Tachikawa, Appl. Phys. Lett. 25, 94 (1974).

25. K. Inoue, T. Kuroda, and K. Tachikawa, IEEE Trans. on Magn. MAG-15, 635 (1979).

26. B. S. Brown, J. W. Hafstrom, and T. E. Klippert, J. Appl. Phys. 48, 1759 (1977).

27. T. Luhman and D. Dew-Hughes, J. Appl. Phys. 49, 936 (1978).

28. M. Decroux, O. Fischer, and R. Chevrel, Cryogenics 17, 291 (1977).

29. N. E. Alekseevskii, M. Slinski, N. M. Dobrovolskii, and V. I. Tsebro, JETP Lett. 23, 412 (1976).

30. S. A. Alterovitz, J. A. Woolam, L. Kammerdiner, and H. L. Luo, Appl. Phys. Lett. 31, 233 (1977).

31. T. H. Geballe and J. K. Hulm, IEEE Trans. on Magn. MAG-11, 119 (1975).

32. J. E. Kunzler, Revs. Modern Phys. 33, 501 (1961).

33. K. Tachikawa and Y. Tanaka, Japan J. Appl. Phys. 5, 834 (1966).

34. A. R. Kaufman and J. J. Pickett, Bull. Am. Phys. Soc. 15, 838 (1970).

35. J. D. Livingston, to be published in Trans. of IEEE.

36. Y. Furuto, T. Suzuki, K. Tachikawa, and Y. Iwasa, Appl. Phys. Lett. 24, 34 (1974).

37. K. Tachikawa, Y. Tanaka, Y. Yoshida, T. Asano, and Y. Iwasa, IEEE Trans. on Magn. MAG-15, 391 (1979).

38. K. Tachikawa, K. Itoh, and Y. Tanaka, IEEE Trans. on Magn. MAG-11, 240 (1975).

39. D. G. Howe and T. L. Francavilla, Reports of NRL Progress, 21, June (1977).

40. E. R. Parker et al., LBL Report 425, 128 (1971).

41. M. R. Pickus, V. F. Zackay, E. R. Parker, and J. T. Holthuis, International J. Powder Metallurgy 9, 3 (1973).

42. K. Hemachalam and M. R. Pickus, IEEE Trans. on Magn. MAG-13, 466 (1977).

43. M. R. Pickus and J. L-F Wang, Modern Developments in Powder Metallurgy 11, 314 (1977).

44. C. C. Tsuei, J. Appl. Phys. 45, 1385 (1974).

45. S. Foner, R. Roberge, J. L. Fihey, R. Flükiger, R. Akihama, E. J. McNiff, Jr., and B. B. Schwartz, 8th Symposium on Eng. Problems of Fusion Research, Nov. 13-16, 1979 - San Francisco, CA.

46. J. Beyk, F. Habbal, C. J. Lobb, and G. Duclon, to be published in Adv. in Cryo. Eng., Vol. 26.

47. J. D. Verhoven, E. D. Gibson, C. V. Owen, J. E. Ostenson, and D. K. Finnermore, Appl. Phys. Lett. 35, 270 (1979).

48. T. Luhman, Treatise on Materials Science and Technology V. 14, 224 (1979), Ed. T. Luhman and D. Dew-Hughes, Academic Press, and the references quoted in this article.

49. T. W. Eager and R. M. Rose, IEEE Trans. on Magn., MAG-11, 214 (1975).

50. D. E. Harasyn and L. E. Toth, J. Appl. Phys. 46, 2232 (1975).

51. S. Ceresara, M. V. Ricci, N. Sacchetti, and G. Sacerdoti, IEEE Trans. on Magn. MAG-11, 263 (1975).

52. R. Flükiger, R. Akihama, S. Foner, E. J. McNiff, Jr., and B. B. Schwartz, Appl. Phys. Lett. 35, 810 (1979).

53. R. Bormann, L. Schultz, and H. C. Freyhardt, Appl. Phys. Lett. 32, 79 (1978).

54. S. Foner and R. Akihama, private communication.

55. M. Hong and J. W. Morris, Jr., unpublished results.

56. J. S. Caslaw, Cryogenics 11, 57 (1971).

57. A. W. West and R. D. Rawlings, J. Mater. Sci., 12, 1862 (1977).

58. J. D. Livingston, Phys. Status Solidi (a) 44, 295 (1977).

59. J. Bevk and J. P. Harbison, J. Mater. Sci. 14, 1457 (1979).

60. M. Hong and J. W. Morris, Jr., submitted to Appl. Phys. Letters.

61. J. Bevk, private communication.

62. K. Lo, J. Bevk, and D. Turnbull, J. Appl. Phys. 48, 2597 (1977).

IV. DIRECT "SOLID-STATE PRECIPITATION" PROCESS AND EXPERIMENTAL PROCEDURE

A. Direct "Solid-State Precipitation" Process

A15 compounds are intrinsically brittle and special processing techniques must be used to form them into wires or tapes. A number of manufacturing techniques have been suggested for laboratory or commercial use. As discussed in the previous chapter, these techniques include the well-developed "Bronze" process, the "In-Situ" (Tsuei's) method, the "liquid infiltration" method, the "cold" or "hot" powder metallurgical process, and others. While considerable success has been obtained with these various manufacturing methods, they have the common drawback of being metallurgically elaborate and difficult to accomplish in practice. Furthermore, a solid-state diffusion reaction between Nb(V) and Sn(Ga) is required to form the A15 compounds for most of the processes mentioned above. From the standpoint of phase stability and thermodynamics of the A15 compound formation as mentioned in Chapter III, most of the processes can only be applied to the fabrication of the first-class A15 materials. Only a few processes have the possibilities of being applicable to the fabrication of the second-class A15 compounds; for these processes, however, very high ($\geq$ 1600° C) aging was used to obtain superconducting A15 phases with high T_c's and $J_c(H)$'s. The high temperature heat treatment on the final wire or tape product might not be acceptable because of the low melting points of the stabilizing material such as Al or Cu. In order to produce superconducting wire of second-class A15 compounds, some novel metallurgical techniques must be invented and developed.

The metallurgically simplest method of wire manufacture involves casting an ingot of the desired composition and extruding or drawing the cast

material into a wire. Virtually all conducting wires, including ductile Nb-Ti superconducting wires, are manufactured in this way. It is possible that variations in conventional wire making practice may also be used for the manufacture of high T_c superconducting wires or tapes.

A monolithic processing technique (see Fig. IV.1) which should succeed in producing superconducting wires containing A_3B phases is simple to design in theory, and it is illustrated in Fig. IV.2 with reference to the V-Ga phase diagram[1,2]. The V_3Ga phase is an ordered phase which is present in the equilibrium phase diagram in the isolated region shown to the left hand side. The region of preference of the V_3Ga phase lies below a well-defined critical temperature, above which V and Ga form a solid solution. One may hence design a monolithic process in which a V/Ga ingot of composition near V_3Ga is made homogeneous by annealing at temperatures above the ordering temperature. In theory the ingot could be subsequently cooled at a rate sufficient to suppress the formation of the V_3Ga ordered compound, producing a supersaturated solid solution of Ga in V. The resultant BCC solid solution is relatively ductile and amenable to processing through wire drawing or extrusion. After deformation, the superconducting phase could then be introduced by heat treatment at a temperature below the ordering temperature but high enough for the precipitation of the V_3Ga phase to proceed at a kinetically reasonable rate.

A process of this type is most straightforward in the V-Ga system, whose phase diagram contains a solid solution region above the ordered V_3Ga compound but modifications of this technique could easily be designed for other systems of A15 materials.

While the monolithic processing described above is simple and appealing in theory, its practical implementation faces substantial difficulties. The obvious problems are the following:

(1) Sample preparation. For any A15 (A_3B) system, the difference in melting points between elements A and B is tremendous, e.g., 1900° C for V, 2468° C for Nb 29.8° C for Ga, 660° C for Al, etc. For some systems the boiling point of element B is even lower than the melting point of element A; the boiling point of Al is 2450° C, which is lower than 2468° C, the melting point of Nb. Consequently, the ingots prepared from these elements often have surface defects, internal cracks, and porosities. These problems have been encountered in several research laboratories[1,3] where the arc-melting method was used for sample preparation.

(2) Quench Cracking. One can achieve a homogeneous solid solution by annealing ingots in the high temperature range of the BCC phase region. To produce a homogeneous solid solution at room temperature, requires that the ingot be cooled sufficiently rapidly to suppress the formation of the A15 phase. However, the rapid cooling of alloys frequently results in a phenomenon known as "quench-cracking", in which the alloy spontaneously fractures due to thermal stresses on cooling. This problem is usually attributed to chemical segregation during high temperature annealing. Quench-cracking-like phenomena have, in fact, been encountered in previous attempts to form A_3B superconducting compounds by monolithic processes.

(3) Low temperature Brittleness. Even though the sample can be successfully quenched to form a homogeneous solid solution at low temperatures, it still does not follow that the sample can be successfully formed into a tape or wire. The matrix phases of interest, V or Nb, are BCC-structure

refractory metals which typically have high ductile-to-brittle transition temperatures, with the result that their solid solutions may prove to be extremely brittle at low temperature.

(4) Interstitial Impurities. The deformability of V or Nb based alloys depends very heavily on the levels of interstitial impurities, e.g., oxygen and nitrogen in the material. A high concentration of oxygen and nitrogen inside the ingots is unavoidable if one uses the more economical raw starting materials of 99% or 99.9% purity.

(5) Non-Stoichiometric Precipitation. The A_3B compounds of interest as high-field superconducting phases permit relatively large deviations from stoichiometry, as indicated by the breadth of the stability field of the V_3Ga in the V-Ga phase diagram and the off-stoichiometry of the A15 phase in the Nb-Al phase diagram (see Figs. IV.3[4] and IV.4[5]). It is well known that the superconducting properties of the A15 compounds deteriorate as the compounds deviate from the true A_3B composition[1,6]. It may, therefore, prove difficult to achieve good superconducting transition temperatures if the alloy is intentionally made lean in solute so as to facilitate melting and wire and tape fabrication.

The problems and possible promise of monolithic processing are indicated by the prior work of Das et al.[1] and Pan et al.[7] in the V-Ga system, and Webb et al.[3,8] and Pan et al.[9] in the Nb-Al system. In the work of Das et al.[1] ingots of V-(13-40 at.%)Ga were cast, homogenized, and then slowly cooled or cooled and annealed to develop the A15 V_3Ga phase. Substantial quench-cracking was found in the as-cast samples. Moreover, there was a substantial decrease in superconducting transition temperature when the Ga content of the ingot fell below (or rose above) the stoichiometric composition. For example, a V-20.5 at.% Ga ingot exhibted a

superconducting transition temperature <10 K, in contrast to the transition temperatures above 15 K obtainable with V-25.6 at.% Ga.

The work of Pan et al.[7] concentrated on samples of lower Ga content, V(6-16 at.%) Ga. They reported success in overcoming the quench-cracking problem to produce samples which could be successfully made into wire or tape. The superconducting phase was then introduced through a subsequent aging treatment. However, to achieve reasonable superconducting transition temperatures they apparently found it necessary to introduce a third element, cerium in ~ 1 at.% concentration. They attributed the resulting high values of the transition temperatures (~14° K) to a beneficial effect of Ce on the phase diagram.

In the work of Webb et al.[3,8], small ingots of Nb-25 at.% Al weighing about 1 gm were cast, homogenized, and then quenched in a room temperature Ga-In eutectic liquid bath. A BCC phase of Nb_3Al was obtained by quenching. However, a serious quench-cracking problem appeared. Upon manipulation with tweezers, the samples broke apart until they appeared as a collection of individual crystals, cracking along grain boundaries. The isolated individual crystals were ductile and could be deformed. The A15 phase was introduced by an aging heat treatment. Critical current densities about 10^5 A/cm^2 at 200 KG and 4.2 K were obtained for these samples which contained brittle intermetallic compounds A15 (Nb_3Al) and σ (Nb_2Al) phases, and were thus unavoidably brittle.

For the Nb-Al system, Pan et al.[9] also concentrated on samples of lower Al content, Nb-7~14 at.% Al. No quench-cracking problem was encountered in their work. They also claimed that the critical current densities were about 10^4 A/cm^2 at 60 KG and 4.2 K.

In the following discussion in this chapter we show the experimental procedure of the monolithic "solid-state precipitation" process. In Chapter V, we show that V-Ga alloys having Ga contents up to 18.5 at.% can be monolithically processed into tape, and made superconducting through direct precipitation of the A15 phase so that high critical transition temperatures are obtained without the addition of a third element; reasonably good $J_c(H)$ data is also achieved. No quench-cracking problem was encountered in this work. The cerium addition, however, was found to play an important role in removing oxygen and nitrogen from the cast samples.

Results of the monolithic "solid-state precipitation" processed Nb-Al specimens are presented in Chapter VI. Large quantitites of the samples weighing about 30 gms could be quenched; a ductile material with a BCC phase was obtained and no quench-cracking was observed. The overall J_c's of the tape made from the ingot containing 18 at.% Al are about 10^4 A/cm^2 at 140 KG and 4.2 K.

B. Experimental Procedure

1. Materials Preparation

For the V-Ga system, the alloys investigated were prepared by arc-melting pure starting components under an argon atmosphere. The starting materials were V, 99.8% pure, and Ga, 99.999% pure. The arc furnace employed a water cooled non-consumable tungsten electrode and a copper hearth. The atmosphere was high purity argon, 99.995%, which was passed over heated zirconium to remove residual oxygen and nitrogen, and through a cold trap to condense moisture before being introduced into the furnace. During melting, the samples were inverted on the copper hearth and remelted at least four

times to achieve complete alloying between the V and Ga. There was, of course, a loss of Ga during melting through vaporization. The composition of the starting mixture of V and Ga was chosen so as to achieve a desired Ga content after melting and high-temperature homogenization. The nominal composition of the final product was then calculated on the assumption that the observed sample weight loss was due to the vaporization of Ga. This method of computing the nominal composition appears reasonable as evidenced by chemical analysis, which yields Ga contents differing by no more than a fraction of an atom percent from those computed.

Ingots prepared by the method described above have very high oxygen and nitrogen levels. In order to remove the oxygen and nitrogen, cerium, a rare-earth element, was added in some samples during arc-melting.

The samples investigated in this work had nominal compositions in atom percent, V-14~19 at.% Ga.

The arc-melting procedure was the same for the Nb-Al system as for the V-Ga system. No cerium was added to the Nb-Al system. The Nb-Al samples investigated had nominal compositions in atom percent. Nb-13~22 at.% Al.

2. Homogenization and Quenching

Both homogenization and quenching were accomplished in an Abar-type vacuum furnace. A schematic diagram, shown in Fig. IV.5, illustrates the essential parts of the furnace. Either tungsten or tantalum was used to construct the cylindrical-shape heating element. Temperatures at the center of the heating element were calibrated by using a W-Re thermocouple and an optical pyrometer. A tantalum rod with a hole in it was used as a heating objective. Since different metals have different coefficients of emissivity, it is necessary to use the hole as a black body. The W-Re

thermocouple was inserted into the hole of the Ta rod. The temperature readings were verified by an optical pyrometer which read temperatures from the hole of the Ta rod. Since the furnace was used either under vacuum or in the back-filled He condition, calibration was done for both cases and the results were plotted as power (P≡current times voltage) versus T^4 in Fig. IV.6.

For the V-Ga system, the homogenization treatment was done at 1600° C for 20 minutes and 1350° C for 15-30 minutes. For the Nb-Al system, the homogenization treatment was done at 1930° C for one hour.

Quenching was also performed inside the Abar furnace. For the V-Ga samples, the quenching could be achieved by simply dropping the samples on the copper plate which was located at the bottom of the furnace. For the Nb-Al samples the quenching rate even with the help of copper was not fast enough to prevent the precipitation of the A15 phase. It was necessary to quench the Nb-Al samples in a Ga-In bath in order to meet the cooling rate requirement[2]. In this work, however, a novel approach was used, i.e., an ice-brine quench. The brine solution was placed in a graphite crucible which was enclosed in a quartz tube with one end open to the furnace chamber (see Fig. IV.5). The whole thing was cooled down to 77° K by immersion in liquid N_2, and then inserted into the bottom of the furnace which was surrounded by liquid N_2. Due to the low vapor pressure of the solid brine at 77° K, it was possible to pump the furnace down to 10^{-5} Torr range within a short period of time. After the whole chamber was cleaned, the main valve was closed and back-filled with a high-purity He gas at a level of 250 Torr. Under these conditions, the temperature could be raised without fear of contaminating or oxidizing

the samples. Just before finishing the homogenization, the solid brine was melted by an outside heater and the samples were then dropped in the ice-brine solution. This method provided the quenching rate necessary to retain the high-temperature BCC phase.

3. Mechanical Deformation

Due to the high-temperature homogenization, the as-quenched samples have a very large grain size. Since the ductile-to-brittle transition temperature of the BCC alloy is known to increase with grain size, the samples are therefore, in general, brittle at room temperature. However, the samples could be deformed at somewhat elevated temperatures. In order to prevent oxidation, tested samples were inserted into stainless steel tubes, whose ends were sealed by welding.

For V-Ga samples, the deformation temperatures were in the range of 600° C to 800° C, while for the Nb-Al samples, they were between 300~400° C.

In this work, flat rolling, form rolling, and swaging were used to deform the specimens.

4. Aging Treatments

For both the V-Ga and Nb-Al samples, the aging treatments at temperatures between 600-1000° C were carried out by wrapping the samples in Ta foils and sealing them in quartz tubes under an argon atmosphere. The purpose of wrapping the samples in Ta foils is to prevent the chemical interaction between the samples and the quartz; for example, this had led to an erroneous result in the V-Ga system[10] as indicated by van Vucht et al.[2].

5. Critical Transition Temperature (T_c) Measurements

The critical temperature is usually determined either by directly measuring the electrical resistance as a function of temperature or by an inductive method. This latter method uses the change in the induction or frequency of a coil with the specimen as a core at the instant of normal-superconducting transition (see Fig. IV.7). In general, the T_c's measured by the resistive method are higher than those measured by the inductive method.

In measuring T_c by the resistive method, one uses a sample with four-point contacts (see Fig. IV.8), two of which act as current leads and the other two as voltage leads. By using the inductive method, the relative proportions of normal and superconducting phases in the sample may be determined. In principle, the method relies on the fact that the self-inductance of a coil wound around the sample varies in direct proportion to the sample's magnetic permeability, which is equal to the induction B divided by the external field H. The inductive method has the advantage that it requires no direct electrical contact with the sample and thus shapes of the samples could be irregular.

The inductive method was used in detecting the normal-superconducting transitions of the samples. Temperatures were measured with a calibrated germanium (Ge) resistance thermometer.

6. Critical Current Density $J_c(H)$ Measurements

The critical current is a very important parameter since it determines the possible practical use of materials with high values of T_c and H_{c2}. The critical currents were measured by a standard four-probe technique under transverse applied magnetic fields (see Fig. IV.8). Most of the

measurements were done at the Francis Bitter National Magnet Laboratory at the Massachusetts Institute of Technology. A few measurements were performed at the Accelerator and Fusion Research Division of the Lawrence Berkeley Laboratory at the University of California, Berkeley. After the sample was cooled to a specific temperature (4.2 K in this work) and its orientation relative to the applied field was established (90° in this work), one of the following procedures was used:

a. The field was made equal to a specific value and the current was increased until a potential drop appeared at the voltage leads.

b. The current was made equal to a constant value, and the field was increased until a potential drop appeared at the voltage leads.

The tested samples, V-Ga and Nb-Al systems, were covered with a thin layer of Cu (~ a few hundred Å's) using a sputtering technique. An indium (80)-silver(5)-lead(15) alloy was used to solder the current leads and the ends of the specimen. The voltage leads soldering was done by a silver paste or an In-Ag-Pb alloy. The intrinsic characteristic of the V-I curve is shown in Fig. IV.9(a). If, however, the voltage leads are close to the current leads (see Fig. IV.8), the resistivity of the current leads, in addition to that of the specimen can be detected, thus leading to a current transfer characteristic of the V-I curve shown in Fig. IV.9(b).

Critical current I_c is defined here as the current at which the potential drop across the voltage leads (spaced 5 mm apart) exceeds 1 μV. The overall critical current density J_c was then determined by calculating I_c/A where A is the total cross-sectional area of the specimen consisting of both superconducting and non-superconducting phases.

7. Optical Microscopy

Specimens for optical microscopy were cut from arc-cast, homogenized, quenched, deformed, and aged samples. The specimens were mounted either in Koldmount or in Bakelite. After grinding with successive emery papers up to 600 grade under water-flood cooling, polishing was done on 6 μm and then finally 1 μm diamond paste on a rotary wheel. The V-Ga samples were etched with a solution of $5HNO_3$, 2HF and $25H_2O$ while the Nb-Al samples were etched with another solution of $1HNO_3$, 1HF, and $5H_2O$. The microstructures were studied under a Carl Zeiss Universal Photomicroscopy Ultraphoto II.

8. Scanning Electron Microscopy (SEM)

Fracture surfaces of tested specimens were examined with an AMR 1000 scanning electron microscopy operated at 20 KV. Because of the large field depth of the SEM, this instrument is excellent for studying the fracture mode.

9. Transmission Electron Microscopy (TEM)

Specimens for transmission electron microscopy were obtained by very carefully grinding the tested samples down to the thickness of 0.2 mm, and then spark-cutting 3 mm diameter thin discs using an EDM machine. The thin discs were ground and polished down to a thickness of 0.1 mm or below by using emery papers of 600 grade. Ion milling was found to be the most effective way to produce sufficiently uniform thin areas and a Philips EM301 electron microscope, operating at 100 KV voltage, was used for thin foil examination. The identification of the A15 precipitate was carried out by using selected area diffraction (SAD) and dark field (DF) imaging techniques.

10. X-Ray Diffraction

For all diffraction measurements, the tested specimens were either in a powder form or in a chunk form with one polished flat surface. Most of the measurements were performed using a diffractometer, while a few of them were done by the Dehye-Sherrer method. Cu or Fe radiation was used in this work.

IV. REFERENCES

1. B. N. Das, J. E. Cox, R. W. Huber, and R. A. Meussner, Met. Trans. 8A, 541 (1977).

2. J. H. N. van Vucht, H. A. C. M. Bruning, H. C. Donkersloot, and A. H. Gomes de Mesquita, Philips Res. Rep. 19, 407 (1964).

3. G. W. Webb, Appl. Phys. Lett. 32, 773 (1978).

4. V. M. Pan and V. I. Latysheva, Metallofizika 33, 38 (1971).

5. C. E. Lundin and A. S. Yamamoto, Trans. AIME 236, 860 (1966).

6. S. Moehlecke, Ph.D. Thesis, Universidad Estudial de Campinas, Brazil (1977).

7. V. M. Pan, Yu. I. Beletskiy, V. S. Flis, S. A. Firstov, and G. F. Sarzhan, Fiz. metal. metalloved., 40, 706 (1980).

8. J. A. Woolam, S. A. Alterovitz, E. Haugland, and G. W. Webb, Appl. Phys. Lett. 36, 706 (1980).

9. V. M. Pan, V. I. Latysheva, Ye. N. Khusid, V. N. Minakov, and Ye. V. Turtsevich, Fiz. metal. metalloved., 40, 512 (1975).

10. J. W. Wernick, F. J. Morin, S. L. Hsu, D. Dorsi, J. P. Maisa, and J. E. Kunzler, High magnetic fields, ed. by Kolm, Lax, Bitter and Miles, John Wiley and Sons, New York, 609 (1962).

FIGURE CAPTIONS

Fig. IV-1. Direct "solid-state precipitation" process for making high-field hard Type II superconducting wire.

Fig. IV-2. The relevant portion of the V-Ga equilibrium phase diagram as reported by van Vucht et al. (see Ref. 2), dot-dash lines and modified by Das et al. (see Ref. 1), solid lines.

Fig. IV-3. The Nb-Al equilibrium phase diagram by Pan et al.[4],

Fig. IV-4. The Nb-Al equilibrium phase diagram by Lundin et al.[5].

Fig. IV-5. Schematic diagram of Abar furnace:

1. back filling port,
2. tantalum wire,
3. electrical leads,
4. heating element (tungsten or tantalum),
5. specimen
6. radiation shields
7. water cooled wall
8. vacuum connection
9. quartz tube
10. graphite crucible
11. iced brine or ice-brine solution

Fig. IV-6. The temperature-power calibration chart for the Abar furnace.

Fig. IV-7. The tested sample surrounded by a coil in the inductive-T_c measurement.

Fig. IV-8. The standard four-probe technique which can be used for measuring the resistive-T_c or the $J_c(H)$ data.

Fig. IV-9(a) Schematic representation of the voltage-current characteristics of the superconducting to normal state transition in two regions: (a) far from the current contact where the tested sample undergoes the usual resistive transition as the current approaches a critical value and

Fig. IV-9(b) (b) near the current contact where the characteristic exhibits a linear region at low currents.

THE CONTROLLED PRECIPITATION PROCESS FOR MAKING HIGH-FIELD HARD TYPE II SUPERCONDUCTING WIRE

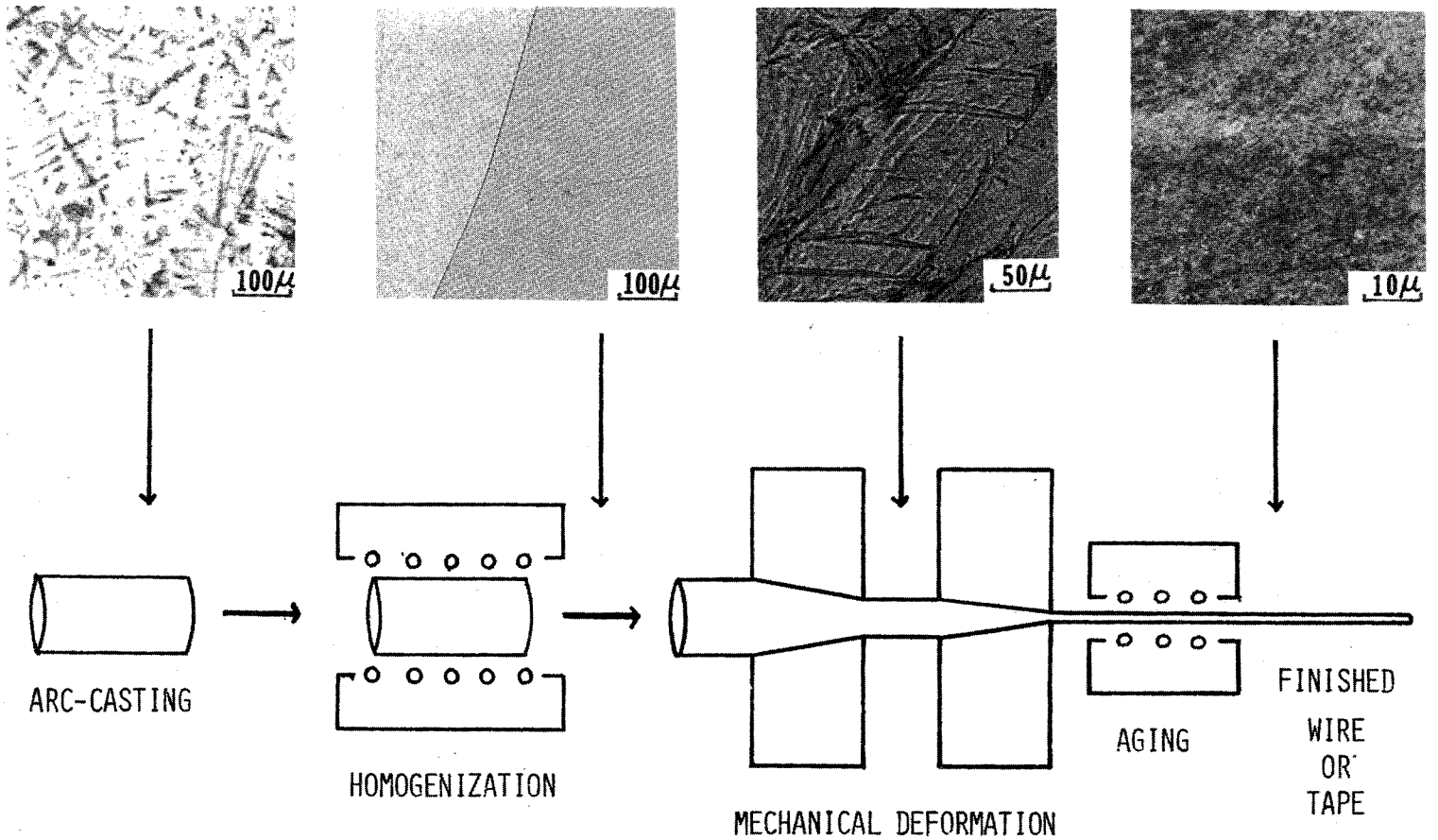

XBB 801-1144

Fig. IV-1

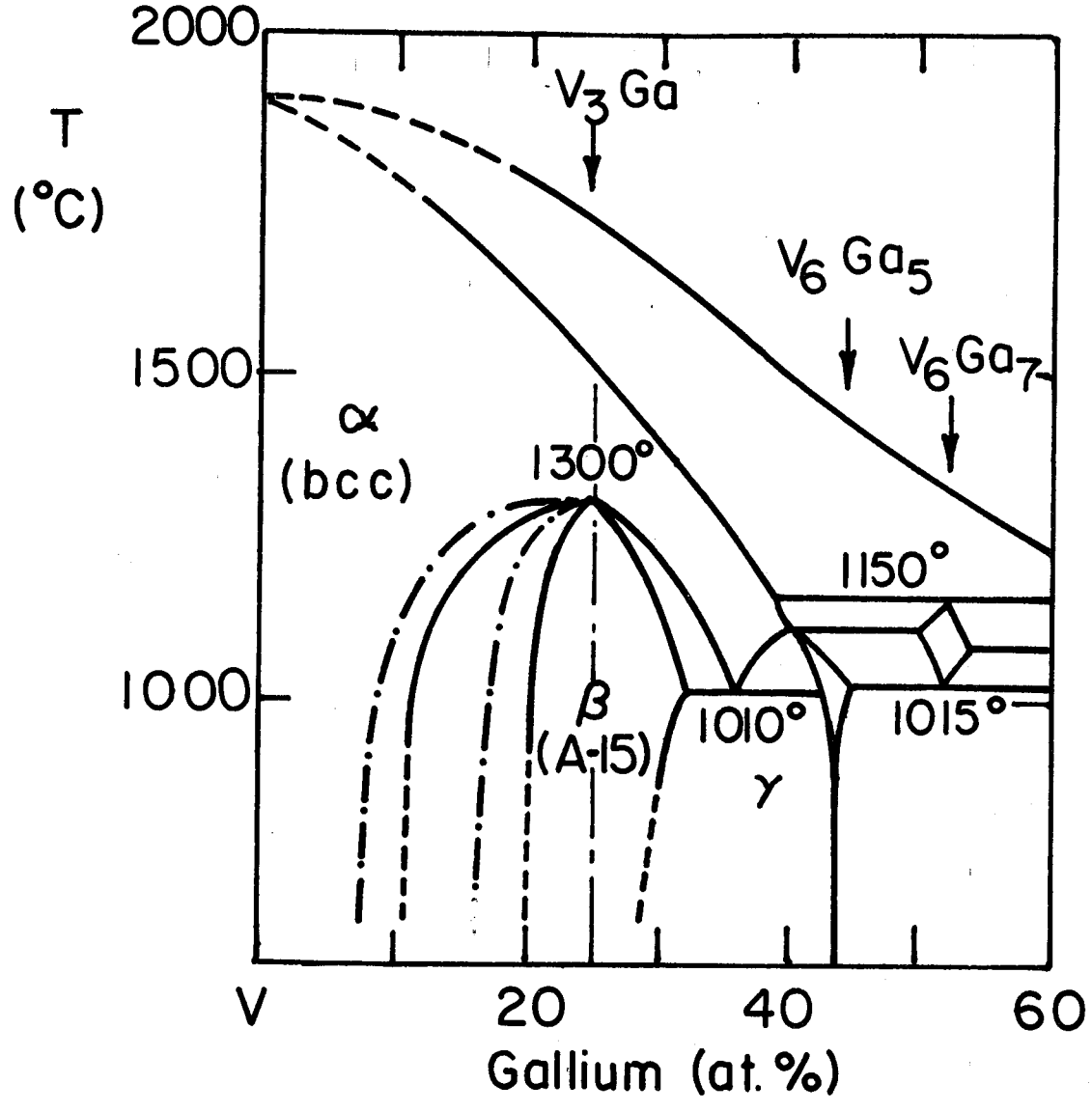

XBL 793-5872

Fig. IV-2

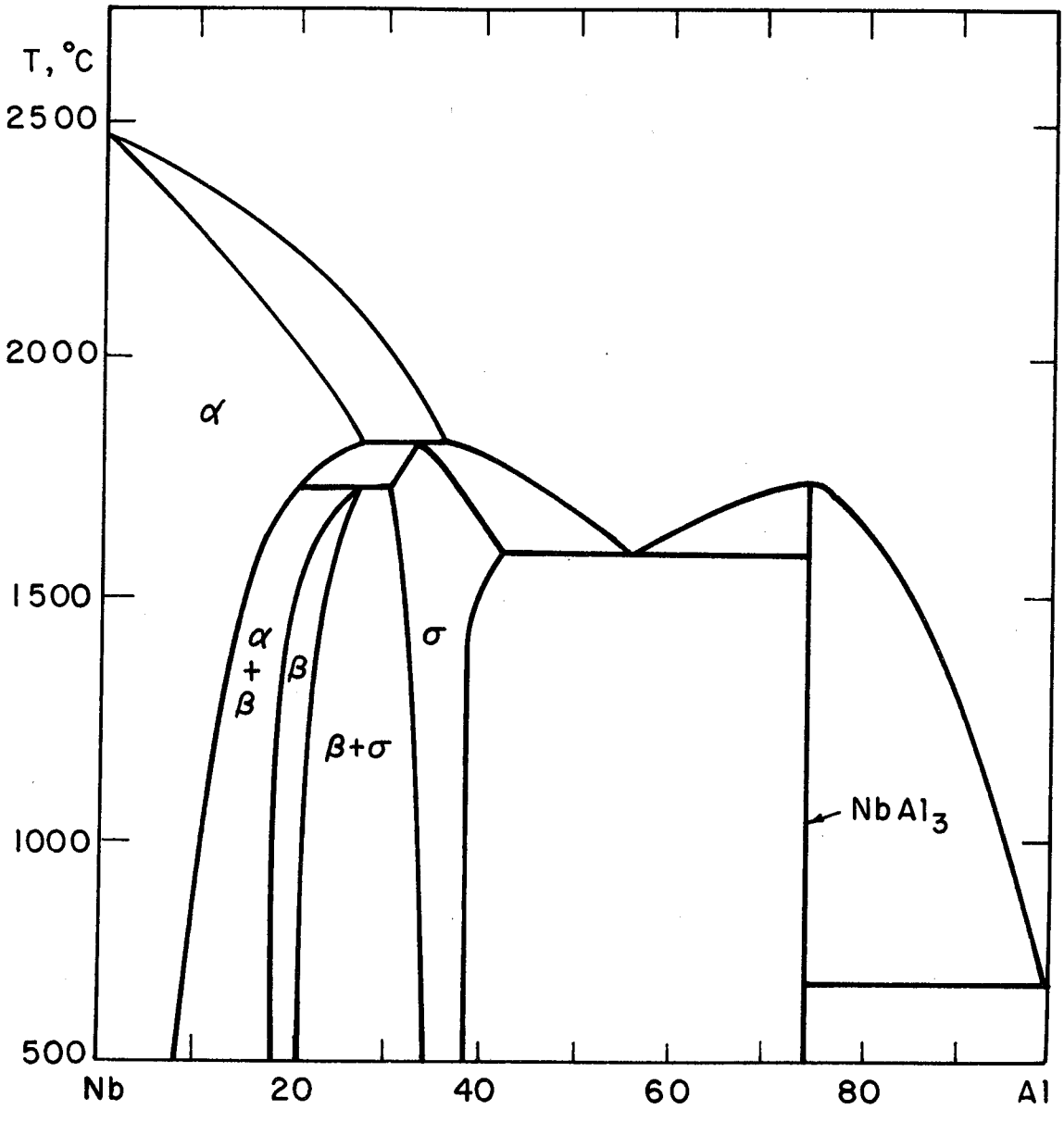
T, °C
2500
2000
1500
1000
500
Nb
20
40
60
80
Al
α
α + β
β
β+σ
σ
NbAl3
XBL 7810-6018

Fig. IV-3

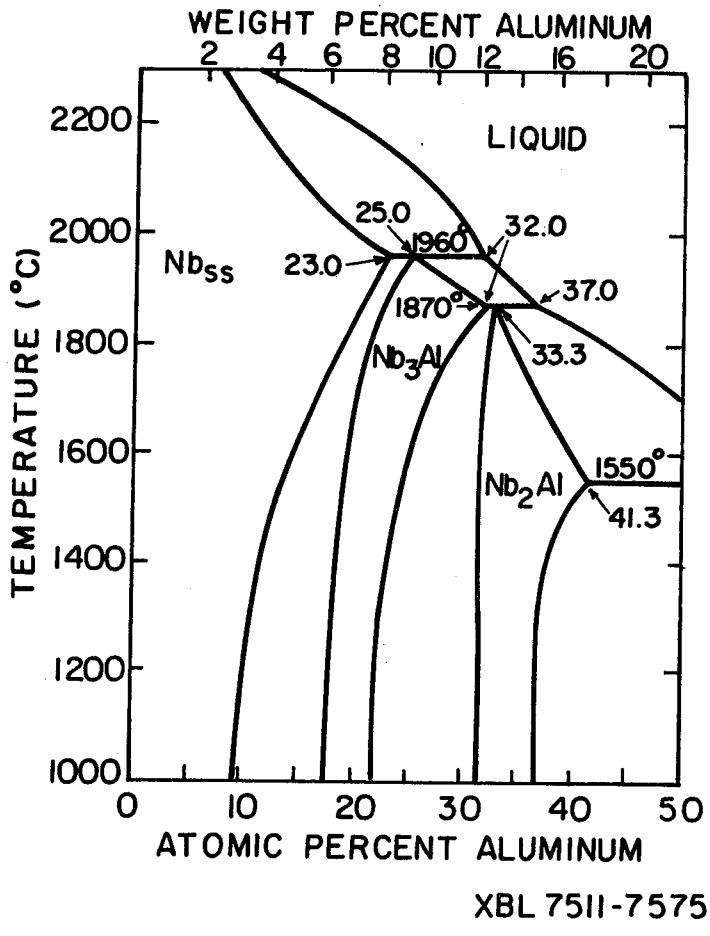
WEIGHT PERCENT ALUMINUM
2
4
6
8
10
12
16
20
2200
2000
1800
1600
1400
1200
1000
TEMPERATURE (°C)
LIQUID
25.0
1960°
32.0
Nbss
23.0
37.0
1870°
Nb3Al
33.3
1550°
Nb2Al
41.3
0
10
20
30
40
50
ATOMIC PERCENT ALUMINUM
XBL 7511-7575

Fig. IV-4

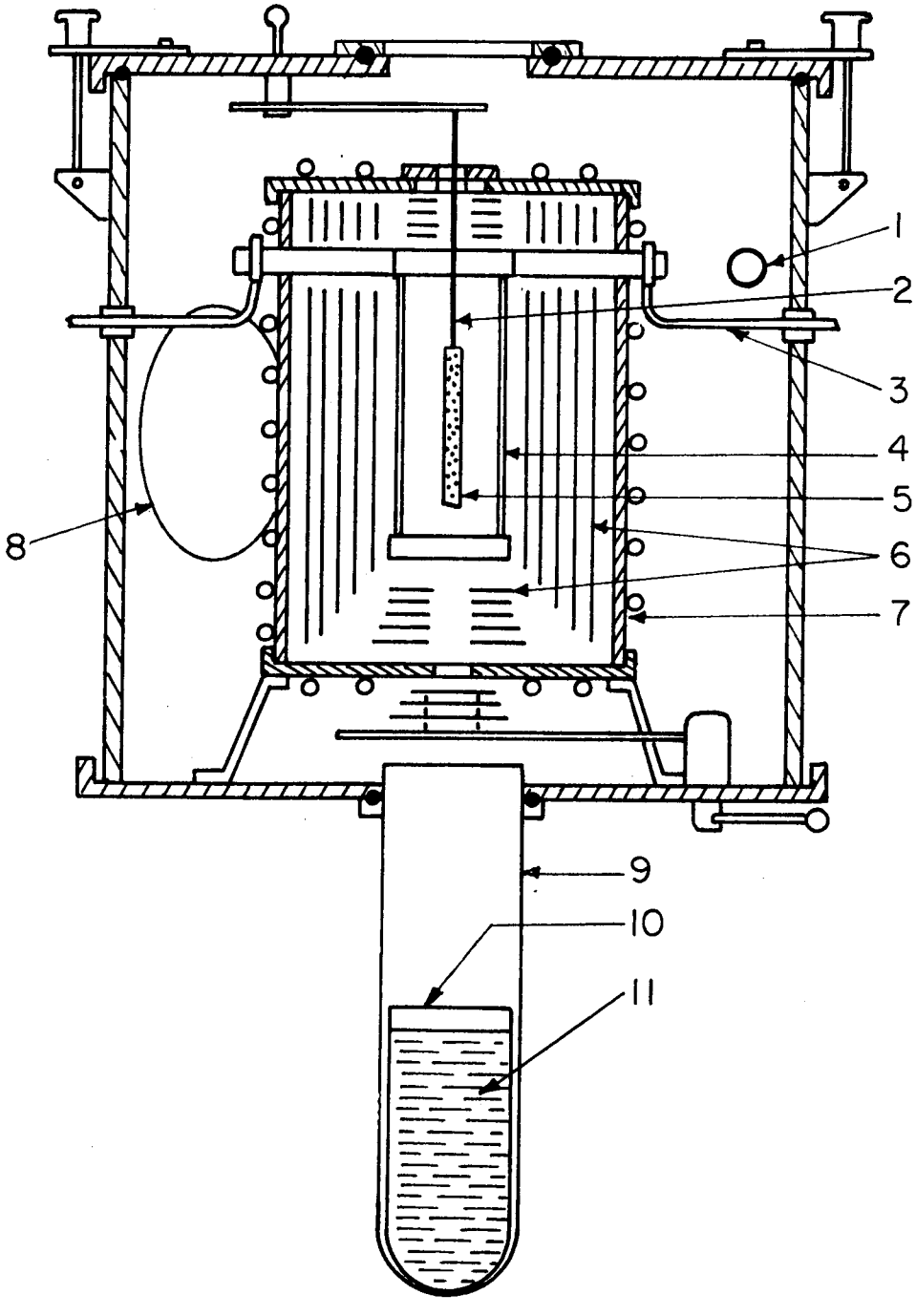

Fig. IV-5

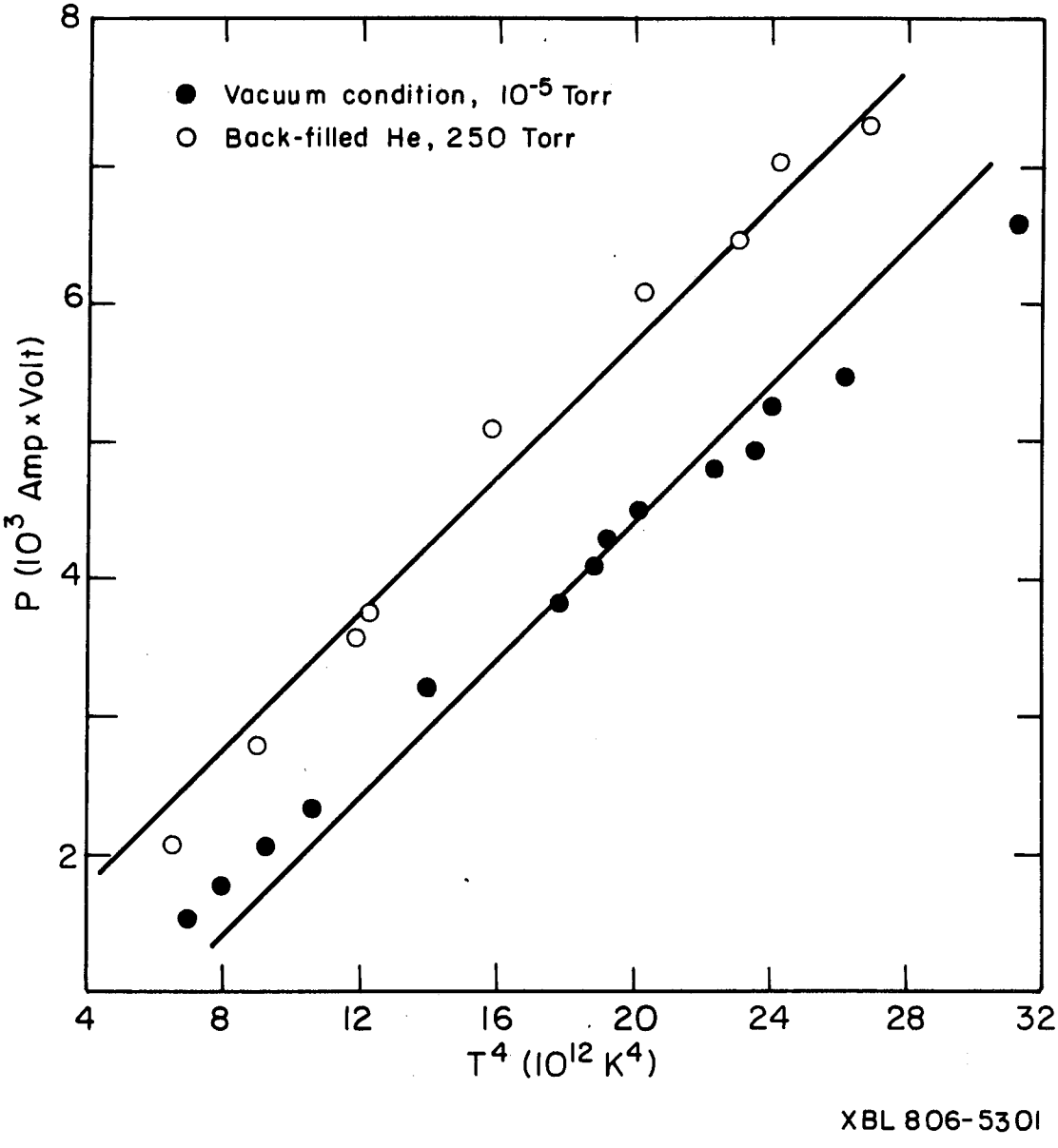
Vacuum condition, 10^{-5} Torr
Back-filled He, 250 Torr
P (10^3 Amp x Volt)
T^4 (10^{12} K^4)
8
6
4
2
4
8
12
16
20
24
28
32
XBL 806-5301

Fig. IV-6

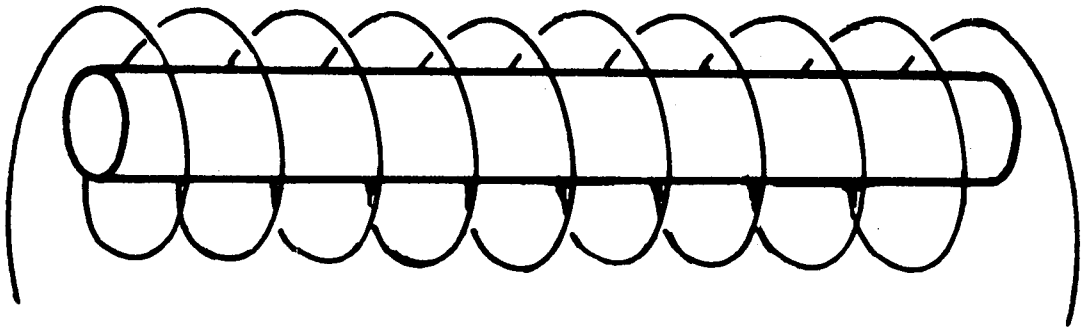

XBL806-5299

Fig. IV-7

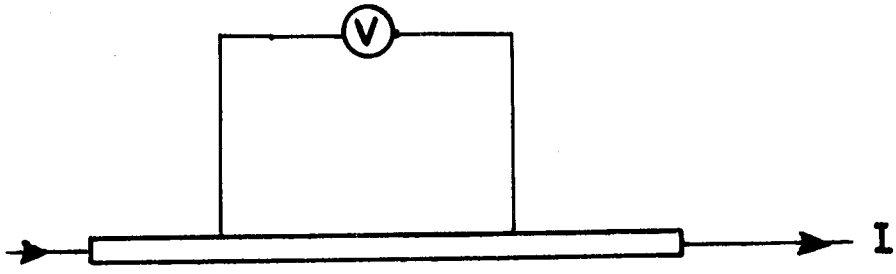

XBL 806-5300

Fig. IV-8

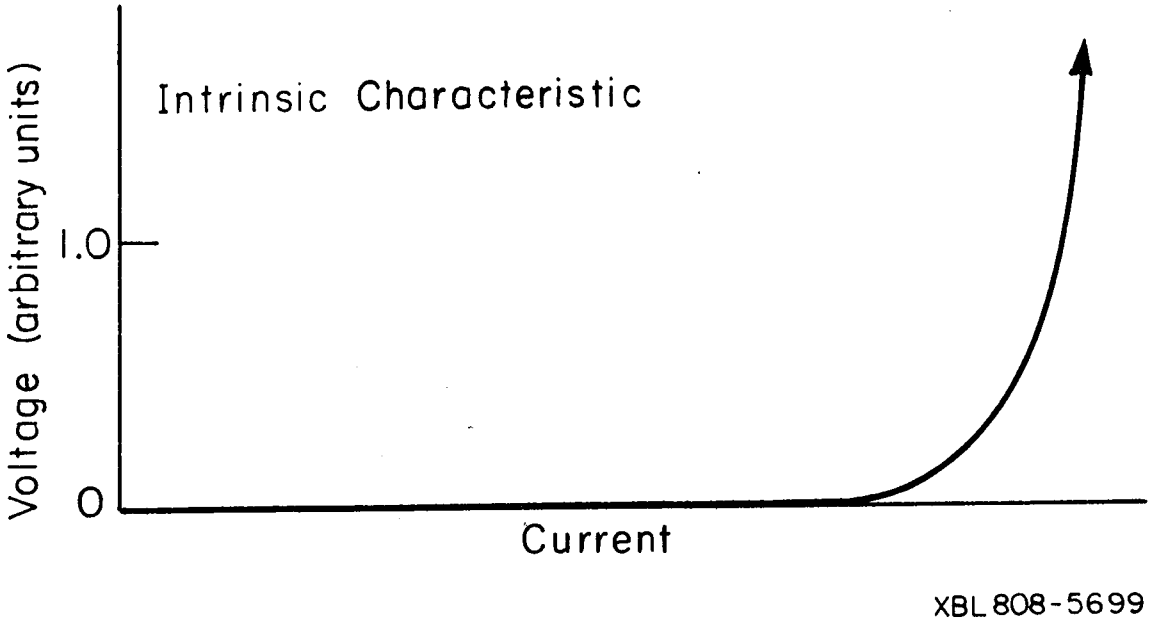
Intrinsic Characteristic
Voltage (arbitrary units)
1.0
0
Current
XBL 808-5699

Fig. IV-9(a)

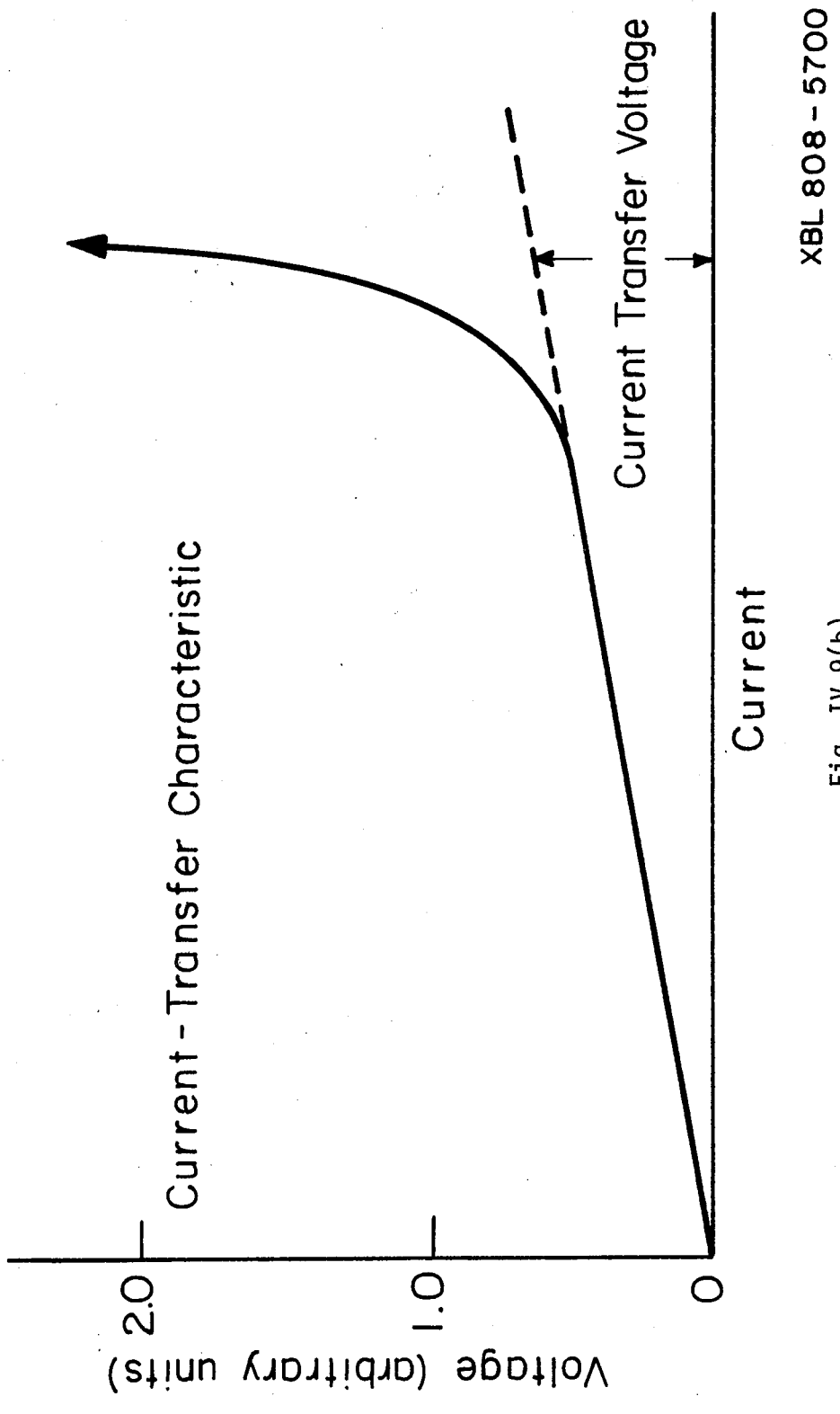
Current-Transfer Characteristic
Current Transfer Voltage
Current
Voltage (arbitrary units)
2.0
1.0
0
XBL 808-5700

Fig. IV-9(b)

V. A15 SUPERCONDUCTORS THROUGH DIRECT "SOLID-STATE" PRECIPITATION: V_3Ga

A. Introduction

V_3Ga, a stable first-class A15 compound, is important both as a practical superconductor[1] and as a research material[2,3] for studying the compositional and structural effects on the superconducting properties. The advantages of the V-Ga system in investigating these effects are derived from the unique features of the phase relations involving A15 V_3Ga as shown in Fig. IV-2. The broad compositional range of A15 phase spans the stoichiometric V_3Ga composition. This phenomenon makes it easier in studying the correlations between the superconducting properties and the compositional changes of the A15 phase. Also, the A15 phase is formed by a transformation from a BCC phase, rather than a peritectic reaction common to many other systems forming A15 phases[4]. This unique nature makes the V-Ga system a good candidate for studying a fundamental BCC-A15 phase transformation.

As a practical material, V_3Ga, together with Nb_3Sn, has been fabricated through the "Bronze" process[1] and the "In-Situ" (Tsuei) process[5]. Although its T_c is lower than that of Nb_3Sn, the superior current-carrying capacities at high fields (> 100KG), and the excellent mechanical properties make V_3Ga extremely attractive[1,6].

As mentioned in the previous chapter, a monolithic "solid-state precipitation" process is the metallurgically simplest method of wire or tape manufacturing. In this chapter, we will demonstrate that this process is suitable for producing tapes or wires which contain the multifilamentary V_3Ga A15-phase in the relatively ductile BCC phase. The final products have high critical transition temperatures and promising

critical current densities. A systematic study of the correlations among the metallurgical processing, the microstructures, the critical transition temperatures, and the critical current densities will be presented. The explanation for the exceptionally high T_c will also be given.

Samples with compositions ranging from V-14 at.% Ga to V-19 at.% Ga were chosen. They were arc-melted and cast as 12 mm-diameter rods. They were then homogenized at high temperatures and quenched to room temperature to retain the BCC phase. The as-quenched materials could be deformed at some intermediate temperature and the superconducting A15 phases were precipitated out inside the BCC phase after final heat treatments.

The solid-state precipitation process and the experimental procedure have been discussed in Chapter IV. Therefore, they are omitted here.

B. Results and Discussions

1. Casting

After arc-casting, the microstructures of all rod-shaped samples display the evidence of chemical segregation (see Fig. V-1). The segregation arises during the solidification process, which, as indicated by the equilibrium V-Ga phase diagram of Fig. IV-2, proceeds by the formation of the BCC-phase dendrites of lower Ga content than that of the liquid. As the temperature falls, the dendrites grow toward the central part of the rod by creating more solid of higher Ga content. For compositions used here, V-14~19 at.% Ga, the solidification process produces a single-phase (BCC) material but with a Ga-content gradient. The materials with a single BCC-phase have been confirmed by x-ray diffraction analysis on both chunk and powder forms of the tested samples.

However, as indicated by Das et al.[3], for the samples of higher Ga content (22 at.% Ga or more), the A15 phase could appear during the casting.

The casting was done by putting the melted materials on the copper hearth below which the cooling water was surrounding and circulating. The casting technique of being able to suppress the A15 precipitation is similar to the quenching technique described later.

High interstitial contents of oxygen and nitrogen after arc-casting had often been encountered in the early stages of this work (see Table V-1) when only vanadium and gallium were melted together. The samples with high oxygen and nitrogen contents could not be deformed more than 75% reduction in thickness. However, for the samples containing low oxygen and nitrogen, the thickness-reduction could be 90% or more.

In order to consistently obtain samples with low interstitial impurities using the arc-melting method, one phase of this project has been oriented to find the third element addition for removing oxygen and nitrogen from the cast sample. Among the third elements added to the V-Ga melt, small amounts of cerium were found to be very effective in reducing the oxygen and nitrogen contents.

During the melting, cerium, which has a stronger affinity for oxygen than vanadium, reacted with the oxygen in the sample and formed cerium oxides. Since the melting points for the cerium oxides could be as high as 2400°C, the oxides could be in a solid form during melting. The oxides floated on the surface of the melted material, and became "slags" which did not have strong bonding with the specimens and could be easily peeled off. They were verified by the preliminary data of x-ray

diffraction to be CeO_2. After the cerium oxide was removed from the outer surface, the samples were examined by a chemical analysis. As shown in Table V-2, it was found that negligible cerium elements were left inside the samples after melting. This indicated that almost all the cerium reacted with the oxygen, and consequently the oxide thus formed was driven out of the specimen. Therefore, it might be concluded that the cerium strongly reacted with the oxygen, thus reducing the oxygen content in the V/Ga sample, and formed the cerium oxide which were solid during the melting and were eventually separated from the sample.

However, it should be noted here that from the preliminary results of x-ray diffraction, cerium nitride has not been identified from the "slags". Thus, the effect on reducing nitrogen content by the cerium-addition is still not clear. The chemical analysis on the nitrogen content of the "slags" can be used to understand the nitrogen-reducing effects.

With the cerium addition, samples consistently could be deformed more than 95% without creating cracks. It should also be mentioned that the arc-cast microstructures (Fig. V-2) of the cerium-added samples were somewhat different from those of the pure binary V-Ga samples. The chemical segregations and dendritic patterns of the Ce-added samples are not as profound as those of the samples without Ce. From Fig. V-2, it is clear that some Ce-related second phases appeared. The effect of cerium on changing the cast microstructures is still not known at this stage. However, it indicates that with a suitable element addition, the

cast material may be in such a form that they can be deformed without any further heat treatments such as homogenization and quenching.

As a summary of this section, we would like to indicate that for the compositional range, V-14~19 at.% Ga, no surface defects or internal cracks have ever been found in the cast materials with or without Ce addition. However, the cast samples with higher Ga contents (22 at.% Ga or more), which were encountered in the other phase of this project, showed internal cracks and some shrinkage porosities which formed during the cooling.

2. Homogenization and Quenching

Homogenization at 1600°C for 20 minutes and 1350°C for 15-30 minutes was found to be adequate to eliminate the chemical segregation and the dendritic pattern of the cast structure. In order to prevent the severe evaporation of Ga during the high temperature heating, homogenization was performed in the Abar type furnace (see Fig. IV-5) with back-filled helium gas. In order to prevent the sample from being oxidized, a short-time heat treatment was preferable. Therefore, a very high temperature, e.g., 1600°C, was chosen to eliminate segregation in a short time. The reason for using lower second-stage temperature homogenization such as 1350°C was to reduce the thermal stress caused by the quenching step.

Quenching was carried out by dropping the sample either in an ice-brine solution or on a copper plate held at room temperature. The average grain size of the homogenized and quenched sample was about 1000 μm. No quench-cracking was observed during quenching. Moreover, both the optical microscopy and the x-ray diffraction data indicate that the precipitation of the A15 phase was suppressed during the quench.

The suppression of the A15 precipitation was further confirmed by T_c measurements, which showed no T_c above 5K. The homogenization plus an ice-brine-quench or a Cu-plate-cooling hence seems successful in avoiding both quench-cracking and precipitation of the A15 phase.

To form a wire or tape from V/Ga solid solution, it is necessary to prevent spontaneous cracking of the V/Ga ingot during initial quenching, that is, to suppress quench-cracking.

In the case of the V/Ga solid solution, there are three potential sources of quench-cracking which must be guarded against. The first is the formation of brittle interdendritic compounds during the solidification, in this case Ga-rich intermetallic phases. The second is the segregation of embrittling species to grain boundaries during homogenization; and the third is the precipitation of the A15 phase along grain boundaries during quenching.

As mentioned in the previous section, for the compositions (V-14~19 at.% Ga) and the casting technique employed, the brittle interdendritic compounds such as V_3Ga, V_6Ga_5, etc. do not form during the solidification. Thus, the first potential source of quench-cracking is eliminated.

To guard against the presence of crack-inducing interdendritic compounds, the alloys are homogenized within the solid solution field in the phase diagram for an extended period; no grain boundary segregation appears during the homogenization treatment. Following homogenization, a normal water quench or a fast cooling on the copper plate appears sufficient to suppress precipitation of the A15 phase to any significant

extent. With the treatments mentioned above no quench-cracking is encountered.

3. Mechanical Deformation

In the homogenized and quenched condition the V/Ga samples were brittle, and fractured catastrophically on deformation at room temperature. A scanning electron fractographic analysis of broken sample surfaces (Fig. V-3) reveals that the fracture mode is almost entirely quasi-cleavage, indicating that the brittleness of these samples is due to the normal low temperature brittleness of the BCC matrix structure. The ductile-to-brittle transition temperature (DBTT) of BCC alloys is known to increase with grain size. Optical microscopy reveals that during the homogenization treatment substantial grain growth had occurred, giving a typical sample grain size of ~1000 μm. It should be noted that some other factors including the alloying element, e.g., Ga, and the interstitial impurities, e.g., oxygen and nitrogen are also very important in determining the DBTT's.

To avoid low temperature brittleness, the samples were deformed at the intermediate temperatures 600~800°C. The total reduction in thickness accomplished during the warm rolling was ~75% or more, depending on the interstitial impurity levels of the tested samples (see Tables V-1 and V-2).

A measurement of the critical transition temperature of the specimen after 800°C deformation gave T_c ~ 9 - 10K. The existence of the A15 phase could not be detected by x-ray diffraction. This indicated that the amount of the A15 precipitate must be at the level of 1% or less. Inductive measurement of T_c's is known to be more sensitive than x-ray

diffraction in finding a minute quantity of superconducting A15 phase. The study of TEM also confirmed this argument. In searching for the thin area of the specimens after deformation, only the BCC phase was displayed by the selected-area-diffraction (SAD) technique. Fig. V-4 represents the typical region of the as-deformed specimens. It shows a high density of dislocations of the BCC phase, but no evidence of A15 precipitates. Since the existence of the A15 phase was strongly indicated by the inductive T_c measurement, an extensive selection of TEM specimens and a systematic study using high resolution TEM must be able to reveal the location of the small amount of A15 precipitates which are believed to be quite inhomogeneously distributed. Nevertheless, when the deformation temperatures were lower such as 600-650°C, no T_c above 5K could be detected by the inductive method. Fig. V-5 is the optical micrograph of the specimen deformed at 650°C, which shows that no A15 precipitates appeared. This is in contrast to a slight precipitation of the A15 phase for samples deformed at 800°C.

With the samples of low oxygen and nitrogen content, we recently succeeded in deforming the V/Ga alloys at a lower temperature of ~500°C. The lowest oxygen and nitrogen levels of the current samples are around 1000 ppm. It is believed that the deformation temperature could be made even lower if the oxygen and nitrogen contents could be lowered down to 100 ppm. With the lower deformation temperatures, the wire manufacturing practice could be easier, which is very important for the further development of solid-state precipitation processes.

4. Precipitation of the A15 Phase

Following warm deformation the samples were aged to precipitate the A15 phase. The aging treatments were conducted over a range of temperatures from 600°C to 1000°C and for a number of aging times. The critical transition temperatures of the tested specimens were then measured as a function of aging temperature and time. In this section, we are mainly concerned with the data related to optical microscopy and transmission electron microscopy. The results of T_c's and $J_c(H)$'s are given in the next two sections.

A systematic study of optical microscopic examination on the evolution of the microstructures of the deformed and aged samples as a function of aging temperature and time are shown in Figs. V-6~V-9. The composition of the tested specimens was V-17.5 at.% Ga, the deformation temperatures were around 750~800°C, and the reduction in thickness was 75%. From these curves, it is clear that the kinetics of the A15-precipitate formation varies dramatically for different aging temperatures, and the distribution of A15 precipitates is quite inhomogeneous.

Under the condition of 75% thickness reduction, 600°C is probably too low a temperature to obtain a reasonably good kinetic rate of the A15 phase formation. For the samples aged for 10 days, there are still not many A15 precipitates besides those appearing during the deformation at the intermediate temperatures. The optical microscopy of the tested samples aged at 700°C for 10 hours is similar to one aged at 600°C for 10 days. Transmission electron microscopy was used to reveal a more detailed microstructure of the samples aged at 700°C for 10 hours. Due to the severe inhomogeneity of the distribution of A15 precipitates, it was

impossible to find evidence of A15 precipitates. Fig. V-10 is the transmission electron micrograph of the typical region from the thin area of the tested specimens. It shows a dislocation cell structure of the BCC phase. The inability to find the A15 precipitates was also caused by the small amount of precipitates, since the examined condition was an early stage of precipitation.

However, for a longer aging treatment, 700°C for 3 days (see Fig. V-7), it is clear that more A15 precipitates nucleate, grow and form a somewhat continuous and/or semicontinuous network. Figs. V-11~13 are the TEM pictures of the tested samples at this stage. From Figs. V-11~12, it is clear that the A15 precipitates are in an elongated rod-like form with a width around 2000Å and a length of ~1 μm. They are embedded in the BCC matrix and connected to each other like a chain. The separation between chains is around 1000Å. The size of the region containing the cluster of the A15 precipitates is around 5 μm. The continuity of the A15 precipitates and the inhomogeneity of their distribution observed from TEM can be used to explain and verify the observation from optical microscopy.

From the TEM data, it is known that A15 particles are at least connected with each other locally. The important point is whether there is a continuity between clusters such that a continuous network of the superconducting A15 phase is established. This question, however, cannot be fully understood by TEM only. The $J_c(H)$ data may help to clarify this point. The phenomenon will be further discussed in the following sections.

For a much longer heat treatment of 10 days at 700°C, the precipitation of the A15 phase tends to a completion, i.e., the A15 precipitates appear almost everywhere. This kind of A15-precipitation sequence is also observed in the samples aged at 800°C with a different kinetic rate; 3 days at 800°C is long enough to bring the completion of the A15 precipitation. A longer heat treatment will lead to the coarsening of the precipitates.

The optical microscopy of samples aged at 1000°C is displayed in Fig. V-9. It is clear that 0.5 hour aging is enough for the completion of the precipitation and 72 hours aging can lead to a coarsening, thus making discrete A15 particles. A larger magnification of the optical microscopy for the specimens aged at 1000°C is shown in Fig. V-14. From the optical pictures, it can be speculated that the A15 particles are in an elongated form, which confirms the TEM observation shown in Figs. V-11~12. Moreover, for the 10 hours aging, the A15 particles seem to be continuous or semicontinuous while for the 72 hours aging, they coarsen and become discrete.

Based on the TEM and optical microscopy data, an explanation for the nucleation and growth of the A15 precipitates is proposed and shown at the bottom of Fig. V-14. Since there exists a rather large lattice mismatch between the A15 and the parent V/Ga structures, the A15 precipitates should nucleate preferentially along defects within the deformed matrix phase. The initial nucleus is a small elongated rod-like particle of V_3Ga A15 phase which grows into a deformed and supersaturated BCC solid solution. As it grows, it removes gallium atoms from the BCC phase on either side of it. Due to the depletion of Ga atoms surrounding the

A15 particles and the slow diffusion rate of Ga atoms, the next A15 particle will most likely nucleate and grow on the top of or in parallel to the existing one, but at a distance from it. This feature can be seen in Figs. V-11, 12 and 14.

It should be noted that the size and morphology of the A15 precipitates depend on the aging treatment and the prior deformation. This dependence is due in part to the interaction between the precipitation process and the recovery of the deformation-induced defects. As indicated in Figs. V-11 and 12, under 75% prior deformation and three days aging at 700°C, the size of the A15 precipitates is somewhat large; they are 2000Å in width and 1 μm in length. This large grain size of A15 particles probably causes the low $J_c(H)$, which we will discuss in section 6 of this chapter. From the characteristic of the voltage-current curves when measuring $J_c(H)$ data, it is also found that there is a strong internal residual resistance in the tested specimen. This indicates that the A15 precipitates may not be connected with each other and the normal conducting regions between the superconducting precipitates are larger than the "proximity" limit such that the internal resistivity appears[8].

However, for the tested samples under 90% or more prior deformation and some appropriate aging treatment, the $J_c(H)$-values are much higher and no appreciable resistivity was detected. It may be concluded that under 90% or more prior deformation the size of the A15 precipitates is smaller, and the superconducting regions are much closer or even connected with each other. A systematic examination of the consequences of this treatment is now in progress.

5. Critical Transition Temperature (T_c)

For the samples deformed at 800°C, the onset critical transition temperature is plotted as a function of aging temperature and time for the V-18.5 at.% Ga samples in Fig. V-15, for the V-17.5 at.% Ga samples in Fig. V-16, and for the V-14.5 at.% Ga samples in Fig. V-17. For both V-17.5 at.% Ga and V-18.5 at.% Ga it proved possible to obtain T_c in excess of 14K by aging the deformed samples at temperatures between 600°C and 700°C. The maximum T_c measured is ~14.8K, a value which compares favorably to the 14.5~15.8K[3,9,10] which are believed to be the maximum attainable critical temperatures for the compositions near stoichiometric V_3Ga.

For aging temperatures of 800°C or below there is an apparent maximum in the curve of critical temperature versus aging time. The aging time required to reach this maximum increases dramatically as the aging temperature is lowered below 750°C. However, in the case of the 18.5 at.% Ga samples the peak critical temperature is reached after only three hours aging at 750°C. With aging temperatures of 800°C to 1000°C the critical temperatures decrease to a value of 10K or below when the aging time is made long.

For the V-14.5 at.% Ga samples, similar phenomena were observed but the T_c's measured were generally lower.

It has been shown that in the V-Ga system T_c is strongly dependent on the composition of Ga in the A15 phase. van Vucht et al.[10] reported a maximum value of 14.3K at the stoichiometric composition and a rapid decrease in T_c as the composition changed to higher or lower Ga values. Their data was comparable with Wernick et al.'s curve[11] of the dependence

of T_c on the Ga concentration, except the maximum T_c of the latter was higher. van Vucht et al.[10] explained that for Wenick et al.'s experiments[6] the higher T_c was caused by another A15 compound, V_3Si, which was on the surface of the specimen. This was encountered during heat treating V_3Ga specimen in the glass (containing SiO_2) tube without wrapping the tested specimen in some protected metal sheet. It is known that V_3Si has a higher T_c of 17.1K. Efimov et al.[9] reported a maximum value of 15.8K at 26 at.% Ga and also a rapid drop in T_c as the composition deviated to lower or higher Ga contents. The curve of T_c as a function of composition was also reported by Das et al. These curves reported by various authors are plotted in Fig. V-18 for the convenience of discussion.

Reference to the equilibrium phase diagram shown in Fig. IV-2 reveals that for the sample compositions used here (14-19 at.% Ga) and for aging temperatures in the range 600°C to 1000°C the specimens fall within a two-phase region. At equilibrium these samples would therefore be expected to contain an A15 phase of composition determined by the edge of the two-phase region at the particular aging temperature. At 1000°C the predicted composition of the A15 phase is ~20 at.% Ga, which, according to the previous work (see Fig. V-18), has T_c ~ 8K. Because the equilibrium concentration of the A15 phase becomes progressively leaner in Ga as the aging temperature is decreased, successively lower transition temperatures would be expected from equilibrium considerations. However, under the non-equilibrium conditions established during initial aging in the present work, the reverse happens. While aging at 1000°C eventually leads to a T_c near 8K, and aging at 800°C also eventually

yields a rather low T_c, the maximum value of T_c increases when lower aging temperatures are used.

The observation of higher T_c is almost certainly associated with the non-equilibrium conditions of the initial precipitate particles and with the high degree of supersaturation under which they form. The initial A15 precipitates from the supersaturated parent matrix will be expected to differ from the equilibrium A15 phase in two aspects: composition and state of internal strain. Both differences may contribute to the high critical transition temperatures observed.

There are thermodynamic reasons[12] to anticipate that the severe supersaturation present at the time the particles form may cause them to have a more nearly stoichiometric composition than the equilibrium phase diagram would suggest. The thermodynamic argument follows directly from Gibbs who pointed out that the energetic barrier to the formation of a small particle of a new phase within a supersaturated matrix is minimized when the new phase forms in a state such that the chemical potential of each component remains constant. If both the parent and product phases are incompressible then the relevant chemical potential is the relative chemical potential, which is equal to the slope of the free energy versus composition curve of the parent solution measured at its mean composition as illustrated in Fig. V-19. The most favorable composition of initial precipitate phase is that composition at which its free energy versus composition curve, at the same temperature, has an equal slope. The predicted result, illustrated in Fig. V-19, is that initial precipitate particles formed under significant supersaturation will tend to be richer in solute than indicated by the equilibrium phase diagram. This

thermodynamically preferred solute enrichment of the initial precipitate particles currently seems to offer the most plausible explanation for their very high transition temperatures.

Since the A15 phase is in this case formed by solid state precipitation within the solution matrix, and since the A15 phase has a substantial mismatch with the parent matrix one would also anticipate that the initial precipitates would be under a relatively high state of strain. The internal strain of the precipitate particles may be relieved somewhat by preferential nucleation along defects in the matrix such as dislocations or dislocation modes and may be further relieved by the accumulation of thermal vacancies at the precipitate-matrix interface. It still must be expected that particles at relatively low temperature will retain some strain for a rather long aging time. The internal strain is known to influence the critical transition temperature in ways which remain poorly understood. According to T. F. Smith[13], however, the T_c of A15 (V_3Ga) increases with hydrostatic pressure. While the effect measured by Smith is small ($\partial T_c/\partial p = 1.05 \times 10^{-5}$ K/bar), the result does suggest that internal strain may also contribute to the high value of T_c.

In this work, there are another two phenomena which may affect the measured T_c's of the tested samples: ordering parameters[14] and proximity effects[15]. T_c's can be increased by increasing the ordering parameters. Due to the proximity effects, however, the T_c's measured might be lower than the actual values.

The ordering parameter can be increased with longer aging heat treatment. The identification of ordering effects in V_3Ga was also reported by R. Flükiger et al.[14]. They claimed that for the V-24.8 at.%

Ga samples the highest T_c value (T_c = 15.7K) was found after a final annealing of three months at 620°C, while the lowest value (T_c = 13.4K) was obtained after an argon jet quenching from 1260°C.

On the basis of the above reasoning, the variation of critical transition temperature with the time and temperature aging may be rationalized as follows. In the earliest stages of aging at all temperatures, initial precipitates form which are nearly stoichiometric in composition but are too small in size to achieve an optimum critical transition temperature due to proximity effects and a poor order of state. As aging proceeds, the small precipitates coarsen, essentially at constant supersaturation, thus proximity effects diminish because of the increasing size of the superconducting A15 phases, and ordering parameters increase due to longer aging so that the critical transition temperature increases rapidly. Eventually a growth of the precipitate particles and the relief of the supersaturation of the parent matrix causes the composition of the particles to adjust towards the equilibrium value with a gradual loss of critical transition temperature. If the aging temperature is high, 800°C or higher, the "over-aging" adjustment toward an equilibrium composition sets in before a peak critical transition temperature is reached, so that the maximum T_c is rather low. At lower aging temperatures, a critical transition temperature near the optimum value for the V_3Ga phase is approached and maintained for some time before over-aging gradually drives the system toward equilibrium.

The thermodynamic arguments about the enrichment of the solute content inside the initial A15 precipitates under significant supersaturation can be used to explain the difference in the optimal T_c's

obtained by the tested samples with different Ga contents (see Figs. V-16, 17), 13.5K for the V-14.5 at.% Ga samples and 14.8K for the V-17.5 at.% Ga samples. The arguments can also be used to explain the different T_c's of the samples with the same Ga content but different deformation temperatures (see Fig. V-20), 14.8K and 15K for the V-17.5 at.% Ga samples deformed at 800°C and 700°C respectively. The main difference between the V-17.5 at.% Ga and the V-14.5 at.% Ga samples is the different degrees of supersaturation after the samples were quenched from high temperatures. Based on the thermodynamic arguments mentioned above, this leads to the different Ga contents in the initial A15 precipitates as clearly indicated in Fig. V-21. Thus, the different critical transition temperatures were the results of the different Ga contents in the A15 particles (see Fig. V-18).

For the specimens deformed at 800°C, some gallium in the matrix has been consumed to form A15 precipitates during the deformations, while for the specimens deformed at 700°C, less Ga has been consumed. Therefore, after deformation the degrees of supersaturation are different. This again leads to the difference in the Ga contents of the initial A15 precipitates as explained in Fig. V-21. The difference of the Ga contents in the parent V/Ga matrices is not that profound, and consequently the difference in T_c's is only ~0.2K (see Fig. V-20).

It is interesting to examine Fig. V-22 in which T_c values are shown for the deformed and undeformed samples. Maximum T_c's are eventually obtained in both conditions, but the kinetic rate of the A15 phase formation is entirely different for the two cases. Since there are more defects such as the high density of dislocations in the deformed sample,

and the defects can decrease the energy barrier for the A15 phase formation, there are more nucleation sites in the deformed sample than in the undeformed one.

Pan et al.[16] in 1975 used the similar direct "solid-state precipitation" method to deal with the V-Ga system and also obtained a high T_c (~14K) from the V-16 at.% Ga sample with 0.6 at.% Ce addition. They attributed the cause of the high T_c to the dislocation and the addition of cerium. They claimed that the gallium is presumably segregated to dislocations. The deposition of the atoms on dislocations is the main reason why the A15 phase (V_3Ga) with high T_c is formed at early stages of aging in the highly deformed alloys since the initial A15 particle contains more gallium and is closer to the stoichiometric composition. From the V-Ga-Ce phase diagram[17] (see Fig. V-23), their explanation of another reason for the precipitated A15 V_3Ga becoming stoichiometric is the addition of cerium.

We have also obtained an exceptionally high T_c, 15K (1K higher than Pan et al.'s) from the V-17.5 at.% Ga samples. However, our explanation of obtaining a high T_c is different. We explained that high Ga contents are caused mainly by thermodynamic reasons. From the data shown in Fig. V-22, it is clear that the high T_c's can be obtained in both the highly deformed and undeformed samples. This certainly implies that the high T_c can also be obtained without the existence of a high density of dislocations.

The samples which were used in this work to obtain the data shown in Figs. V-15, 16, 20 and 22 had no cerium addition. However, the high T_c's were achieved in those samples.

Furthermore, from Figs. 16, 17, and 20, we know that in our work the maximum T_c's ever obtained from the V-17.5 at.% Ga and V-14.5 at.% Ga samples are 15K and 13.5K, respectively. Therefore, we expect that the maximum T_c from the V-16 at.% Ga samples will be around 14K which was obtained by Pan et al. with their V-16 at.% Ga samples; again, this explains that the high T_c can be obtained without the Ce addition.

6. Overall Critical Current Density (J_c)

The compositions of the samples used to perform $J_c(H)$ measurements are V-15.5 at.% Ga and V-18.0 at.% Ga. The tested samples were deformed at 700°C for the thickness reduction of 90% and then aged at 700°C and 900°C for various periods of time. The sample description is listed in Tables V-3 and 4. The overall $J_c(H)$ data are plotted in Fig. V-24 for the deformed V-15.5 at.% Ga samples under various aging times at 700°C, in Fig. V-25 for the deformed V-15.5 at.% Ga samples under various aging times at 900°C, and in Figs. V-26 and 27 for the deformed V-18.0 at.% Ga samples under various aging times at 700°C. The best overall $J_c(H)$'s from these three treatments mentioned above are plotted in Fig. V-28 for the purpose of comparison.

Under the assumption[18] that for type-II superconductors the flux-pinning force at high fields is limited by plastic shearing of the flux-line lattice, the critical-current density obeys the following relationship:

$$J_c^{\frac{1}{2}} \propto (H_{c_2} - H)H^{-\frac{1}{4}},$$

hence H_{c_2} can be determined from a plot of $J_c^{\frac{1}{2}} H^{\frac{1}{4}}$ versus H by extrapolating to $J_c = 0$. The H_{c_2} values thus determined are listed in Tables V-3 and 4. It is interesting that for the tested samples of compositions V-15.5 at.% Ga and V-18.0 at.% Ga aged at 700°C, there is an apparent maximum of H_{c_2} versus aging time. However, for the tested samples aged at 900°C, no maximum of H_{c_2} was observed. This phenomenon is similar to the curve of T_c's versus aging time (see Figs. V-15, 16, and 17). Since both H_{c_2} and T_c are the intrinsic characteristics of superconductors, for the same materials the H_{c_2} will be higher when the T_c is higher. Therefore, the phenomenon of the similar aging curves of both T_c and H_{c_2} can be explained. It should also be noted that the maximum H_{c_2} estimated in this work is 210 KG which is somewhat lower than 236KG obtained from the stoichiometric pure A15 (V_3Ga) materials[19]. This is not surprising since the T_c's of the majority of the tested specimens are lower than the measured inductive T_c's, which represent the highest critical transition temperatures of the small portion of the tested specimens. This was explained in the previous section.

For the V-15.5 at.% Ga samples deformed at 700°C and then aged at 700°C for 6 hours (see Table V-3), there was no J_c observed although the T_c value was measured by the inductive methods. This indicates that the superconducting A15 precipitates are separated from each other. However, for the samples aged for 24 hours (see Fig. V-24), they were able to carry current at intermediate fields, overall $J_c \sim 2.5\times10^2$ A/cm^2 at 60KG and 4.2K. Furthermore, for the samples aged for 48 hours, not only the overall J_c is increased ($\sim1.0\times10^3$ A/cm^2 at 60KG and 4.2K) but also the H_{c_2} is increased. For a longer aging treatment, the $J_c(H)$ falls off

to the level of those samples aged for 24 hours (see Fig. V-24), and H_{c_2} also decreased. Moreover, for the samples aged for 276 hours, no J_c was observed. The grain growth and coarsening have lead to the larger A15 precipitates and also to the discontinuity of the superconducting A15 particles. This can be used to explain the falling off and disappearing of the $J_c(H)$.

Similar phenomena happen in the V-15.5 at.% Ga aged at 900°C for various periods of time as shown in Fig. V-24 and Table V-3.

The overall $J_c(H)$'s for the V-18.0 at.% Ga samples deformed at 700°C for a 90% thickness reduction are shown in Fig. V-26 for the aging time up to 48 hours, and in Fig. V-27 for the aging time up to 168 hours. As indicated in Fig. V-26, it is clear that both the overall $J_c(H)$ and H_{c_2} are increased as the aging time is increased. This situation can be explained by the following sources: (1) the increase of the amount of A15 precipitates, (2) the increase of the connectivity of superconducting A15 particles, and thus reducing the "proximity effect," and (3) the reasons which are used to explain the increase of T_c's presented in Section 5 of this chapter. The $J_c(H)$ data of the samples for longer heat treatments also show the trend of falling off values with on exception, the samples aged at 168 hours. The reason is not clear at this moment.

Using the "solid-state precipitation" approach in the V-Ga system, we have been able to obtain a continuous or semicontinuous superconducting A15 precipitate network with the overall $J_c \sim 3.5\times10^3$ A/cm^2 at 60KG and 4.2K, and the overall $J_c \sim 10^2$ A/cm^2 at 120KG and 4.2K. These values compare very favorably with the data obtained by Pan et al.[16] using a similar approach. It should be reminded here that the criterion

of defining J_c is the potential drop across the voltage leads exceeding 1 μV, while the criterion of Pan et al.'s work is in the level of a few mV.

The overall $J_c(H)$ values obtained by this approach are lower than those achieved by the conventional "Bronze" process and the "In-Situ" (Tsuei) method. This can be attributed to a larger A15 grain size and a less A15 content. However, the grain size, the morphology, and the volume fraction of the A15 precipitates can be optimized by choosing a proper prior deformation and an appropriate heat treatment. We should indicate that for the V-Ga specimens deformed 75%, the characteristics of the voltage-current curves behave similarly as the one shown in Fig. IV-9(b). During the experiment, we have carefully avoided the problem of putting the current leads and the voltage leads too close. Therefore, for the tested sample deformed 75%, the resistance shown in the V-I curve is caused by the internal resistivity of the tested specimen. This indicates that the superconducting A15 particles are discontinuous, and the normal conducting regions between them cause the resistance measured in the V-I curve.

However, for the tested sample deformed 90%, the characteristics of the V-I curves behave like the one shown in Fig. IV-9(a). No internal resistivity was observed at the 10^{-2} μΩ-cm level. This indicates that the superconducting A15 particles are continuous with each other, or they are discontinuous but very close to each other.

For the tested samples deformed 75% and 90%, not only the characteristics of the V-I curves are different, but also the $J_c(H)$ data are different. The overall $J_c(H)$ could be increased from ~10^2 A/cm^2 at 60KG

and 4.2K for the 75% deformed samples[20] to > 10^3 A/cm^2 at 60KG and 4.2K for the 90% deformed samples. From the experiments performed in the Nb-Al system, which will be presented in the next chapter, it is clear that the $J_c(H)$ values could be enhanced dramatically for more than one order if the sample is deformed for 99% or more. It can be understood that with an increased prior deformation, more dislocations or defects are produced such that the kinetic rate of the A15 formation and the amount of the nucleation-sites for the A15 precipitates are increased. Thus, these lead to finer grain-sized A15 particles. Consequently, the pinning force is increased and so are the $J_c(H)$ values.

V. REFERENCES

1. D. H. Gubser, T. L. Francavilla, D. G. Howe, R. A. Muessner, and F. T. Ormand, IEEE Trans. or Magn. MAG-15, 385 (1979).

2. S. Foner, E. J. McNiff, Jr., S. Moehlecke, and A. Sweedler, Bull. Am. Phys. Soc. 25, 333 (1980); R. Flükiger, S. Foner and E. J. McNiff, Jr., 3rd Conf. on Supercond. on d- and f-band Metals, June 1979, La Holla, Calif.

3. B. N. Das, J. E. Cox, R. W. Huber, and R. A. Muessner, Metall. Trans. 8A, 541 (1977).

4. D. Dew-Hughes, Cryogenics, 5, 435 (1975).

5. C. C. Tsuei, J. Appl. Phys. 45, 1385 (1974).

6. J. Bevk, F. Habbal, C. J. Lobb, and G. Dublon, to be published in Adv. in Cryo. Eng., Vol. 26.

7. D. Dietderich, M. Hong, and J. W. Morris, Jr., presented at the 1980 Annual Meeting of Metallurgical Society of AIME, Las Vegas, Nevada, February 25-28, 1980.

8. S. Foner, private communication.

9. Yu, V. Efimov, V. V. Baron, and E. M. Savitskii, Physics and Metallurgy of Superconductors, pp. 147-153.

10. J. H. N. van Vucht, H. A. C. M. Bruning, H. C. Donkersloot, and A. H. Gomes de Mesquita, Philips Res. Rep. 19, 407 (1964).

11. J. H. Wernick, F. J. Morin, S. L. Hsu, D. Dorsi, J. P. Maisa, and J. E. Kunzler, High Magnetic Fields, H. Kalm, B. Lax, F. Bitter and R. Mills, eds., pp. 609-614, M.I.T. Press, Cambridge, Mass., and New York, N.Y., 1962.

12. J. W. Gibbs, The Scientific Papers of J. Willard Biggs, Vol. 1 Thermodynamics (Dover, New York, 1961).

13. T. F. Smith, J. Low Temp. Phys. 6, 171 (1972).

14. R. Flükiger, J. L. Staudenmann, and A. Treyvand, Proc. 14th Intl. Conf. on Low-Temp. Phys., M. Krusius and M. Vuorio, eds., Vol. 2, p. 1, American Elsevier Publishing Company, New York, N.Y., 1975.

15. G. Deutscher and P. G. de Gennes, Superconductivity, edited by R. D. Parks, vol. 2, p. 1005, Marcel Dekker, Inc., New York, N.Y., 1969.

16. V. M. Pan, Yu. I. Beletskiy, V. S. Flis, S. A. Firstov, and G. F. Sarzhan, Fiz. Meta. Metalloved. 40, 281 (1975).

17. V. N. Svechnikov, V. M. Pan, and A. Ts. Spktor, Sb. Metallofizika 27, Kiev, Naukova dumka, 177 (1970).

18. E. J. Kramer, J. Appl. Phys. 44, 1360 (1973).

19. K. Hechler, G. Horn, G. Otto, and E. Saur, J. Low Temp. Phys. L, 29 (1969).

TABLE V.1

Interstitial Impurity Contents of Arc-Melted Binary V-Ga Alloys

Degree of Deformation (%)	Oxygen (at.%)	Nitrogen (at.%)
> 90	0.46	0.09
< 75	1.04	0.71

TABLE V.2

Interstitial Impurity Contents of Arc-Melted V-Ga Alloys with Small Amount of Ce-Addition

Before Arc-Melting Ce (at.%)	After Arc-Melting Ce (at.%)	Degree of Deformation (%)	Oxygen (at.%)	Nitrogen (at.%)
0.55	0.03	> 95	0.37	0.07

TABLE V-3

V-15.5 at.% Ga

90% Deformation at 700°C

Aging Temperature (°C)	Aging Time (hrs)	Overall J_c at 4.2K and 40KG (10^2 A/cm^2)	Overall J_c at 4.2K and 60KG (10^2 A/cm^2)	H_{c2}* (4.2K) (KG)
700	0	0	0	-
700	6	0	0	-
700	24	6	2.5	140
700	48	18	10	180
700	200	6	2.5	160
700	276	0	0	-
900	0	0	0	-
900	1.5	4	0.4	120
900	6	3.2	-	63
900	24	1.5	-	60

*H_{c2} is determined from a plot of $J_c^{\frac{1}{2}} H^{\frac{1}{4}}$ versus H by extrapolating to $J_c = 0$.[18]

TABLE V-4

V-18.0 at.% Ga

90% Deformation at 700°C

Aging Temperature (°C)	Aging Time (hrs)	Overall J_c at 4.2K and 40KG (10^2 A/cm^2)	Overall J_c at 4.2K and 60KG (10^2 A/cm^2)	H_{c_2} * (4.2K) (KG)
700	0	0	0	-
700	3	2.5	0.54	-
700	6	37	8	92
700	12	> 40	17	163
700	24	> 40	23	210
700	48	120	35	-
700	96	> 40	25	175
700	168	> 40	22	200

*H_{c2} is determined from a plot of $J_c^{\frac{1}{2}} H^{\frac{1}{4}}$ versus H by extrapolating to $J_c = 0.^{18}$

FIGURE CAPTIONS

Fig. V-1. Optical micrograph of an arc-cast V-15 at.% Ga sample.

Fig. V-2. Optical micrograph of an arc-cast V-16 at.% Ga with Ce addition.

Fig. V-3. Scanning electron fractograph of a V-17.5 at.% Ga sample broken after homogenization and quenching. The fracture occurs primarily through transgranular cleavage.

Fig. V-4. Transmission electron micrograph of as-deformed V-17.5 at.% Ga samples showing the high density of dislocations and a BCC phase diffraction pattern.

Fig. V-5. Optical micrograph of V-17.5 at.% Ga samples deformed at 650°C.

Fig. V-6. Optical micrographs of V-17.5 at.% Ga samples deformed 75% and aged at 600°C.

Fig. V-7. Optical micrographs of V-17.5 at.% Ga samples deformed 75% and aged at 700°C.

Fig. V-8. Optical micrograph of V-17.5 at.% Ga samples deformed 75% and aged at 800°C.

Fig. V-9. Optical micrograph of V-17.5 at.% Ga samples deformed 75% and aged at 1000°C.

Fig. V-10. Transmission electron micrograph of V-17.5 at.% Ga samples deformed 75% and aged at 700°C for 10 hrs, showing a dislocation cell structure of the BCC phase.

Fig. V-11. Transmission electron micrograph of V-17.5 at.% Ga deformed 75% and aged at 700°C for 3 days, showing elongated A15 precipitates embedded in the BCC matrix.

Fig. V-12. Transmission electron micrograph of another area of V-17.5 at.% Ga deformed 75% and aged at 700°C for 3 days, also showing elongated A15 precipitates embedded in the BCC matrix.

Fig. V-13. Transmission electron micrograph of the other area of V-17.5 at.% Ga deformed 75% and aged at 700°C for 3 days, showing the BCC phase.

Fig. V-14. Optical micrograph of V-17.5 at.% Ga deformed 75% and aged at 1000°C and a schematic explanation of A15 precipitation.

Fig. V-15. The critical transition temperature of deformed V-18.5 at.% Ga samples as a function of aging time for various aging temperatures.

Fig. V-16. The critical transition temperature of deformed V-17.5 at.% Ga samples as a function of aging time for various aging temperatures.

Fig. V-17. The critical transition temperature of deformed V-14.5 at.% Ga samples as a function of aging time for various aging temperatures.

Fig. V-18. The critical transition temperature as a function of Ga contents reported by Das et al.[3], Efimor et al.[9], and van Vucht et al.[10].

Fig. V-19. Schematic illustration of Gibbs free energy vs. composition at given temperature. C_1 and c_2 are the equilibrium compositions of the hypothetical α and A15 phases at this temperature. C_1* is the composition of the supersaturated solid solution and c_2* is the preferred composition of the initial A15 precipitate.

Fig. V-20. The critical transition temperature vs. aging time for the V-17.5 at.% Ga samples deformed at 700°C and 800°C, respectively.

Fig. V-21. Schematic illustration of Gibbs free energy vs. composition at a given temperature: c_1 and c_2 are the equilibrium compositions of the hypothetical α and A15 phases at this temperature. C_1* and c_2† are the compositions of different degrees of supersaturated solid solutions; c_2* and c_2† are the preferred compositions of the

initial A15 precipitates, accordingly.

Fig. V-22. The critical transition temperature vs. aging time for the V-17.5 at.% Ga samples with 75% deformation and no deformation.

Fig. V-23. The relevant portion of the V-Ga-Ce equilibrium phase diagram as reported by Svechnikov et al.[17].

Fig. V-24. The overall critical current density of deformed V-15.5 at.% Ga samples as a function of transverse magnetic fields for various aging times at 700°C.

Fig. V-25. The overall critical current density of deformed V-15.5 at.% Ga samples as a function of transverse magnetic fields for various aging times at 900°C.

Fig. V-26. The overall critical current density of deformed V-18.0 at.% Ga samples as a function of transverse magnetic fields, aged at 700°C for 3, 6, 12, 24, and 48 hrs.

Fig. V-27. The overall critical current density of deformed V-18.0 at.% Ga samples as a function of transverse magnetic fields, aged at 700°C for 12, 24, 48, 96, and 168 hrs.

Fig. V-28. A summary of the overall $J_c(H)$ data of the V-Ga samples.

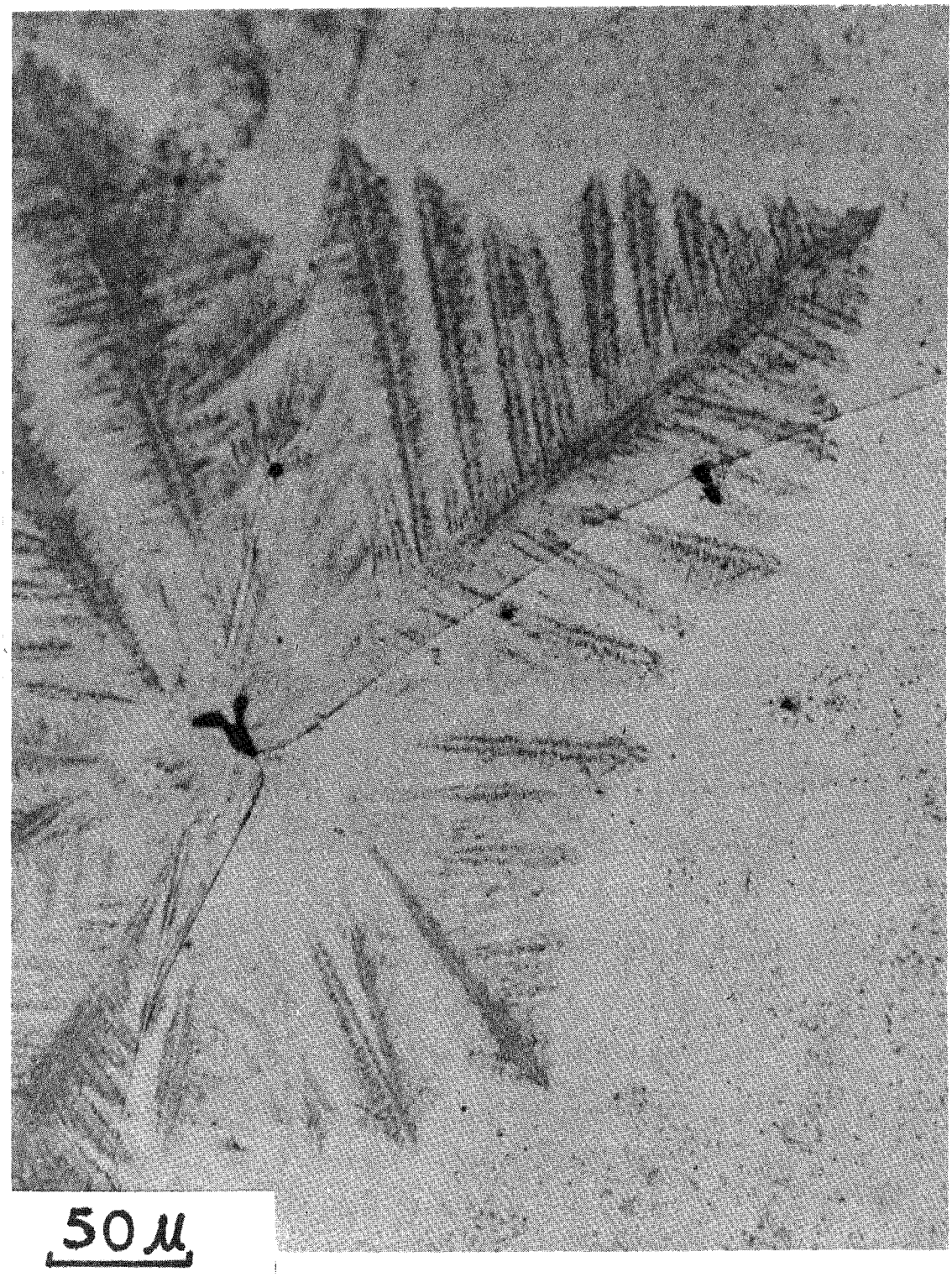

Fig. V-1

XBB 808-9474

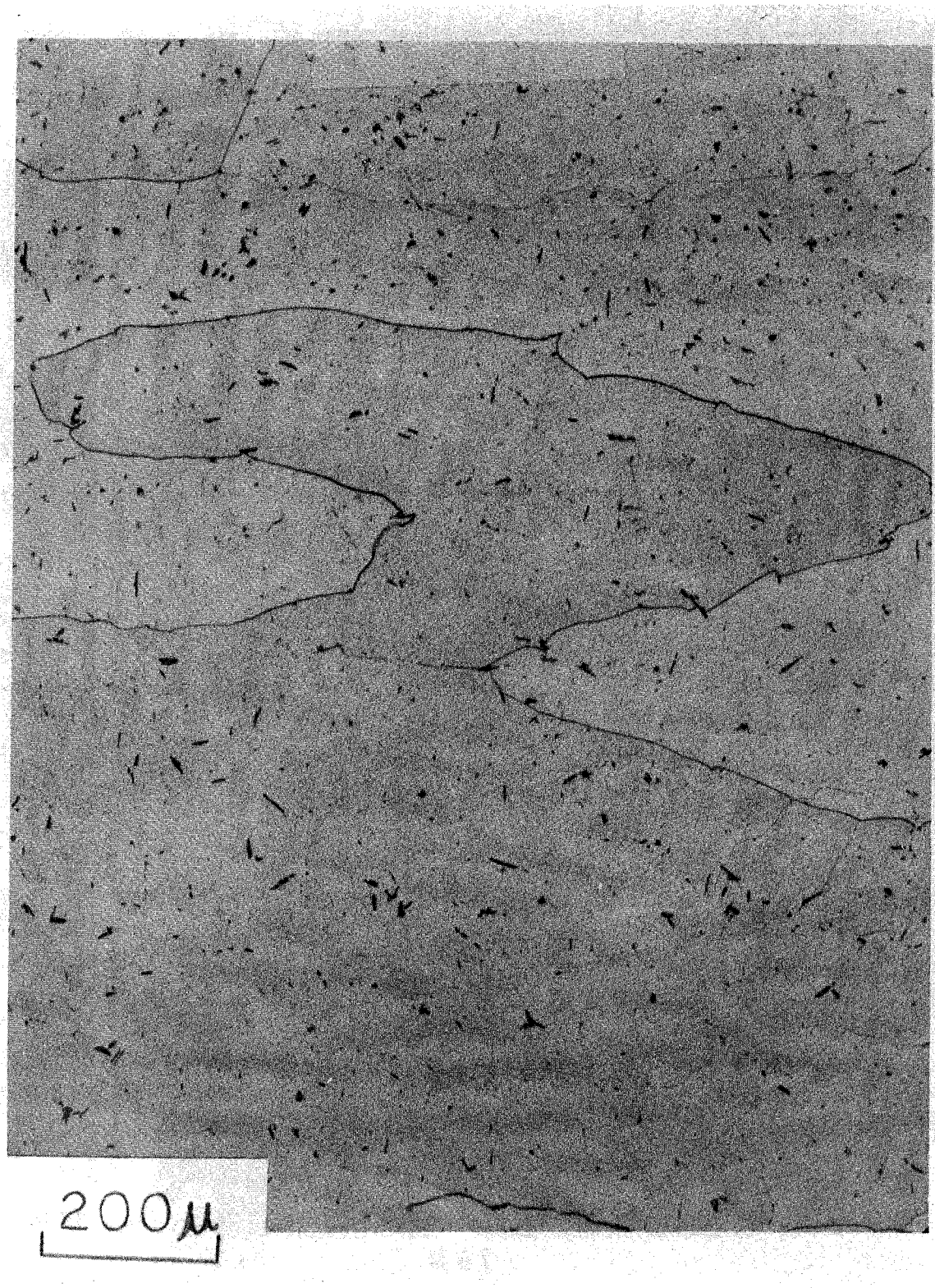

Fig. V-2 XBB 808-9473

Fig. V-3 XBB 798-10315

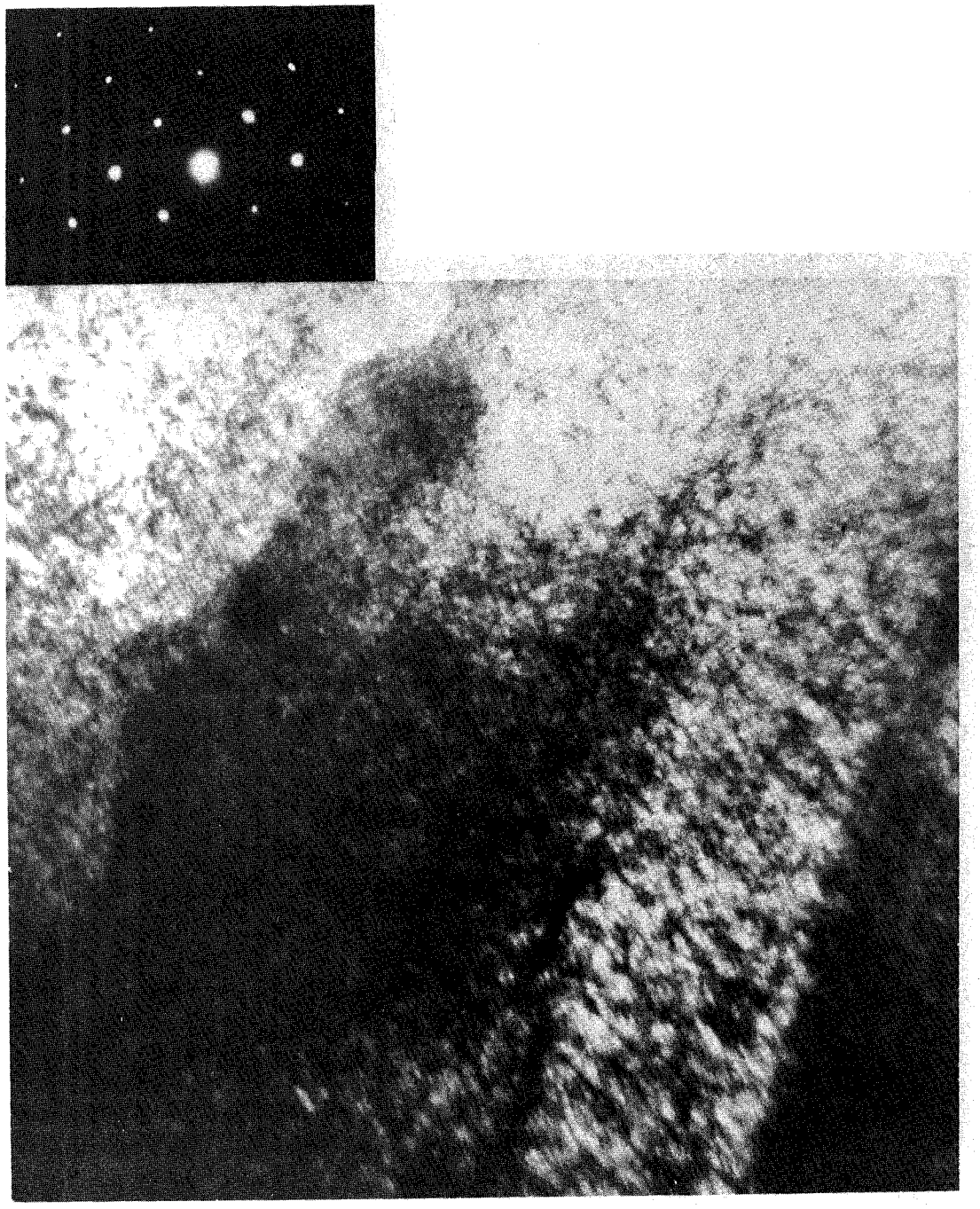

Fig. V-4

XBB 781-678

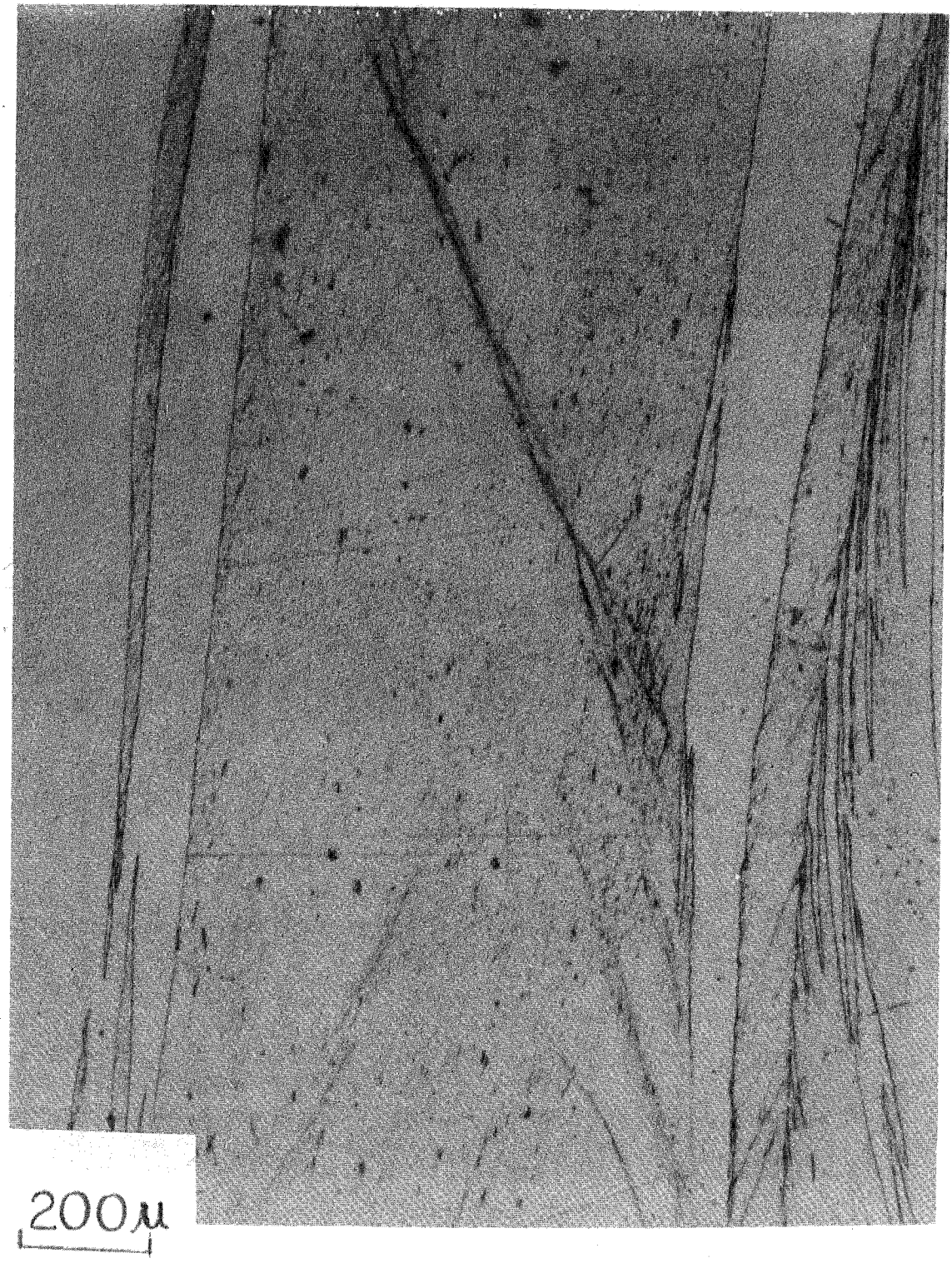

Fig. V-5

XBB 808-9472

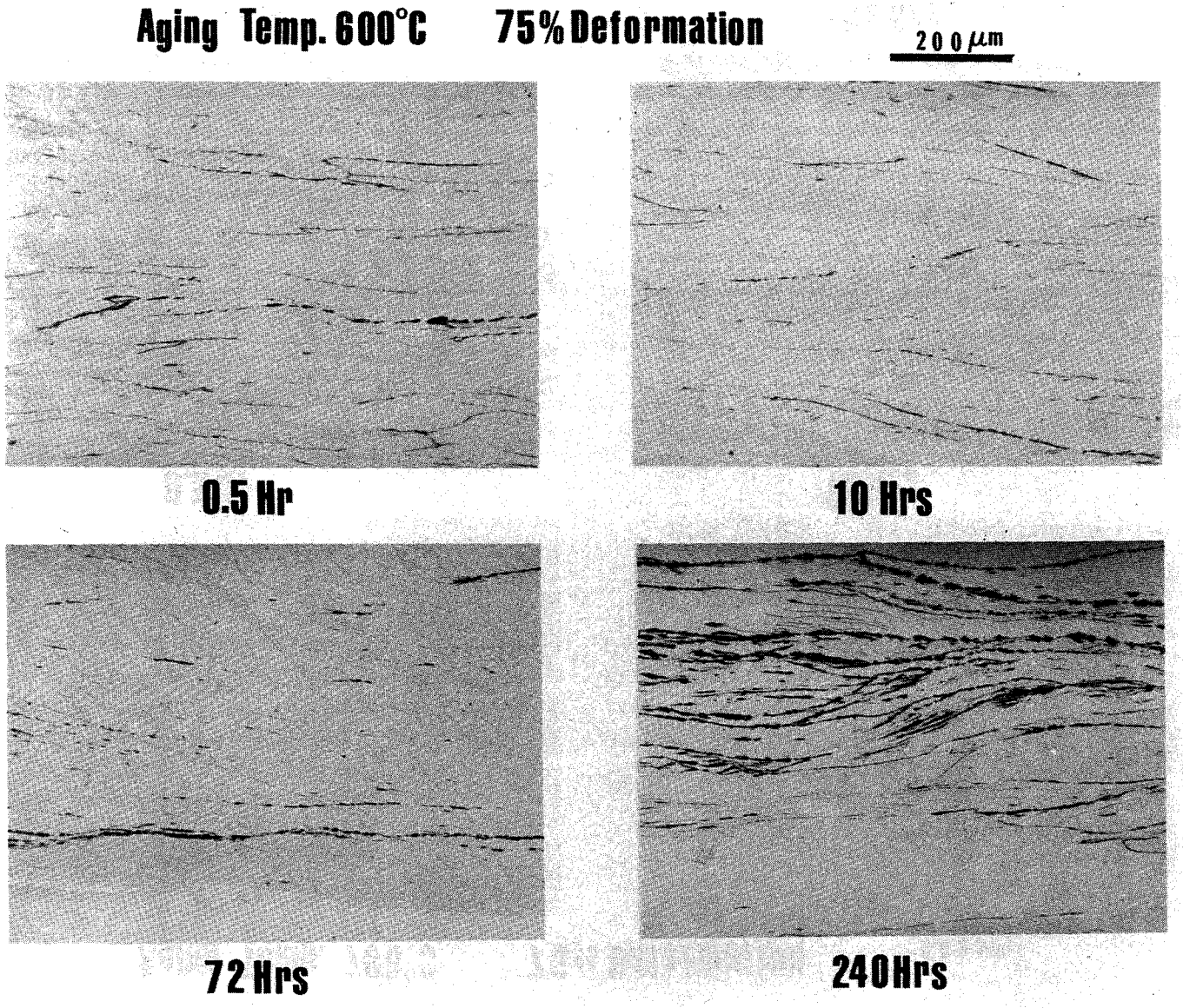

Fig. V-6

XBB 793-3107

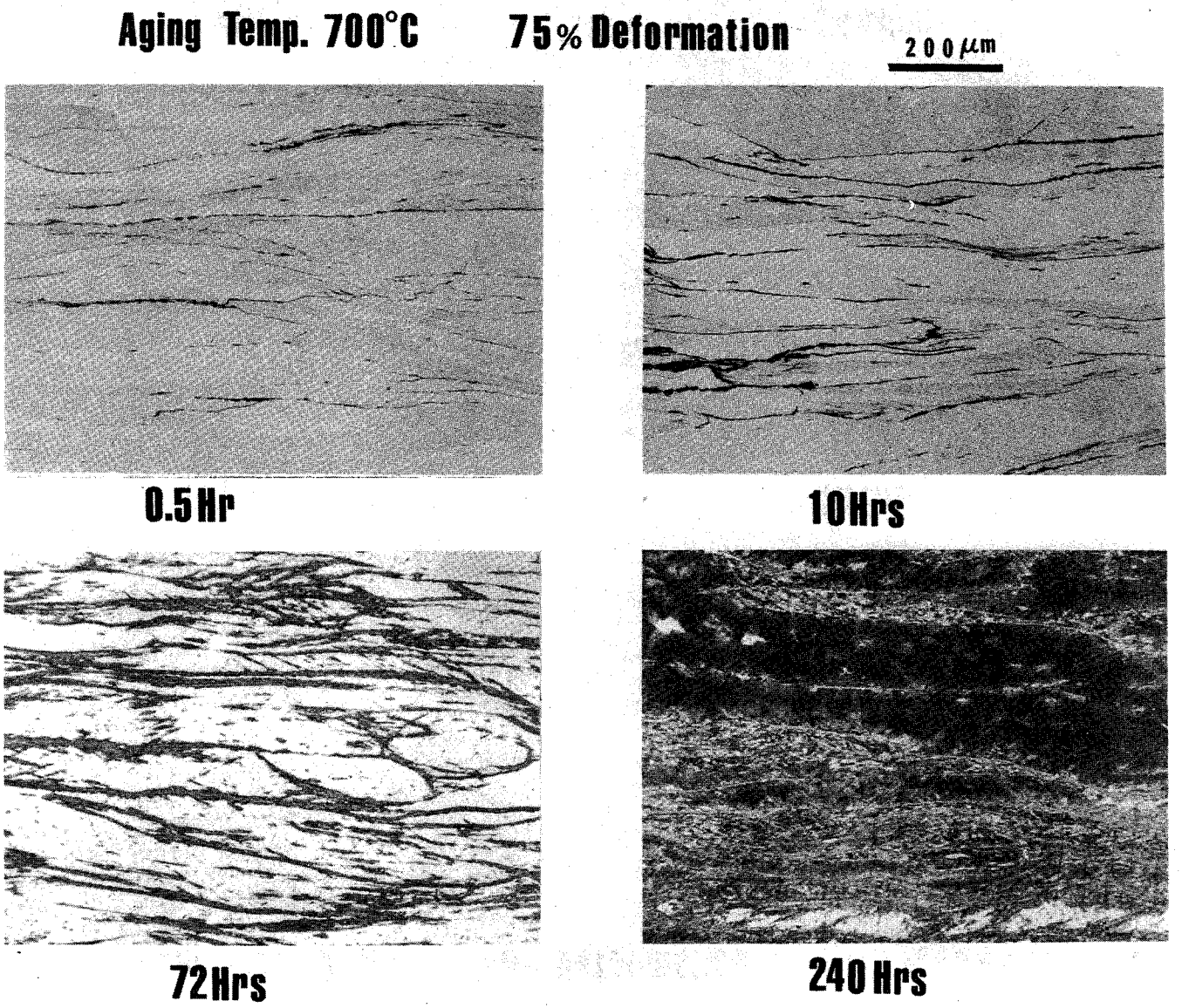

Fig. V-7 XBB 793-3108

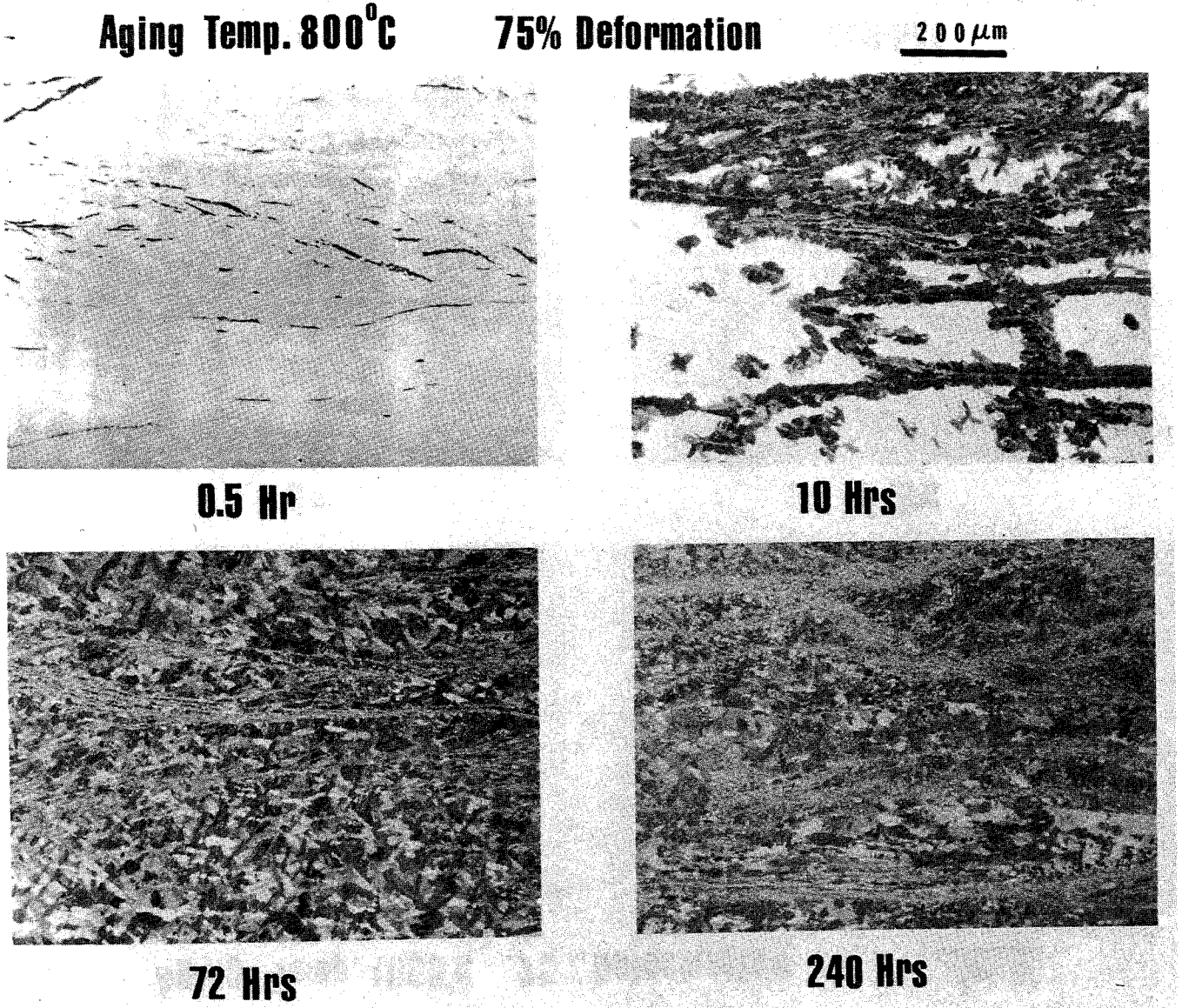

Fig. V-8 XBB 793-3105

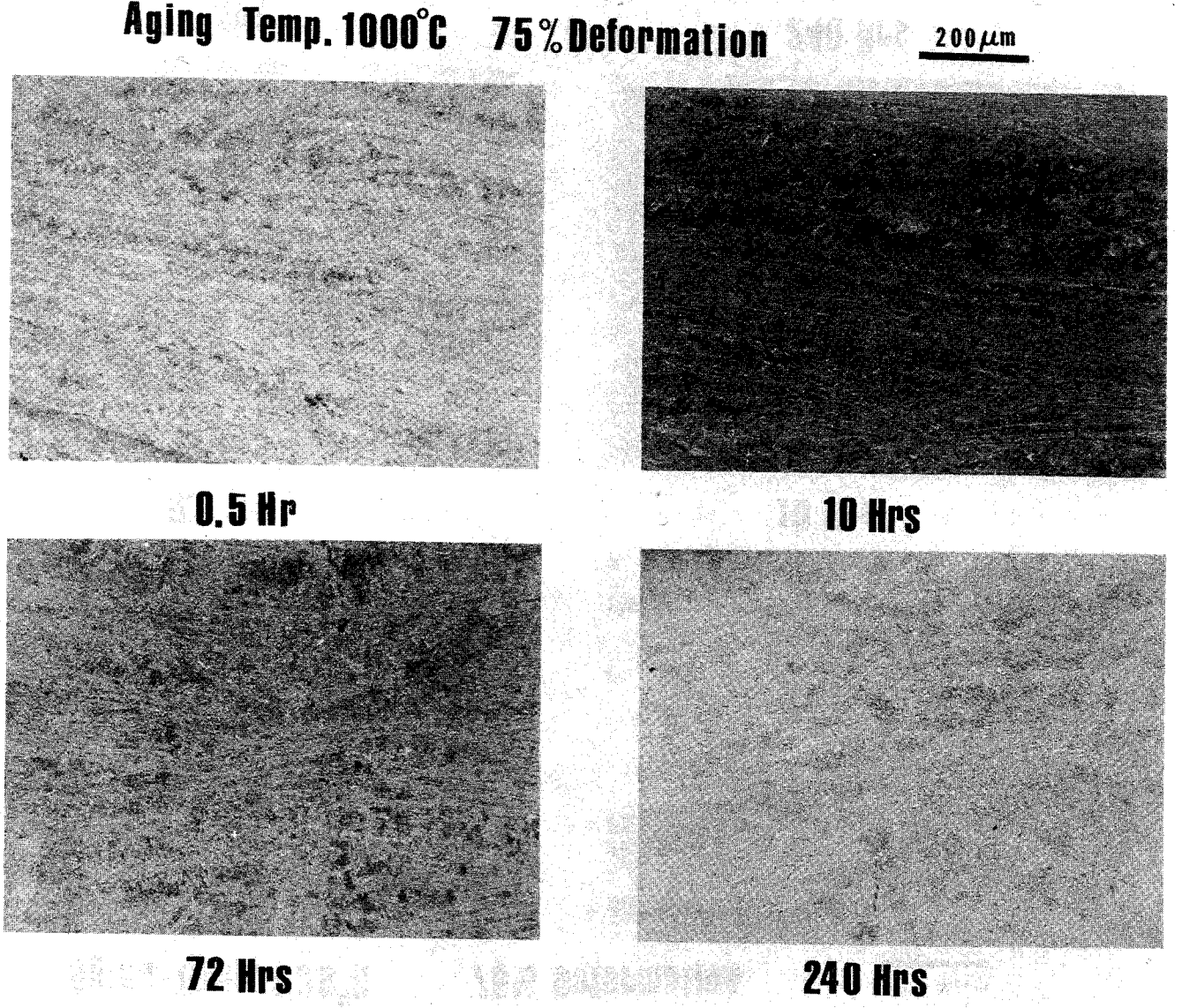

Fig. V-9

XBB 793-3106

Fig. V-10 XBB 802-2121

Fig. V-11 XBB 802-2117

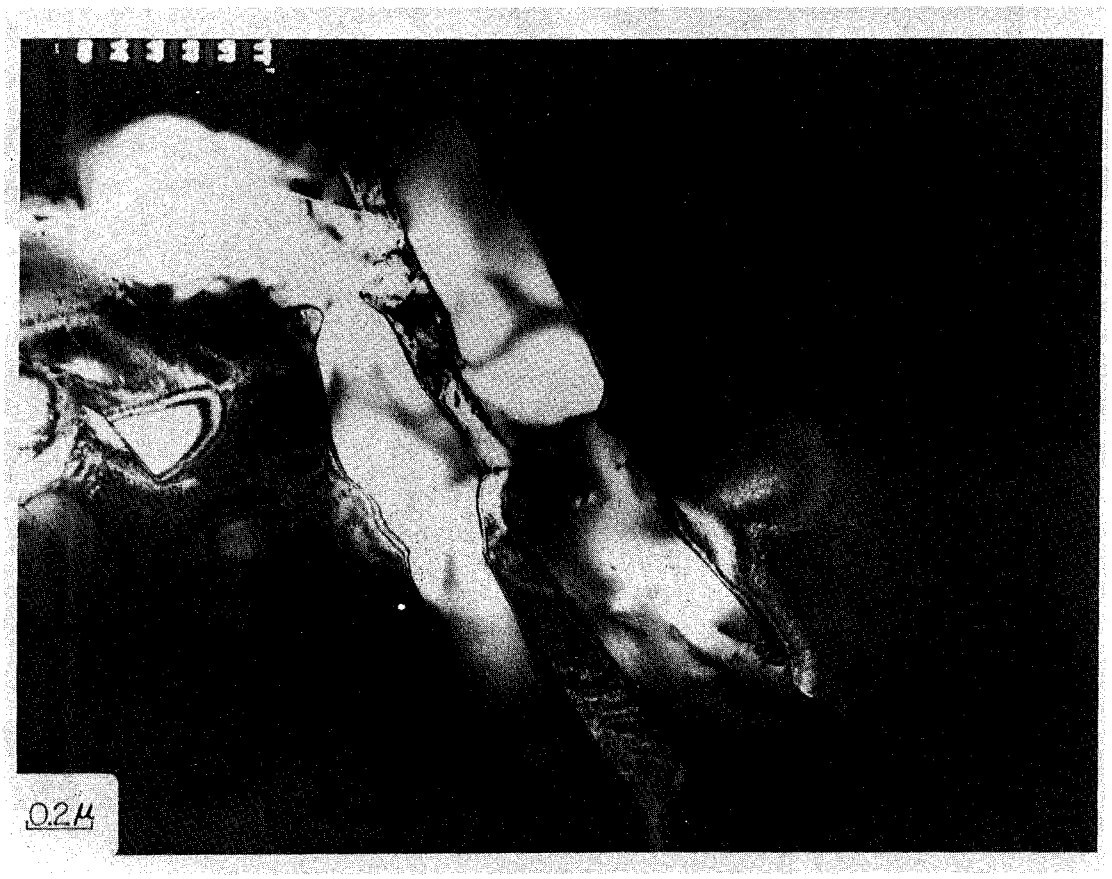

Fig. V-12 XBB 802-2118

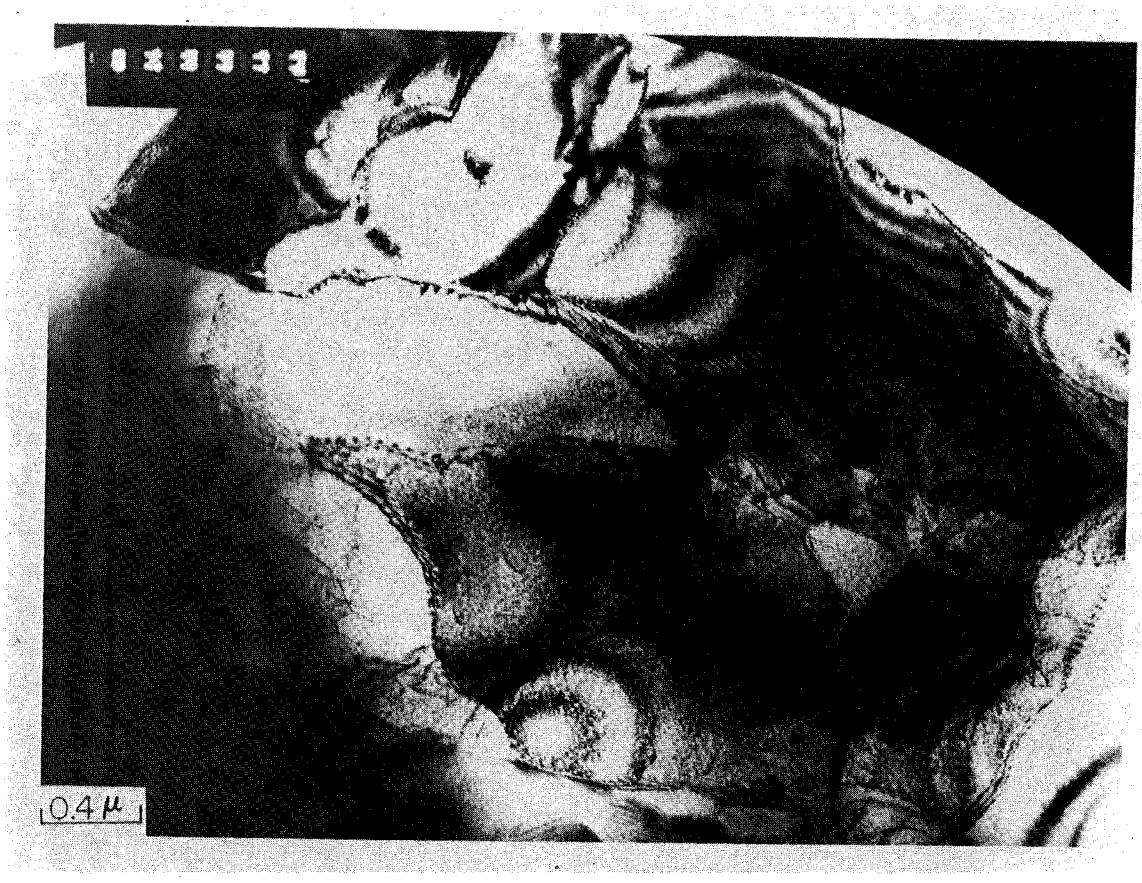

Fig. V-13 XBB 802-2120

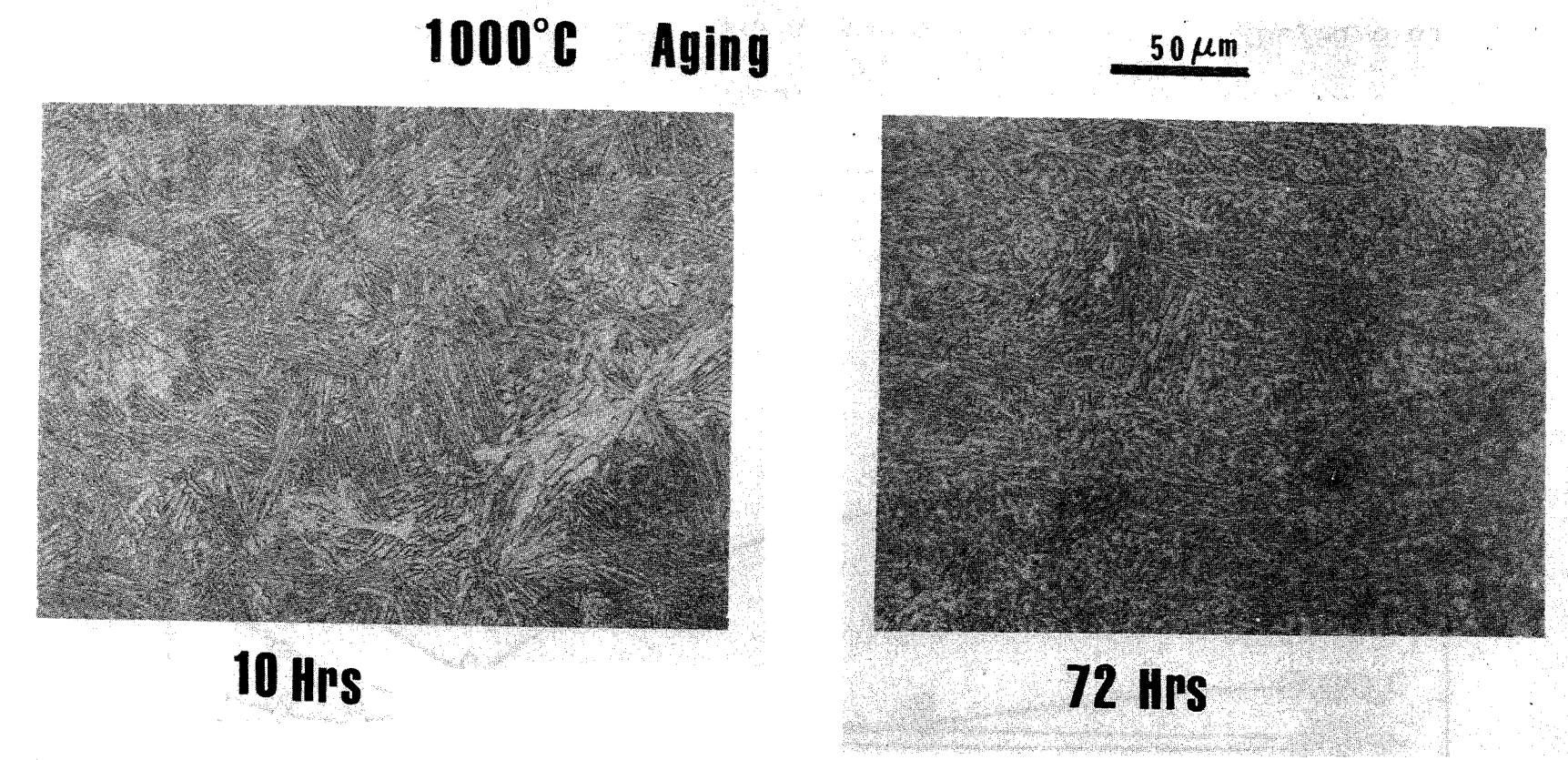

Fig. V-14

XBB 793-3104

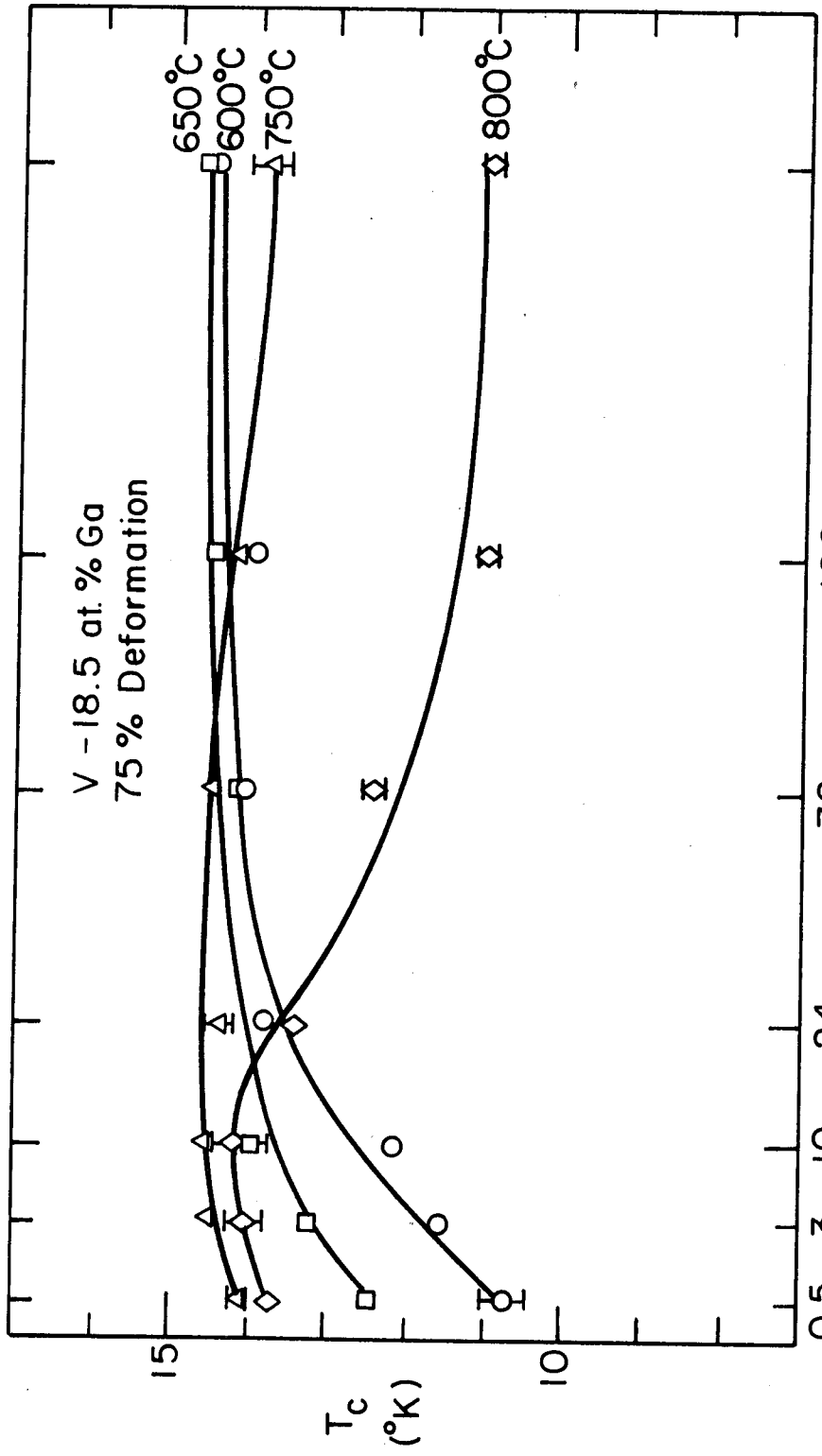

XBL798-6765

Fig. V-15

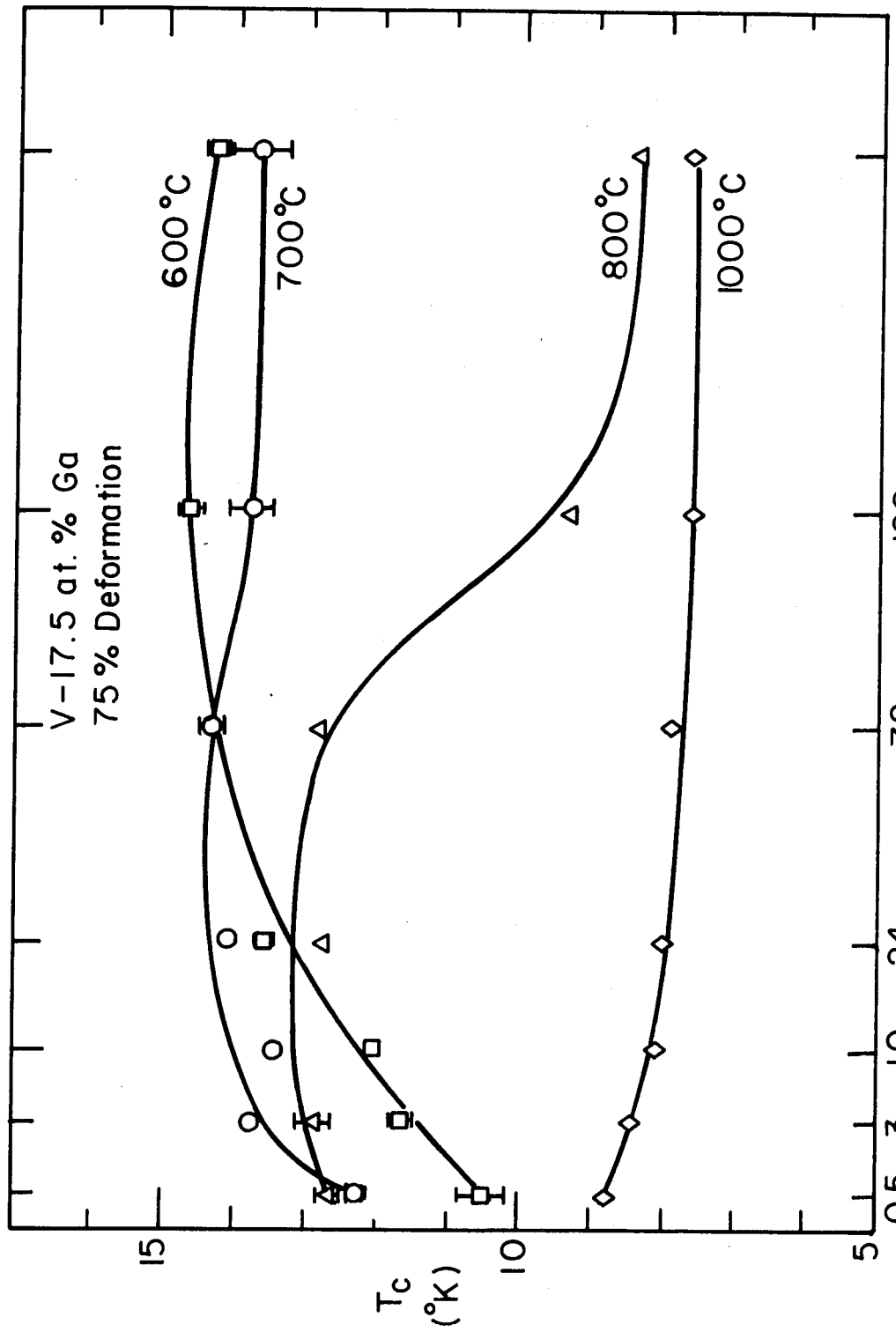

XBL 793-5871

Fig. V-16

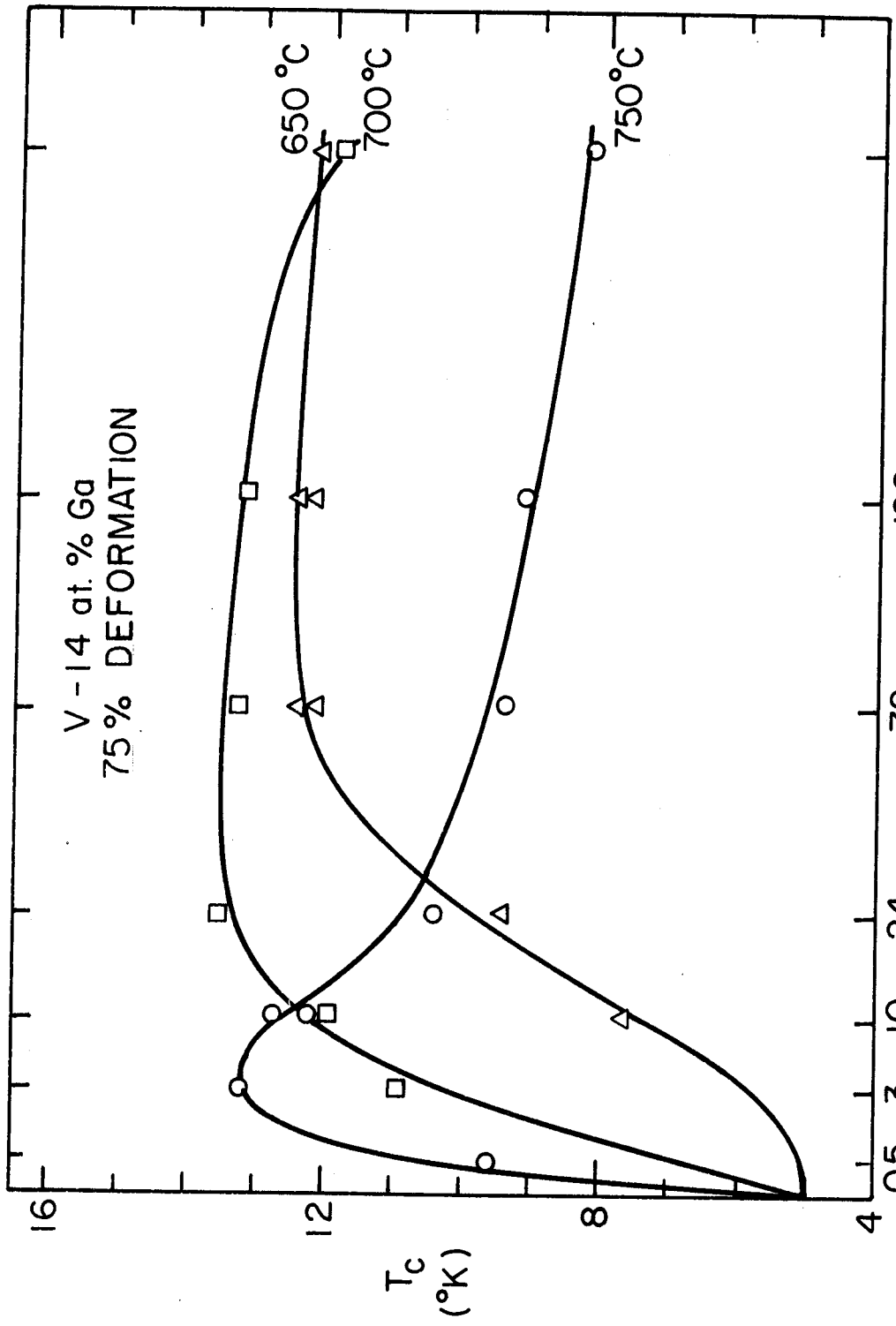

XBL 798-10968

Fig. V-17

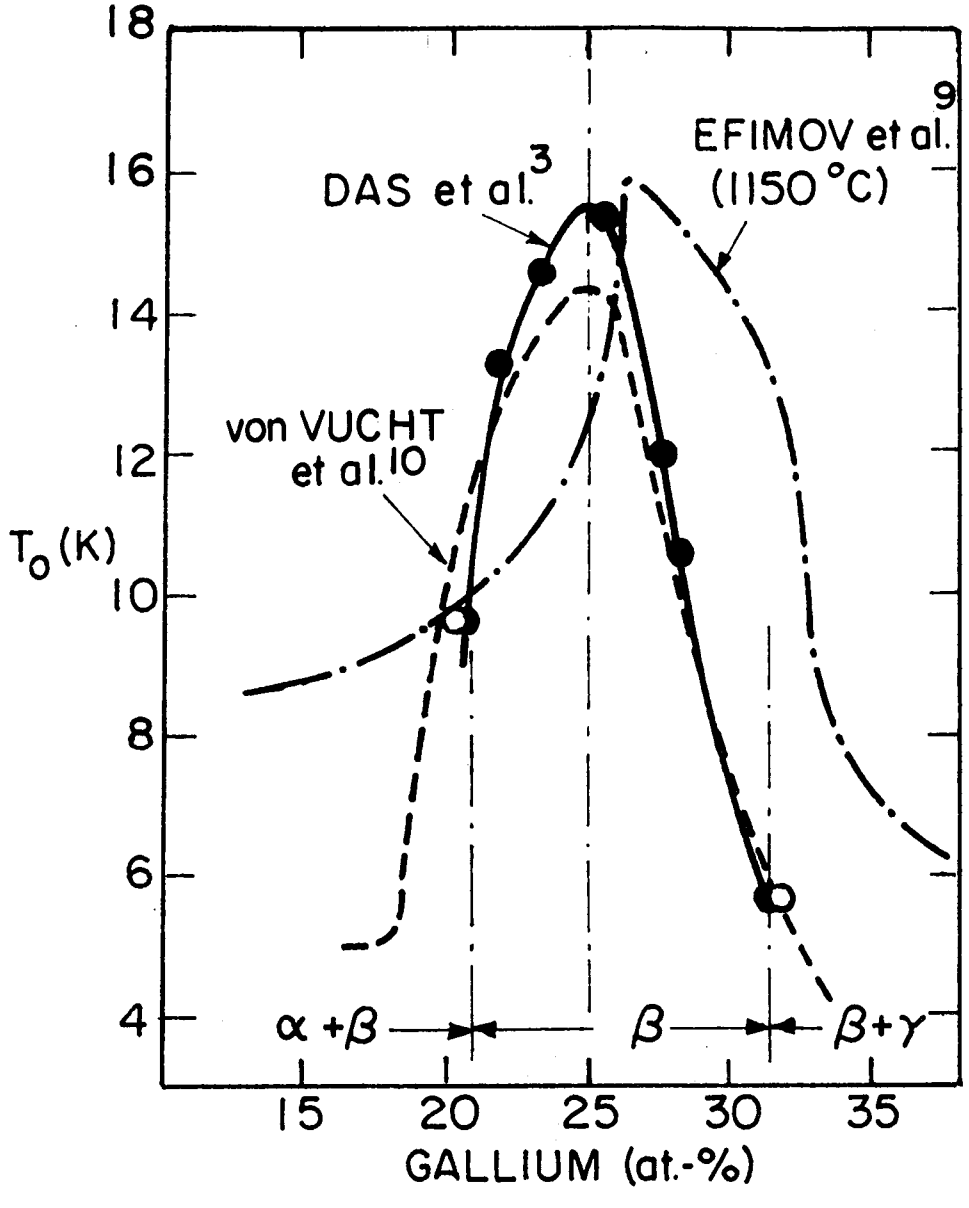
18
16
14
12
10
8
6
4
T_0 (K)
DAS et al.[3]
EFIMOV et al.[9]
(1150 °C)
von VUCHT et al.[10]
α +β
β
β+γ
15
20
25
30
35
GALLIUM (at.-%)
XBL 808-5696

Fig. V-18

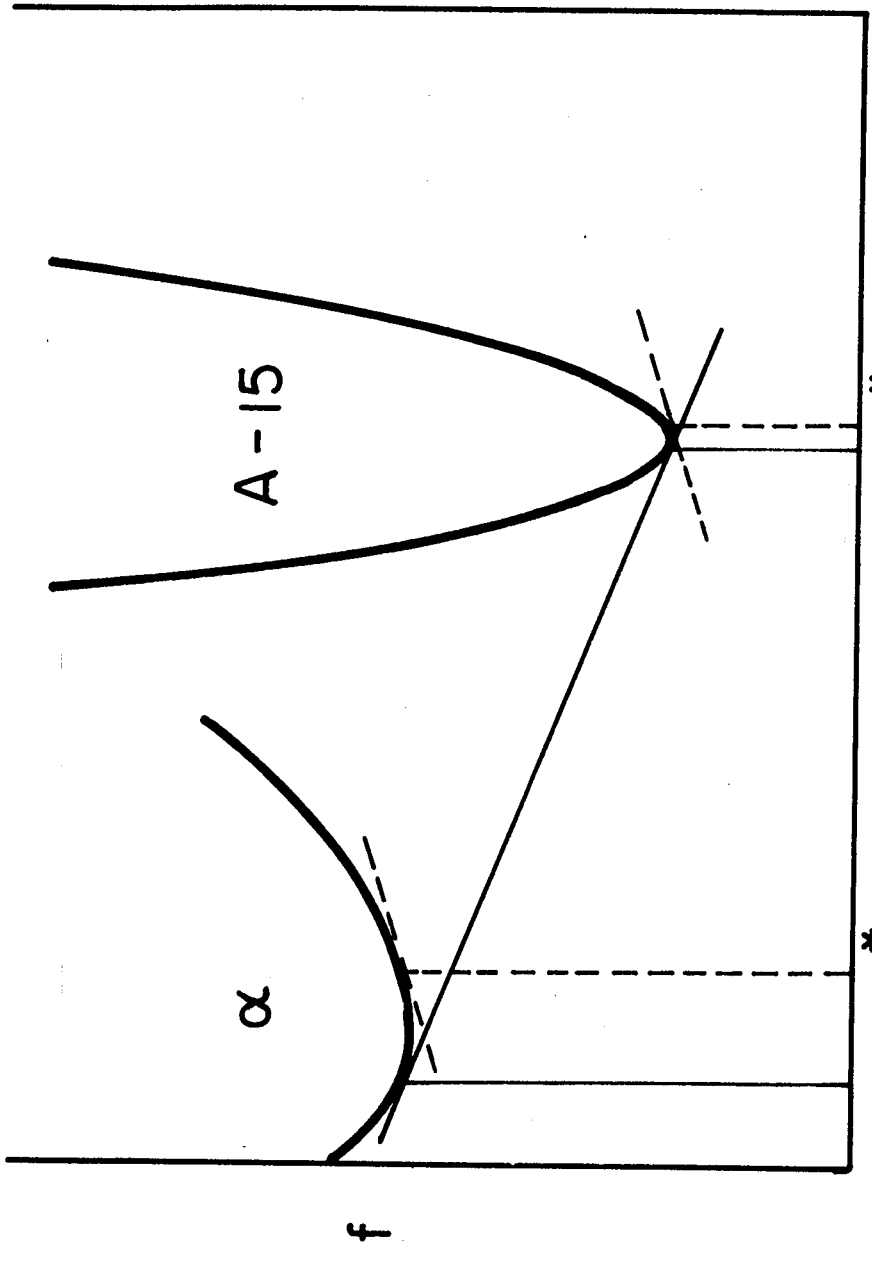

XBL 793-5877

Fig. V-19

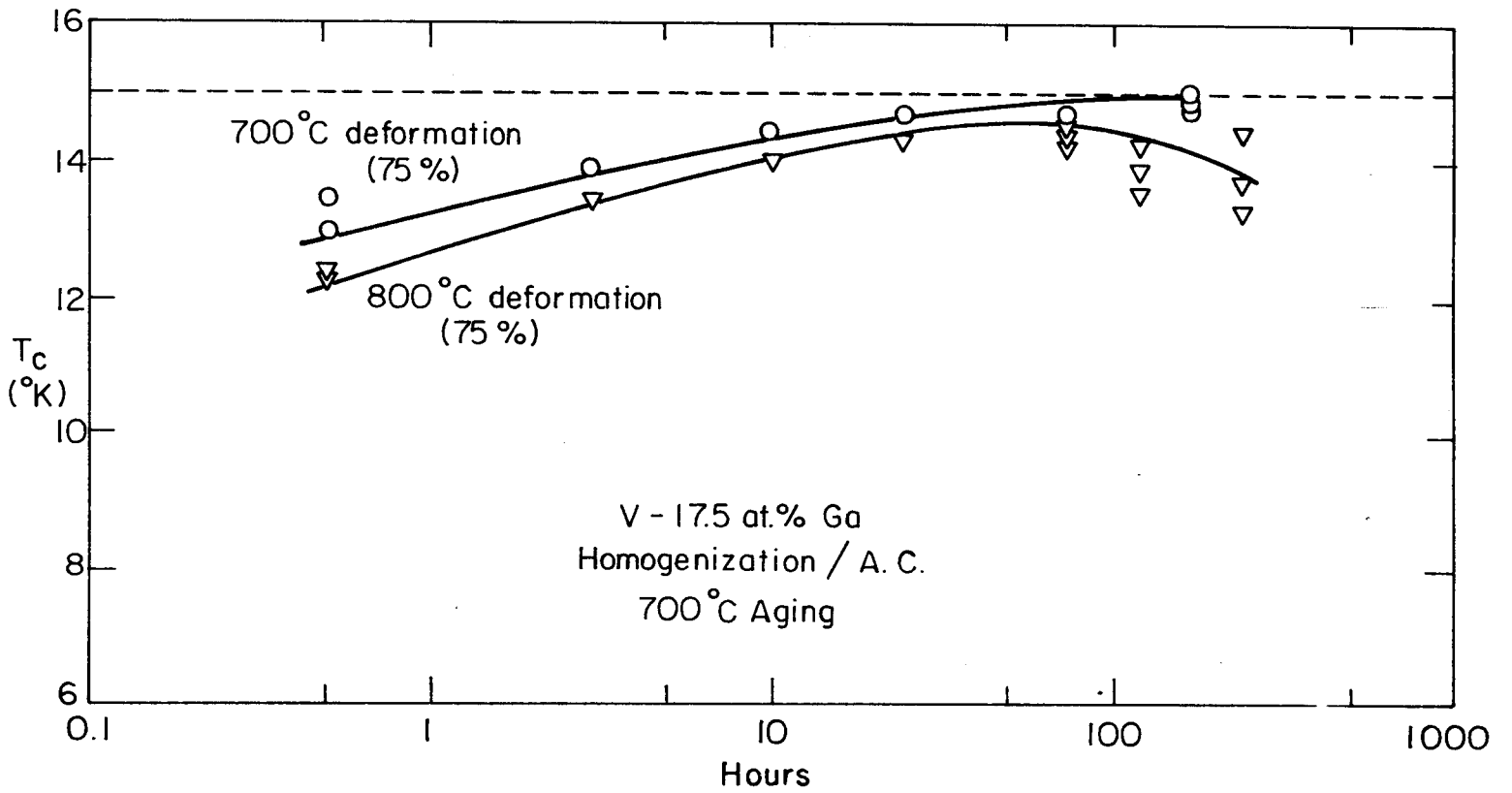
16
14
12
10
8
6
T_c (°K)
700°C deformation (75 %)
800°C deformation (75 %)
V - 17.5 at.% Ga
Homogenization / A. C.
700°C Aging
0.1
1
10
100
1000
Hours
XBL801-4639

Fig. V-20

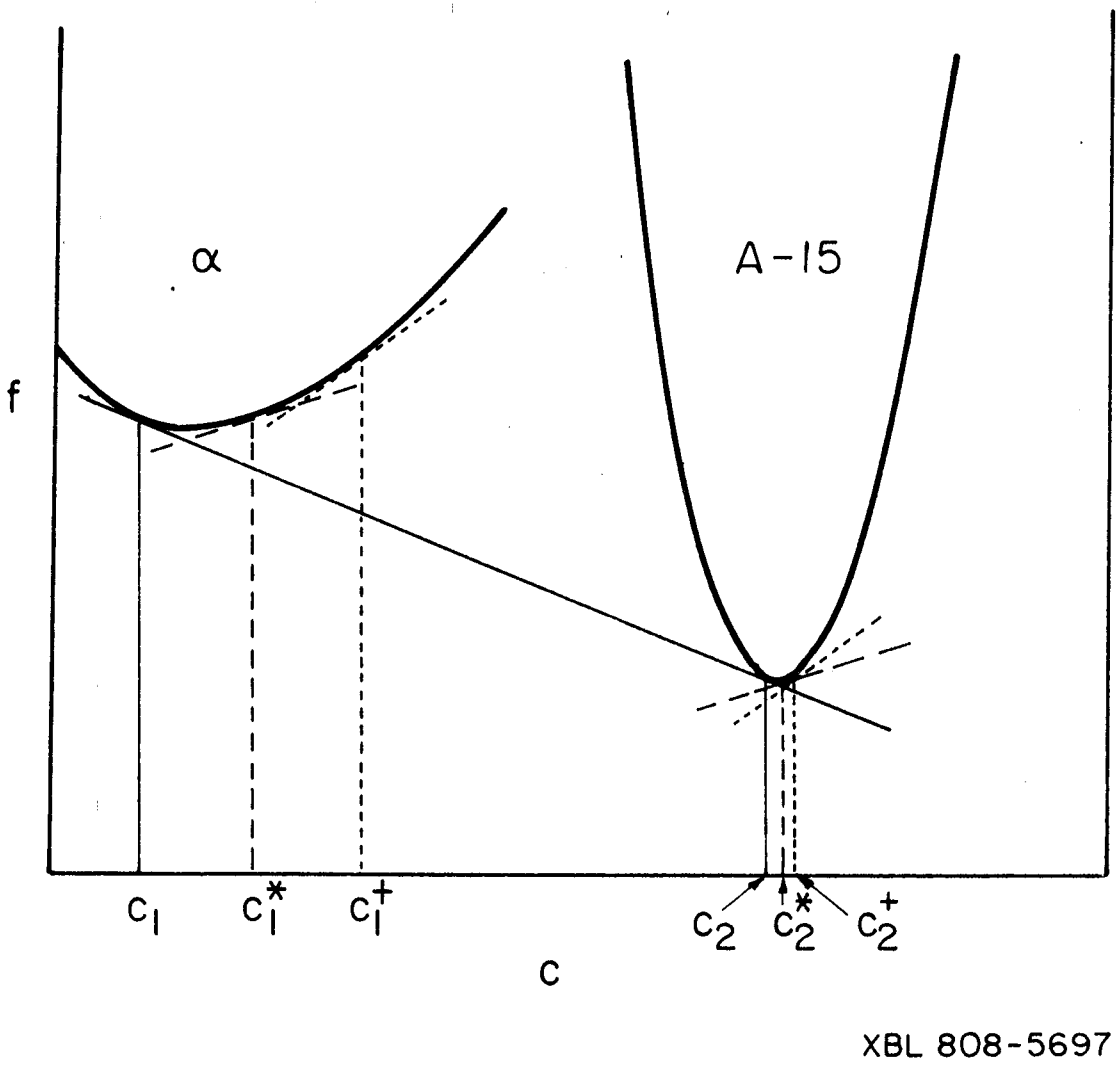

Fig. V-21

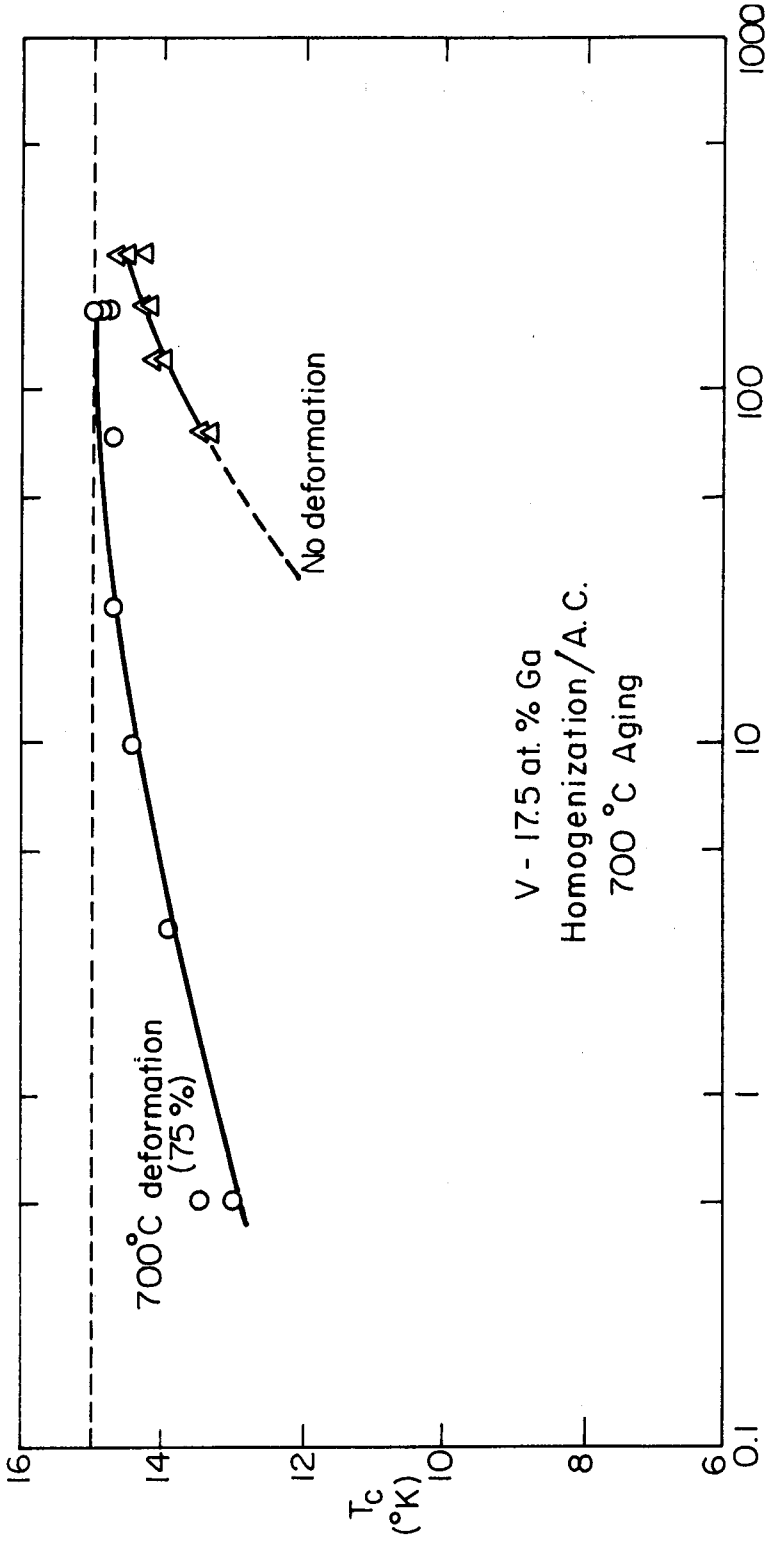

XBL 801-4638

Fig. V-22

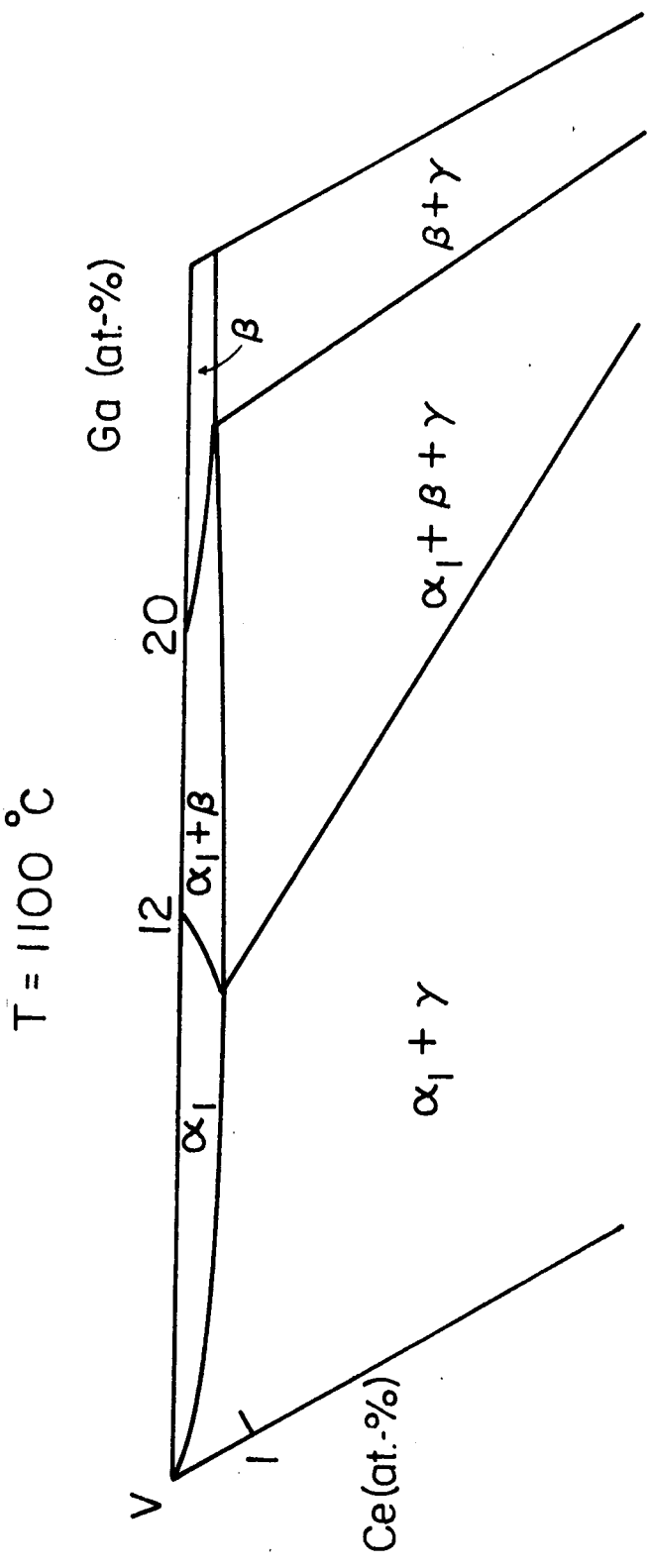

XBL 808-5698

Fig. V-23

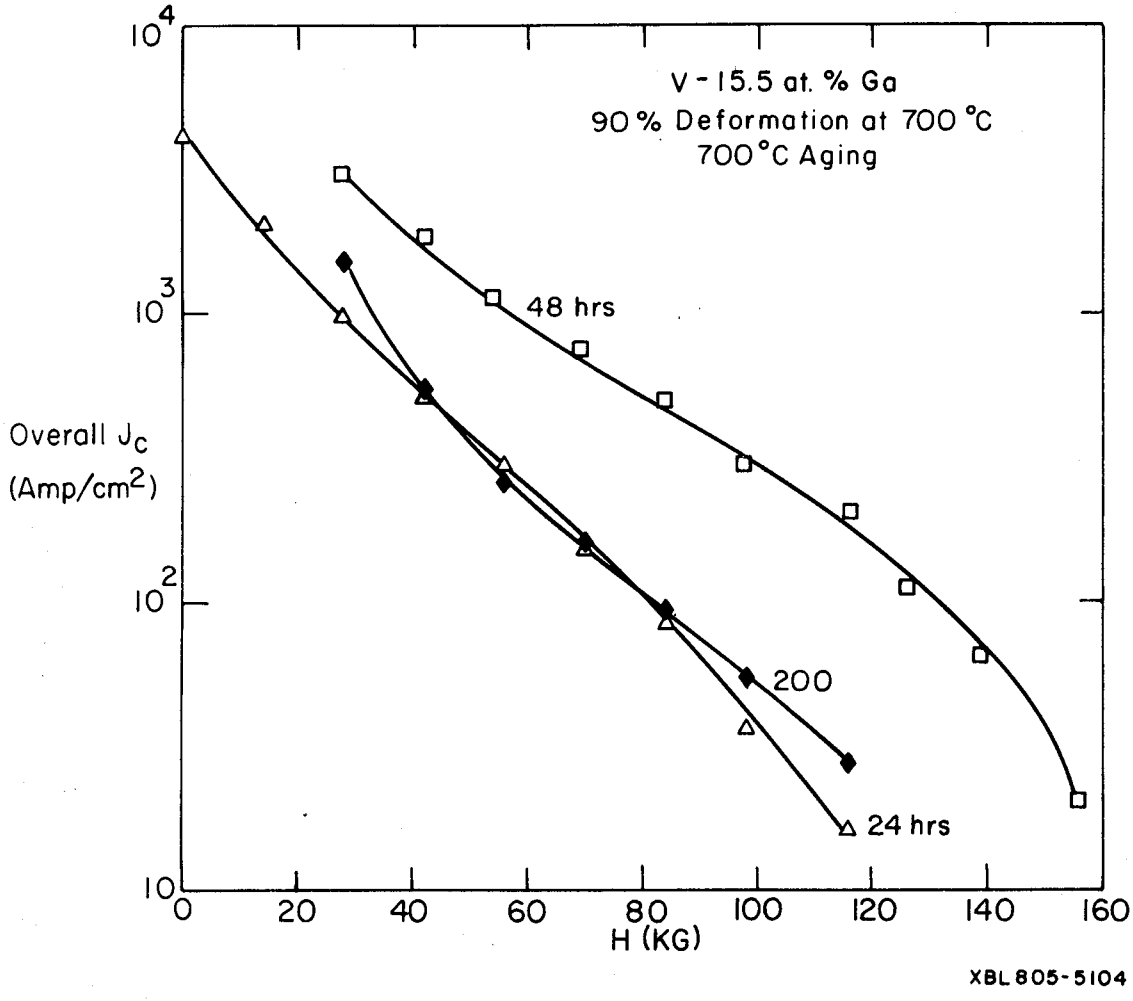
V - 15.5 at. % Ga
90 % Deformation at 700 °C
700 °C Aging
48 hrs
200
24 hrs
Overall J_c
(Amp/cm^2)
10^4
10^3
10^2
10
0
20
40
60
80
100
120
140
160
H (KG)
XBL 805-5104

Fig. V-24

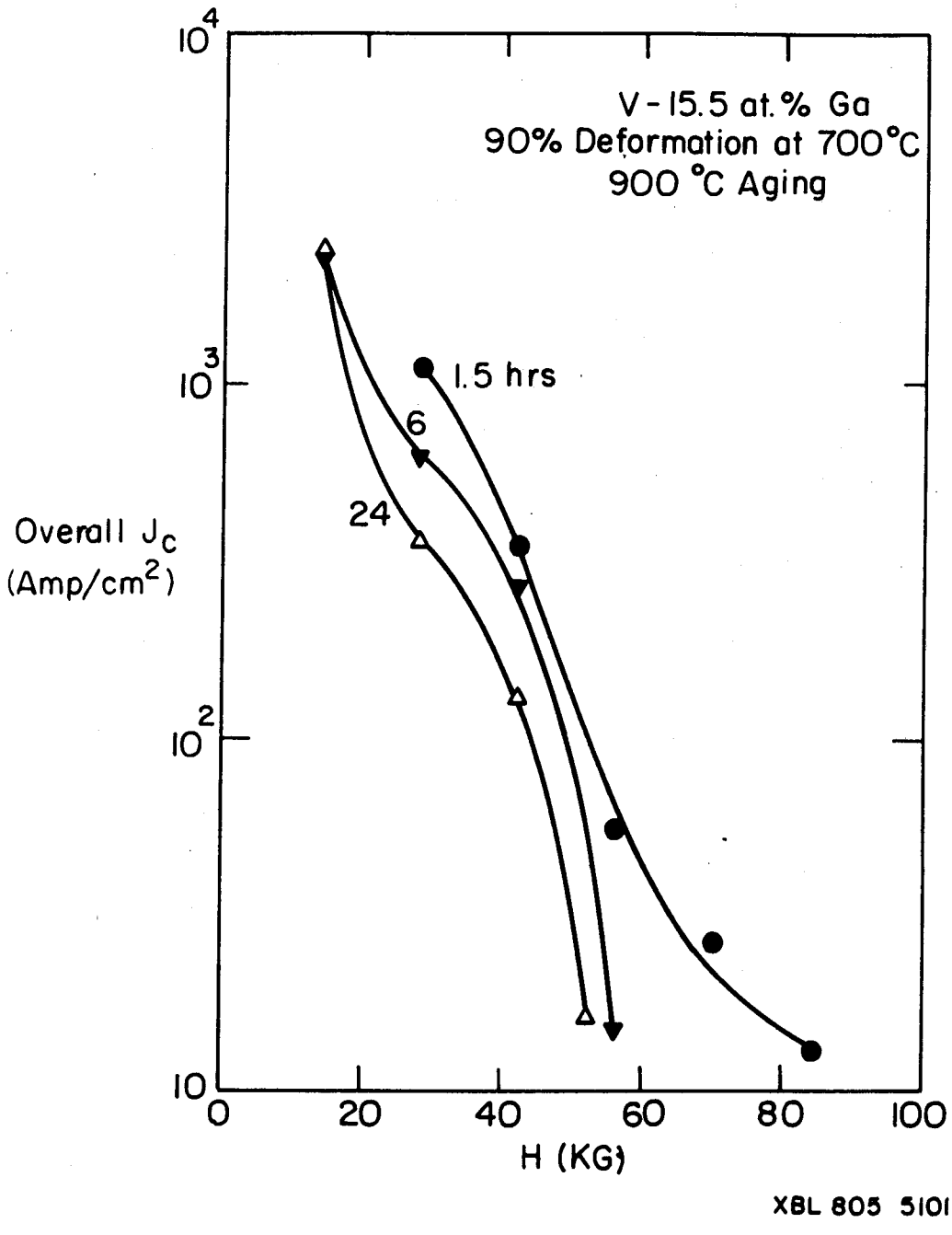
V - 15.5 at.% Ga
90% Deformation at 700°C
900 °C Aging
1.5 hrs
6
24
Overall J_c
(Amp/cm^2)
10^4
10^3
10^2
10
0
20
40
60
80
100
H (KG)
XBL 805 5101

Fig. V-25

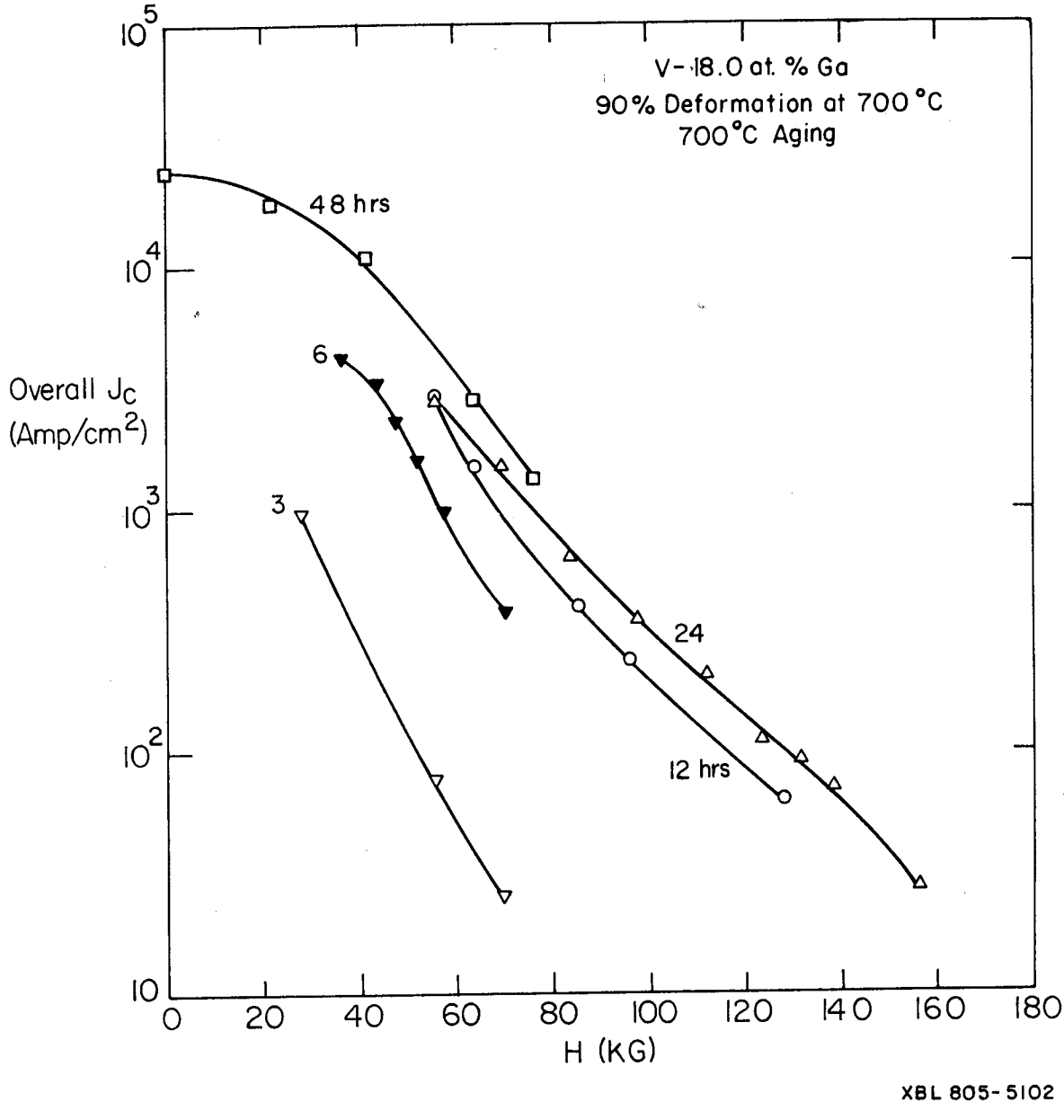
V-18.0 at. % Ga
90% Deformation at 700 °C
700°C Aging
48 hrs
6
3
24
12 hrs
Overall J_C
(Amp/cm^2)
10^5
10^4
10^3
10^2
10
0
20
40
60
80
100
120
140
160
180
H (KG)
XBL 805-5102

Fig. V-26

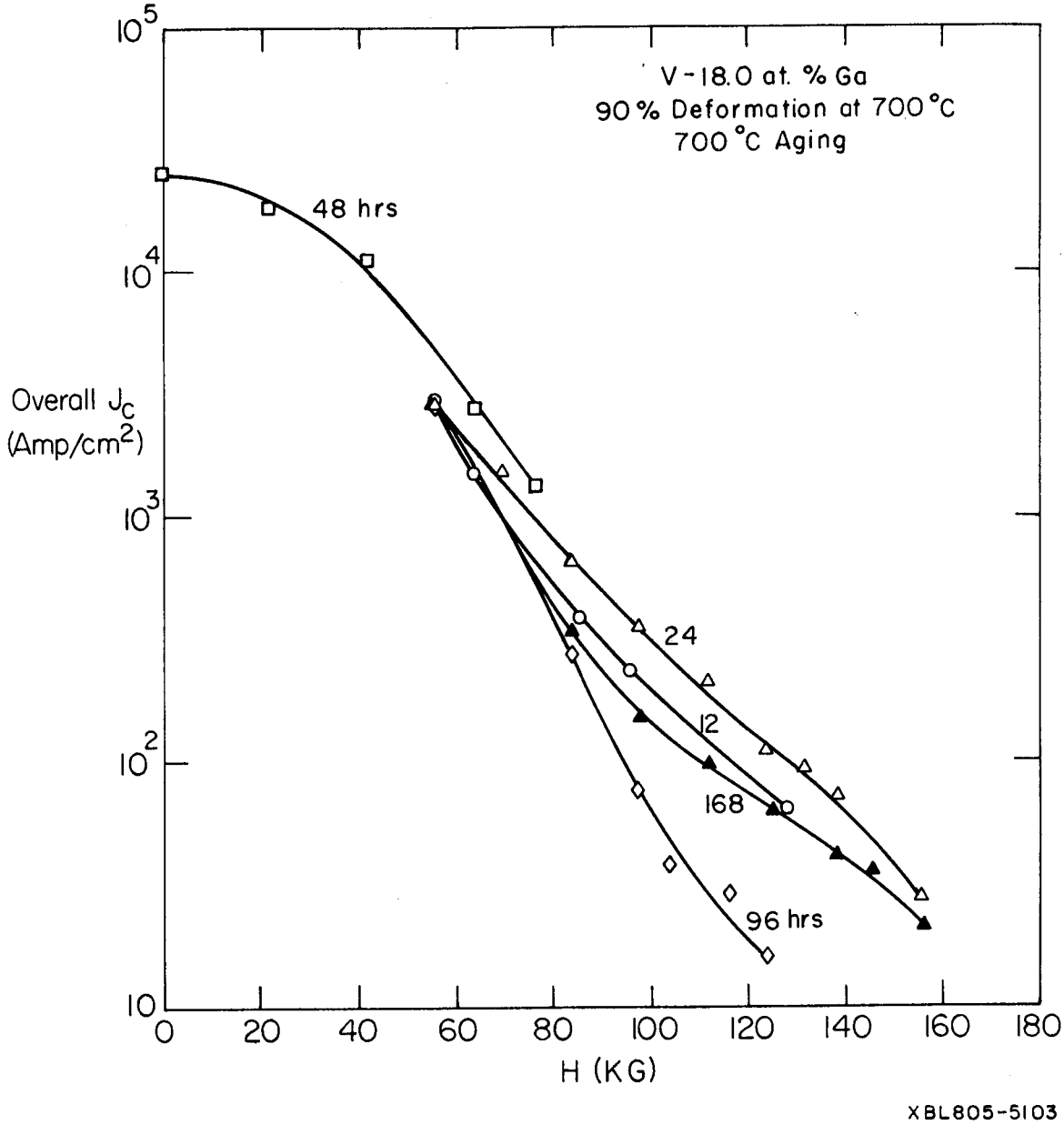
V - 18.0 at. % Ga
90 % Deformation at 700 °C
700 °C Aging
48 hrs
24
12
168
96 hrs
Overall J_c
(Amp/cm^2)
10^5
10^4
10^3
10^2
10
0
20
40
60
80
100
120
140
160
180
H (KG)
XBL805-5103

Fig. V-27

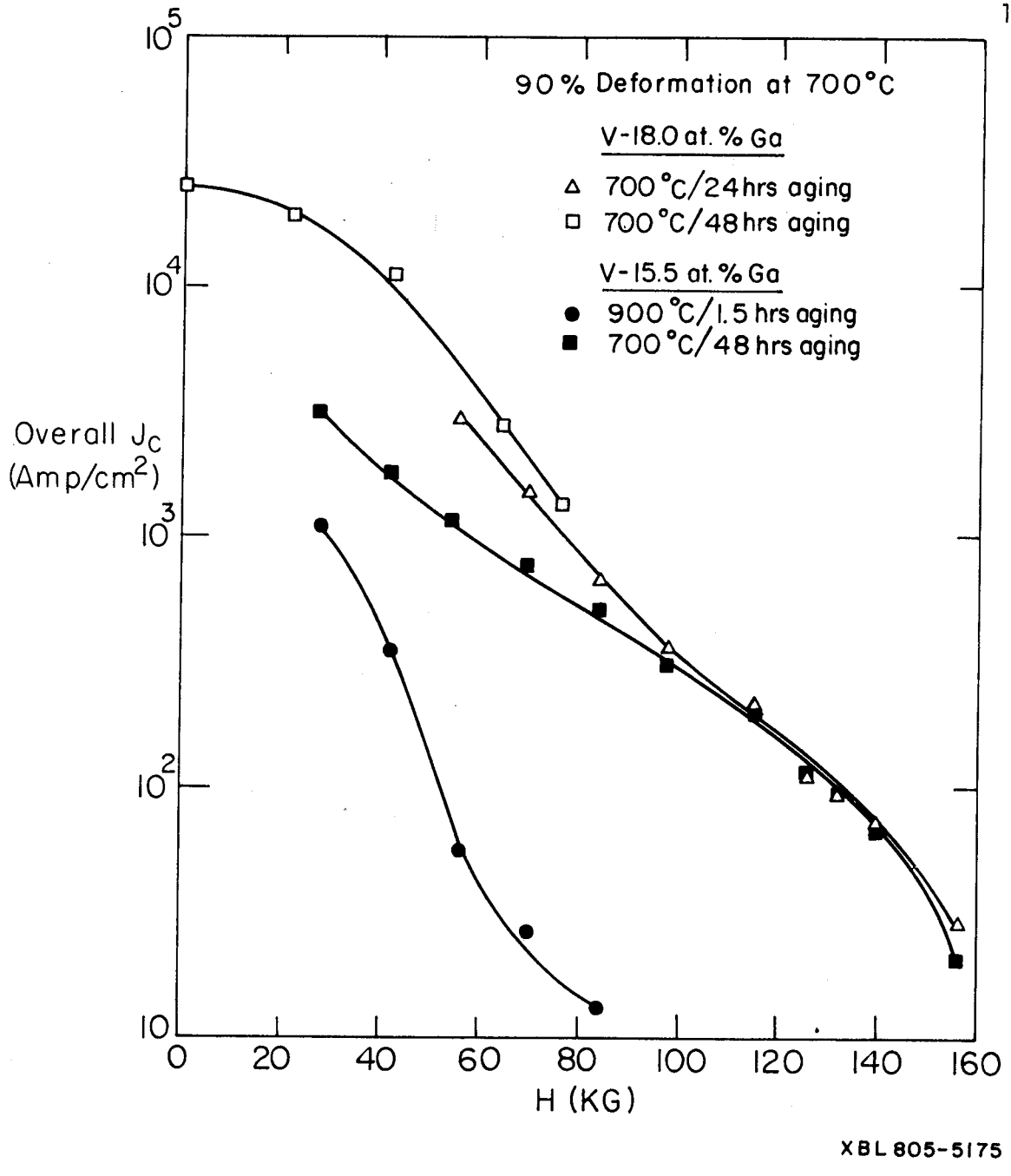

XBL 805-5175

Fig. V-28

VI. A15 SUPERCONDUCTORS THROUGH DIRECT "SOLID-STATE" PRECIPITATION: Nb_3Al

A. Difficulties in Synthesizing A15 Nb_3Al Compounds

The intermetallic compound Nb_3Al with A15 crystal structure was found to be a superconductor with a T_c of 17.5 K[1,2]. The T_c onset was then raised to 18.8 K by some variety of heat treatments[3]. The Nb-Al system is one of the high-T_c second-class A15 superconducting materials which is always Nb rich (compared with the 3:1 stoichiometric ratio) when prepared from melt, by equilibrium solid-solid reactions, or by equilibrium solid-liquid reactions (see the equilibrium Nb-Al phase diagram, Fig. IV-3 or IV-4). Unlike forming the stable high-T_c first-class A15 superconductors, it is extremely difficult, if not impossible, to synthesize the high-T_c A15 Nb_3Al compound in obtaining both a perfect ordering state and a 3:1 stoichiometry at the same time. A nearly stoichiometric A15 compound of the Nb-Al system may be obtained by some non-equilibrium method. The ordering parameter can be increased by aging the tested material for a long time; however, as indicated in the Nb-Al equilibrium phase diagram, the Al-content of the A15 compound becomes lean with a long aging treatment. The heat capacity experiments showed a much broader superconducting to normal state transition for the Nb_3Al than the Nb_3Sn[3-5]. This evidence indicates that the high T_c (~18 K) part of the Nb_3Al prepared by the existing methods, conventional bulk[3] or thin film techniques[6], is only a small portion of the whole specimen. Furthermore, resistivity measurements on Nb_3Al invariably showed a low resistivity ratio, less than 2.0[7], which indicates strong electron scattering by impurities, defects, or disorder (see Eq. II.1).

B. Excellent Superconducting Properties of A15 Nb_3Al Compounds

Despite the small portion of the high T_c region and the inhomogeneous distribution of the composition in the Nb_3Al A15 materials, the upper critical magnetic fields have been found to be over 300KG[8]. Moreover, after systematically studying their specimens prepared by the electron-beam coevaporation technique, Kwo et al.[6,9] have recently shown a correlation between the H_{c2}'s and T_c's as indicated in Table VI-1; they showed that an $H_{c2}(0)$ of 300KG has been found to be in the specimen with a T_c of 16K. $H_{c2}(0)$'s of 230KG and 150KG are found to be in the specimens with T_c's of 14.5K and 11.4K, respectively. It should be noted that for the Nb_3Sn sample having a T_c of 18K, its $H_{c2}(0)$ was found to be 240KG. However, with some "dirtying" efforts, e.g., decreasing the ordering parameter, the H_{c2}'s of the Nb_3Sn samples were raised to about 280KG, although the T_c's were made lower to 16K. These experimental data about the Nb_3Sn specimens coupled with the low resistivity ratio of the Nb_3Al specimens suggest that the high H_{c2} of the Nb-Al A15 phase is probably caused by, in addition to the intrinsic characteristics, the inhomogeneities of the Nb_3Al sample.

Webb et al.[12-14] recently used a somewhat similar monolithic solid-state precipitation process to obtain Nb_3Al A15 structure converted from cold-worked BCC structure; the critical current densities at 20 T and 4.2K have been shown to be about 10^5 A/cm^2. It is known that for the A15 superconducting materials, the $J_c(H)$ values can be increased with a finer grain size of the A15 phase. Using the liquid-quenched method, Lo et al.[15] were also able to obtain high $J_c(H)$ data, 10^6 A/cm^2 at 150KG and 4.2K, in the Nb_3Al samples doped with silicon (Si). The exceptionally

high $J_c(H)$ values obtained by both groups can be explained by the fine grain size of Nb_3Al (A15) phase and/or the existence of Nb_2Al (σ) phase; the grain boundaries and the second phases (superconducting or non-superconducting) are believed to be the very important flux pinning centers: the stronger the flux pinning, the higher the $J_c(H)$ values.

The research materials exhibiting those exceptional properties were, however, made using processes which cannot be scaled up to produce superconducting wires in useful lengths; moreover, the tapes produced by the methods mentioned above[12-15] consist of the intermetallic compounds, Nb_3Al and Nb_2Al, and are thus unavoidably brittle. Since the "Bronze"[16] and "In-Situ"[17] (Tsuei) processes used in the manufacture of multifilamentary Nb_3Sn and V_3Ga superconducting wires are inapplicable to Nb_3Al for thermodynamic reasons[18], the practical utility of Nb_3Al depends on the identification of new and suitable wire manufacturing techniques. Relevant research is hence underway in a number of laboratories[19-22].

C. Processes in Making A15 Nb_3Al Superconducting Materials

Due to the excellent superconducting properties of Nb_3Al A15 materials, many methods have been developed to produce useful forms of the Nb-Al systems. Some of the early attempts are discussed in the following:
(1) Isao et al.'s[23] and Kohr et al.'s[24] efforts in which Nb foil strips were coated with Al, the whole samples were heat treated at low temperatures (800-900°C) to allow Al to diffuse into Nb foils, and then reacted at very high temperature (~1870°C) to form Nb_3Al compounds.

(2) Rose et al.'s[25,26] method in which Nb and Al powders were mixed, pressed, inserted into tubes, then swaged or rolled into wires or tapes, and finally reacted at very high temperatures to form A15 Nb_3Al compounds, and

(3) cold-welding processes including: (a) aluminum tube swaged onto niobium rod[25], (b) niobium tube swaged onto aluminum rod[25], (c) Nb and Al sheets put together in a composite[26] or spiral form[21] and then swaged or rolled to final forms; in all cases, a final heat treatment was used to form an A15 Nb_3Al layer.

The common feature of the methods mentioned above is that the Nb_3Al A15 phase was formed by chemical reactions between solid Nb and liquid Al. For most methods, equilibrium conditions were used in the final heat treatments; according to the published equilibrium phase diagrams (see Figs. IV-3, 4) the high T_c Nb_3Al compounds, i.e., the closer stoichiometric A15 compounds, can only be obtained by heat-treating the tested samples at very high temperatures (~1600°C) under the equilibrium conditions.

Heat treatments at high temperatures to form superconducting phases are usually avoided due to the folliwing reasons: first, the difficulty in finding stabilizing materials such as copper and aluminum which are necessary in constructing real conductors for preventing thermal instabilities, and are usually low melting point materials; second, the inevitability in producing large A15 grains which are not desirable in enhancing the critical current density $J_c(H)$, since in the A15 superconducting materials, grain boundaries are believed to be strong flux pinning centers. Smaller grain-size A15 superconducting materials may

also be beneficial to the mechanical properties such as less degradation of superconducting properties under strain. The small A15 grains can be obtained by heat treating the tested samples at the low temperatures. Under equilibrium conditions, however, as indicated in the Nb-Al phase diagrams the superconducting A15 phase obtained has the Al-content somewhat less than 21 at.% and the superconducting properties such as T_c's are thus poor[6,27] (see Fig. VI-1).

Nevertheless, under non-equilibrium conditions high T_c A15 phases can be obtained by the solid-liquid reactions at lower temperatures (1100°C or lower): Using this approach, Ceresara et al.[21] were able to obtain reasonably good results, $T_c \sim 15.6K$ and $J_c \sim 10^5$ A/cm^2 at 4.2K and 6 T. These optimal conditions can be obtained by choosing appropriate amounts of Nb and Al elements (either in foil or powder forms), the final particle sizes of Nb and Al involved in the reactions, the reaction temperatures, and the heat-treatment time. Accordingly, a powder metallurgy method can be more effective in reaching the optimal conditions than the technique used by Ceresara et al.[21]. This powder approach includes mixing the appropriate amounts of Nb and Al powders, putting and pressing them into a Cu-Ni or Be-Cu tube, swaging the tube down to the final product, and then heat treating it at low temperatures to produce the superconducting phase. The research on this approach is now underway in a number of laboratories[20,22]. A systematic work is now being carried out on the study of the microstructure and chemistry of the final fine wire under various aging temperatures and different periods of time.

It should be noted that in both the powder metallurgy approach and the method used by Ceresara et al., the brittle A15 phase is embedded in a ductile matrix of Nb.

The superconducting A15 phase for all the methods mentioned above is formed through the solid Nb-liquid Al reaction. In the following, we will discuss a different method in making the Nb-Al superconducting materials. As described in the last two chapters, a newly developed monolithic process called the direct "solid-state precipitation" method has been used to produce superconducting materials from the V-Ga which have high critical transition temperatures and reasonable overall critical current densities[28,29]. The purpose of this chapter is to report the results from similar research on the Nb-Al system.

Samples with compositions ranging from Nb-13 at.% Al to Nb-22 at.% Al were chosen. They were arc-melted and cast as 12 mm-diameter rods, weighing around 30 gms for each sample. They were then homogenized at high temperatures and then quenched to an ice-brine solution to retain the BCC phase. It requires a much faster quenching rate in the Nb-Al system than in the V-Ga system in order to prevent the formation of the A15 phase. The as-quenched materials were deformed at 400°C or below. The brittle superconducting A15 phases were precipitated out and embedded in the relatively ductile BCC phase after final heat treatments.

D. Results and Discussions

1. Casting, Homogenization, and Quenching

Chemical segregation appears in the microstructures of the cast materials, as shown in Figs. VI-2, 3. The segregation and the dendritic pattern arise during the solidification process. For the cast samples

with the Al content being 16 at.% or more, the A15 and the BCC phases were both found by x-ray diffraction analysis. For the samples with the less Al content, however, the A15 phase was not found by the same technique. These phenomenon can be explained in terms of the Nb-Al phase diagram (see Fig. IV-3 or 4); for the higher Al content samples, the A15 phase precipitates at high temperatures (~1700°C) during the casting, and the kinetic rate of the A15 formation is fast at high temperatures. It should be noted here that the Nb-Al samples were cast on the water-cooled copper hearth. It took less than 10 minutes to cool samples from high temperatures down to room temperature. For the lower Al content samples, e.g., Nb-13 at.% Al, the A15 phase begins to precipitate at ~1100°C. At these low temperatures, it is not favorable to form the A15 in a very short period of time.

For the arc-cast Nb-Al samples, the level of oxygen and nitrogen interstitial impurities is quite low (~0.01 w/o N and ~0.05 w/o O), comparing with that of the cast V-Ga samples (see Tables V-1 and 2).

For the cast samples with compositions ranging from Nb-13 at.% Al to Nb-20 at.% Al, no internal crack or shrinkage porosity was found. However, the cast samples with higher Al compositions (more than 21 at.% Al) showed severe internal defects, such as cracks, porosities, and large-scale inhomogeneities. This kind of sample preparation problem was also encountered in the research of other laboratories[12]. The effort to improve and/or solve the situation of the severe defects in the cast materials is now underway.

Homogenization at 1930°C for 1 hr was found to be adequate to eliminate the chemical segregation and the dendritic pattern of the cast

structure. In order to obtain the supersaturated BCC solid solution in the Nb-Al system, quenching had to be carried out by dropping the sample in an ice-brine solution. The contrast of the requirement of the quenching rate between the V-Ga and the Nb-Al systems is probably due to different diffusion rates of Al in the Nb-Al samples and Ga in the V-Ga samples. In Fig. VI-4, we show the optical micrograph of the BCC phase, which resulted from an adequate homogenization and quenching. However, for the inadequate treatments some residual second-phase particles may still exist in the as-quenched condition.

As a summary of this section, we would like to indicate that for the cast samples with compositions of 20 at.% Al or below, no internal cracks were found. Furthermore, samples of Al compositions up to 22 at.% weighing 30 gms could be homogenized and quenched to retain the BCC phase. Besides the internal cracks which already existed in the high Al composition samples (<21 at.% Al) during the casting, no other quenching cracks were observed.

2. Mechanical Deformation

Given the integrity of the as-quenched specimens they could be deformed severely at room temperature without catastrophic failure. However, some cracking did occur during cold deformation. A scanning electron microscopic examination of these fractures revealed a mixed cleavage and dimpled fracture mode (Figs. VI-5 and 6), which suggests that the cracking has its source in the relatively large grain size established during homogenization. The relevant properties which affect the ductile-to-brittle transition temperature (DBTT) of BCC alloys were discussed in the previous chapter. To avoid low temperature brittleness,

the samples were warm-rolled into tape at temperatures between 300° C and 400° C. At these temperatures deformation of up to 99% could be accomplished without fracture.

A measurement of the critical transition temperature of the tested samples after 400° C deformation gave no T_c above 5 K. The existence of the A15 phase could not be detected by x-ray diffraction analysis. The optical micrographs of the Nb-18 at.% Al samples, deformed 90% at 400° C, are shown in Figs. VI-7,8. Fig. VI-9 is the TEM picture of the as-deformed condition in which only the BCC phase was observed. We would like to mention that the as-deformed samples of the BCC phase are ductile; they can be bent or even folded without breakage.

3. Precipitation of the A15 Phase

Following deformation, the samples were annealed for various periods of time at temperatures in the range of 600° C to 900° C to precipitate the A15 phase. A systematic examination of the consequences of these aging treatments is now in progress. However, preliminary results show a marked dependence of the size and morphology of the A15 precipitates on the aging treatment and the prior deformation, a dependence which is due in part to the interaction between the precipitation process and the recovery of the deformation-induced defects. Fig. VI-10 shows a transmission electron micrograph of a Nb-17.7 at.% Al sample which was deformed 99%, then aged for 3 hrs at 900° C. In this case, almost all of the deformed BCC solution has transformed to the A15 phase. The grains of the A15 phase are large and elongated, having widths on the order of 1000 Å and lengths closer to 5000 Å.

Both the A15 phase and the residual matrix are low in dislocation density. A similar sample aged 3 hrs at 750°C, however, has a very different microstructure (Fig. VI-11). The dislocations present in the deformed BCC matrix have apparently recovered into sub-cells a few microns in size. Fine, equi-axed A15 particles of diameters near 300 Å are precipitated along the cell walls in a continuous or semi-continuous network. Since a fine A15 grain size is expected to enhance the critical current density through strong flux pinning at the grain boundaries, the latter microstructure should be conducive to a high critical current, provided, of course, that the A15 particles have good inherent superconducting properties and are present in a reasonable fraction.

There is a strong contrast in the precipitation mode between the Nb-Al and the V-Ga systems. In the V-Ga system, nucleation of the A15 phase is heterogeneous (Figs. VI-12, V-6~9), while in the Nb-Al system, it is homogeneous (Figs. VI-13~15). Figure VI-12 is an optical micrograph of the V-14.5 at.% Ga samples, which were homogenized, air-cooled, and then aged at 900°C for 1 day and for 4 days. It is clear that the A15 phase precipitated mainly along grain boundaries and later grew toward the interior of the grains. The heterogeneity can also be observed in Figs. V-6~9.

For the Nb-Al system, however, the precipitation of the A15 phase is entirely different. An optical micrograph of the Nb-16 at.% Al samples is shown in Fig. VI-13, which were homogenized, quenched, and then aged at 750°C for 1 day. Clearly, the feature of the precipitation is homogeneous. Optical micrographs of the Nb-17.7 at.% Al samples deformed and aged at 900°C and 750°C for 3 hrs are shown in Figs. VI-14 and VI-15, respectively The homogeneity of the A15 phase nucleation is indicated in these two figures. Of course, the more detailed microstructures can only be obtained.

using high resolution transmission electron microscopy. The initial TEM results were shown in Figs. VI-10,11.

It should be noted here that the Nb-17.7 at.% Al sample, deformed 99% and then aged 3 hrs at 750°C, can be bent without fracture. This means that the product is flexible even with the existence of the brittle Al5 precipitates (see Fig. VI-11). However, the samples, deformed 99% and aged 3 hrs at 900°C (see Fig. VI-10), are brittle. The ductility of the sample is determined by the microstructures which are controlled by the prior deformation and the aging treatment. We expect that a higher degree of deformation and a lower temperature aging could create a microstructure with finer Al5 grains and a more uniform distribution of these precipitate particles; with this microstructure, a better overall J_c and mechanical property may be produced.

4. Superconducting Properties: Critical Transition Temperature (T_c) and Critical Current Density (J_c)

Three ingots were processed to provide specimens for initial tests of superconducting properties. The specimen compositions were Nb-16 at.% Al, Nb-17.7 at.% Al, and Nb-18.8 at.% Al.

For the T_c measurements, the specimen compositions and treatments were (1) Nb-17.7 at.% Al, deformed 90%, followed by aging for various periods of time at 750°C and 900°C; (2) Nb-18.8 at.% Al, deformed 90%, followed by aging for various periods of time at 750°C and 900°C; (3) Nb-16 at.% Al, not deformed, only aged for various periods of time at 750°C. The onset T_c as a function of aging time is plotted in Figs. VI-16~20 for various cases.

Figure VI-16 shows T_c values of the Nb-17.7 at.% Al samples, deformed 90%, followed by aging at 750°C and 900°C. The aging response at 900°C

of the tested specimens shows an increase of T_c to a first plateau at ~12.5 K, with another increase of T_c to a second plateau at ~13 K. The aging response at 750°C, however, gives a first plateau of T_c at ~13 K with a second plateau of T_c at ≥14 K. Similar phenomena were observed for the T_c values of Nb-18.8 at.% Al samples (see Fig. VI-17).

It is interesting to examine the effect of Al composition on the T_c values. Figures VI-18,19 show T_c values of both the deformed Nb-17.7 at.% Al and Nb-18.8 at.% Al samples, aged at 750°C and 900°C, respectively. It is clear that the curves are almost parallel to each other, with a higher T_c (~0.7 K) in the Nb-18.8 at.% Al samples in the case of 750°C aging and a higher T_c (~1 K) in the Nb-18.8 at.% Al samples in the case of 900°C aging.

A more profound characteristic of the T_c vs. aging time was found in the non-deformed Nb-16 at.% Al sample, followed by aging at 750°C. The aging response of the samples shows an increase in T_c to a plateau at ~11.5 K, with a second increase to T_c near 17 K after extended aging.

Reference to the equilibrium phase diagrams shown in Figs. IV-3,4 and the curve of T_c as a function of Al content shown in Fig. VI-1 reveals that for the sample compositions used here (16-18.8 at.% Al) and for aging temperatures of 750°C and 900°C, T_c's of the specimens fall below 10 K. It is the non-equilibrium Nb_3Al A15 phase which gives the exceptionally high T_c.

In Chapter V, we gave various reasons to explain the curves of the T_c vs. the aging time in the V-Ga system. Those arguments can be used to explain the similar phenomena in the Nb-Al system. Nevertheless, the shapes of the curves are entirely different between the V-Ga and the Nb-Al systems. In the V-Ga system, the T_c's increase smoothly as the aging time

is made longer, reach the maxima and then decline due to over-aging. In the Nb-Al system, however, the T_c's increase with the longer aging time, reach a plateau, and then increase again to reach another plateau. Even though this phenomenon was present in all the tested Nb-Al samples, the explanation for this observation is not yet clear. Longer heat treatments, such as overaging, are now being carried out in order to obtain the whole spectrum of the aging curve.

The compositions and treatments of the specimens which were used for measurements of the critical current densities at 4.2 K and high magnetic fields, are listed in Tables VI-2~4; they were (1) Nb-17.7 at.% Al, deformed 90%, followed by aging for various periods of times at 750°C and 900°C; (2) Nb-17.7 at.% Al, deformed 99%, followed by aging for 3 hrs at 750°C; (3) Nb-18.8 at.% Al, deformed 90%, followed by aging for various periods of time at 750°C and 900°C. The first two specimens were intended to show the effect of increased pre-aging deformation. The third was made to explore the effect of increased Al content.

Critical current densities were measured using a standard four-probe technique in transverse applied magnetic fields up to 190 KG in water-cooled Bitter solenoids. The critical current was taken to be that current at which the potential difference across the voltage leads (spaced 5mm apart) exceeds 1 μV, and the overall current density, J_c, was taken to be the critical current divided by the total cross-sectional area of the specimen. It should be noted that this total cross-sectional area consists of an A15 phase, a BCC phase, and/or a Nb_2Al (σ) phase. Therefore, the values of the true critical current densities are higher than those of the overall critical current densities, depending on the cross-sectional area of the superconducting A15 phase. The results of the

overall critical current densities under the transverse magnetic fields are plotted in Figs. VI-21,22, we know that for the samples with the composition NB-17.7 at.% Al, deformed 90% at 400°C, and followed by aging at 900°C, 45 minutes of aging is the optimal condition with the results of 4.0×10^3 A/cm^2 at 80 KG and 5.5×10^2 A/cm^2 at 100 KG. With an aging time longer than 45 minutes, the $J_c(H)$ values are decreased although the corresponding T_c values are increased. This can be attributed to the larger grain size which was caused by a longer heat treatment. Similar phenomena were also observed in the Nb-17.7 at.% Al samples aged at 750°C (see Fig. VI-23); 12 hrs aging at 750°C gives the $J_c(H)$ data of $\sim 10^4$ A/cm^2 at 80 KG and $\sim 10^3$ A/cm^2 at 100 KG. For the sample with the same composition but with a 99% thickness reduction, the $J_c(H)$ values are even better; they are 2×10^4 A/cm^2 at 80 KG and 5.5×10^3 A/cm^2 at 100 KG (see Fig. VI-24).

Increasing the Al content by 1%, to the 18.8 at.% Al, causes a still more profound increase in critical current density (see Figs. VI-25,26). After a 90% area reduction followed by aging at 900°C for 22.5 minutes, J_c of 1.8×10^4 A/cm^2 at 120 KG and 2.5×10^2 A/cm^2 at 150 KG. Aging at 750°C for 6 hrs raises $J_c(H)$ to an even better value: 2.5×10^4 A/cm^2 at 120 KG and 2×10^3 A/cm^2 at 150 KG.

Figure VI-27 is plotted to show the strong influence of the overall critical current density by both the prior deformation and the sample composition.

The $J_c(H)$ values are much higher in the Nb-Al system than in the V-Ga system, even though the onset T_c's of the V-Ga samples are higher than those of the Nb-Al samples. This can be attributed to a finer A15 grain size and/or a better connectivity of the A15 precipitate particles in the Nb-Al system. For the V-Ga and the Nb-Al systems, the different

microstructures are probably caused by the different precipitation mechanisms. A fundamental study of the precipitation in the A15 family is necessary if we want to obtain an optimal microstructure of the final product.

The overall critical current densities of $\geq 10^4$ A/cm^2 at 140 KG obtained in this work is much better than J_c of $\sim 10^4$ A/cm^2 at 60 KG obtained by Pan et al. using a similar approach[30].

The metallographic studies needed to complete the interpretation of these results are in progress, but initial metallographic observations suggest that the increase in J_c with prior deformation is associated with a finer grain size and distribution of the A15 phase. This is due to increased dislocation density and a finer cell structure. The principal effect of increasing Al content appears to be an increase in the volume fraction of the A15 phase, which improves both the connectivity of the superconducting phase and its areal fraction in the sample cross-section. Research toward further improvement of the overall critical current density of samples made by solid-state precipitation is in progress.

VI. REFERENCES

1. E. A. Wood, V. B. Compton, B. T. Matthias, and E. Corenzwit, Acta Crystallogr. 11, 604 (1958).

2. E. Corenzwit, J. Phys. Chem. Solids 9, 93 (1959).

3. R. H. Willens, T. H. Geballe, A. C. Gossard, J. P. Maita, A. Menth, G. W. Hull, Jr., and R. R. Soden, Solid State Commun. 7, 837 (1969).

4. A. Junod, J. L. Staudenmann, J. Müller, and P. Spitzli, J. Low Temp. Phys. 5, 25 (1971).

5. L. J. Vieland and A. W. Wicklund, Phys. Rev. 166, 424 (1968).

6. J. Kwo, R. H. Hammond, and T. H. Geballe, J. Appl. Phys. 51, 1726 (1980).

7. G. W. Webb, Z. Fisk, J. J. Engelharat, and S. D. Bader, Phys. Rev. B15, 2624 (1977).

8. S. Foner, E. J. McNiff, Jr., T. H. Geballe, R. H. Willens, E. Buehler, Physica 55, 534 (1971).

9. J. Kwo and T. H. Geballe, to be published.

10. R. R. Hake, Phys. Rev. 158, 356 (1967).

11. T. P. Orlando, E. J. McNiff, Jr., S. Foner, and M. R. Beasley, Phys. Rev. B19, 4545 (1979).

12. G. W. Webb, Appl. Phys. Lett. 32, 773 (1978).

13. G. W. Webb, IEEE Trans. on Magn. MAG-15, 616 (1979).

14. J. A. Woollam, S. A. Alterovitz, E. Haugland, and G. W. Webb, Appl. Phys. Lett. 36, 706 (1980).

15. K. Lo, J. Berk, and D. Turnbull, J. Appl. Phys. 48, 2597 (1977).

16. A. R. Kaufmann and J. J. Pickett, Bull Am. Phys. Soc. 15, 838 (1970).

17. C. C. Tsuei, J. Appl. Phys. 45, 1385 (1974).

18. T. Luhman, Treatise on Materials Science and Technology V. 14, 224 (1979), Ed. T. Luhman and D. Dew-Hughes, Academic Press and the references quoted in this article.

19. M. Hong and J. W. Morris, Jr., Submitted to Appl. Phys. Lett.

20. R. Akihama and S. Foner, (unpublished).

21. S. Ceresara, M. V. Ricci, N. Sacchetti, and G. Sacerdoti, IEEE Trans. or Magns., MAG-11, 263 (1975).

22. M. Hong, J. T. Holthuis, and J. W. Morris, Jr., (unpublished).

23. A. Isao, T. Noguchi, Y. Uchida, and A. Kono, J. Vac. Sci. Technol. 7, 557 (1970).

24. J. G. Kohr, B. P. Strauss, and R. M. Rose, IEEE Trans., N5-18 716 (1971).

25. J. G. Kohr, T. W. Eager, and R. M. Rose, Met. Trans. 3, 1177 (1972).

26. R. Löhberg, T. W. Eager, I. M. Puffer, and R. M. Rose, Appl. Phys. Lett. 22, 69 (1973).

27. S. Moehlecke, Ph.D. Thesis, Universidad Estudial de Campinas, Brazil (1977).

28. M. Hong, D. Dietderich, and J. W. Morris, Jr., J. Appl. Phys. 51, 2774 (1980).

29. M. Hong and J. W. Morris, Jr. (unpublished).

30. V. M. Pan, V. I. Latysheva, Ye. N. Khusid, V. N. Minakov, and Ye. V. Turtsevich, Fiz. Metal. Metalloved., 40, 512 (1975).

TABLE VI-1

Correlation between T_c's and H_{c2}'s of Nb_3Al samples prepared by electron-beam co-evaporation technique[6,*].

Nb-X at.% Al	T_c (K)	$H_{c2}(0)$[**,10] (KG)
22.5	16.0	296
22.3	15.6	243
21.7	14.5	230
20.1	11.4	147

* By the courtesy of Jueinai Kwo

** $$H_{c2}(0) = -0.693\ T_c \left(\frac{dH_{c2}(T)}{dT}\right)_{T \approx T_c}$$

TABLE VI-2

Nb-17.7 at.% Al
90% Deformation at 400°C
and 750°C Aging

Aging Time (hrs)	Overall J_c at 4.2K and 80KG (10^2 A/cm^2)	Overall J_c at 4.2K and 100KG (10^2 A/cm^2)	Overall J_c at 4.2K and 120KG (10^2 A/cm^2)	H_{c2}* (4.2K) (KG)
0	0	0	0	—
1.5	0.25	0.14	—	—
3	18	2.5	0.18	123
12	94	13	0.18	121
24	28	9	—	124
120	19	5.9	0.5	130

Nb-17.7 at.% Al
99% Deformation at 400°C
and 750°C Aging

2	200	55	6	136

* H_{c2} is determined from a plot of $J_c^{\frac{1}{2}} H^{\frac{1}{4}}$ versus H by extrapolating to $J_c = 0$.

TABLE VI-3

Nb-17.7 at.% Al
90% Deformation at 400°C
and 900°C Aging

Aging Time (hrs)	Overall J_c at 4.2K and 80KG (10^2 A/cm^2)	Overall J_c at 4.2K and 100KG (10^2 A/cm^2)	Overall J_c at 4.2K and 120KG (10^2 A/cm^2)	H_{c2}* (4.2K) (KG)
0	0	0	0	—
0.2	3.2	1.2	0.15	130
0.75	40	5.5	0.29	134
3	20	2.5	—	106
6	25	0.6	—	101
12	20	0.3	—	101
24	10	0.1	—	101

* H_{c2} is determined from a plot of $J_c^{\frac{1}{2}} H^{\frac{1}{4}}$ versus H by extrapolating to $J_c = 0$.

TABLE VI-4

Nb-18.8 at.% Al

90% Deformation at 400°C

Aging Temperature (°C)	Aging Time (hrs)	Overall J_c at 4.2K and 120KG (10^2 A/cm^2)	Overall J_c at 4.2K and 150KG (10^2 A/cm^2)	H_{c2}*(4.2K) (KG)
750°C	0	0	0	—
750°C	3	5	—	160
750°C	6	250	20	164
750°C	12	56	10	170
900°C	0.375	180	2.5	153
900°C	0.75	80	0.35	149
900°C	3	80	1.6	151

* H_{c2} is determined from a plot of $J_c^{\frac{1}{2}} H^{\frac{1}{4}}$ versus H by extrapolating to $J_c = 0$.

FIGURE CAPTIONS

Fig. VI-1. The critical transition temperature as a function of the Al content for the A15 phase in the Nb-Al system.

Fig. VI-2. Optical micrograph of arc-cast Nb-21.7 at.% Al samples.

Fig. VI-3. Optical micrograph of arc-cast Nb-15 at.% Al samples.

Fig. VI-4. Optical micrograph of homogenized and quenched Nb-Al samples.

Fig. VI-5. Scanning electron fractograph of a Nb-18.8 at.% Al sample broken at room temperature after homogenization and quenching, which revealed a mixed cleavage and dimpled fracture mode.

Fig. VI-6. A larger magnification of the dimple part in Fig. VI-5.

Fig. VI-7. Optical micrographs of as-deformed Nb-18.0 at.% Al samples.

Fig. VI-8. Larger magnification of optical micrograph of as-deformed Nb-18.0 at.% Al samples.

Fig. VI-9. Transmission electron micrograph of the as-deformed Nb-18.0 at.% Al sample showing a high density of dislocations and a BCC phase.

Fig. VI-10. The transmission electron micrograph of the Nb-17.7 at.% Al sample deformed 99% and then aged 3 hrs at 900°C.

Fig. VI-11. The transmission electron micrograph of the Nb-17.7 at.% Al sample deformed 99% and then aged 3 hrs at 750°C.

Fig. VI-12. Optical micrographs of the V-14.5 at.% Ga sample, homogenized, air-cooled, and aged at 900°C.

Fig. VI-13. Optical micrographs of the Nb-16 at.% Al sample, homogenized, ice-brine quenched, and aged at 750°C.

Fig. VI-14. Optical micrograph of the Nb-17.7 at.% Al sample deformed 90% and aged at 900°C.

Fig. VI-26. The overall J_c vs. the applied transverse magnetic field for Nb-18.8 at.% Al samples, deformed 90%, followed by 750°C aging.

Fig. VI-27. The overall J_c vs. the applied transverse magnetic field for Nb-17.7 at.% Al samples deformed 90%, followed by aging for 3~120 hrs (A), Nb-17.7 at.% Al samples deformed 99%, followed by aging for 2 hrs at 750°C (B), and Nb-18.8 at.% Al samples deformed 90%, followed by aging 6 hrs at 750°C (C).

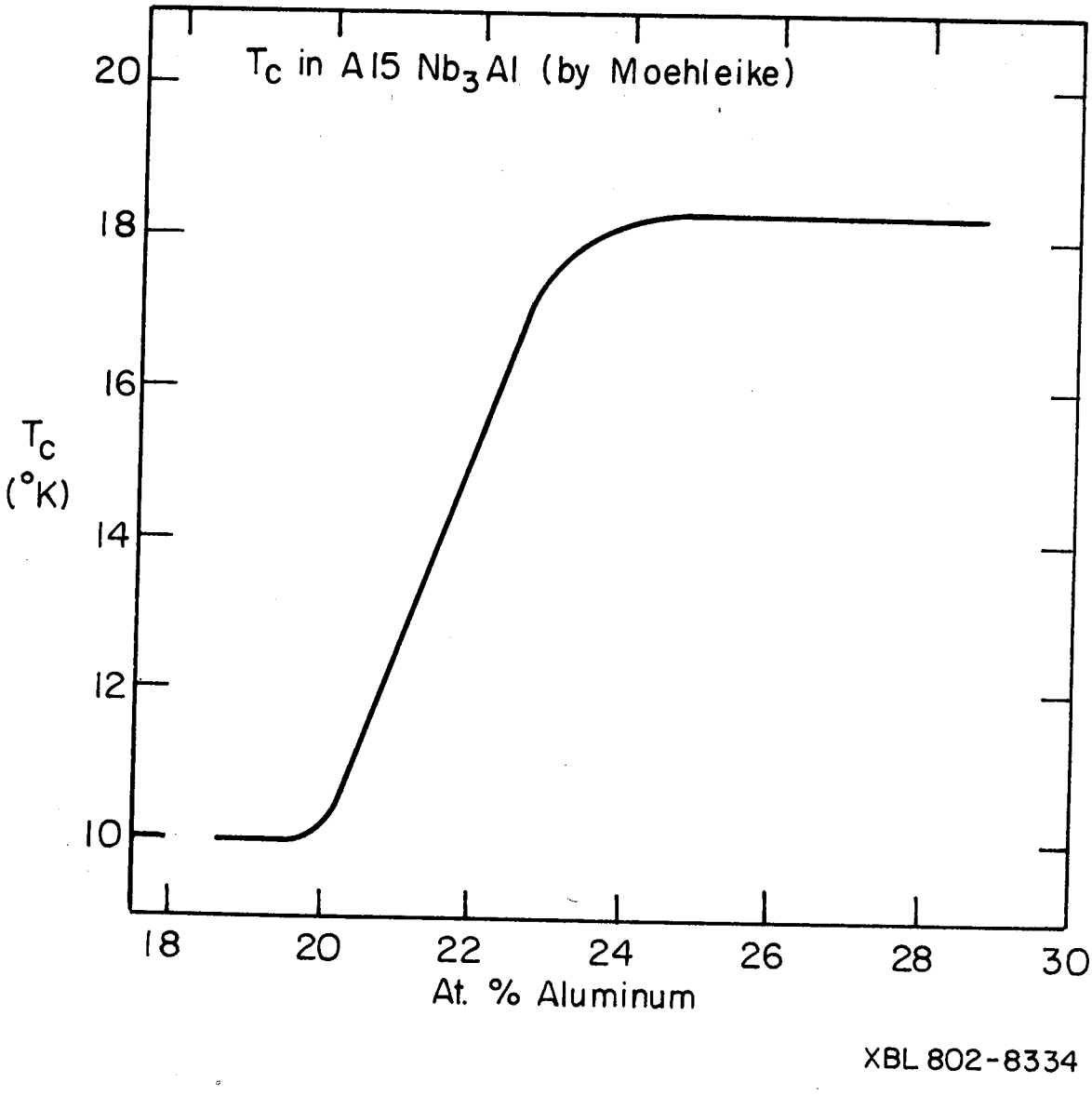
T_c in A15 Nb_3Al (by Moehleike)
20
18
16
14
12
10
T_c
(°K)
18
20
22
24
26
28
30
At. % Aluminum
XBL 802-8334

Fig. VI-1

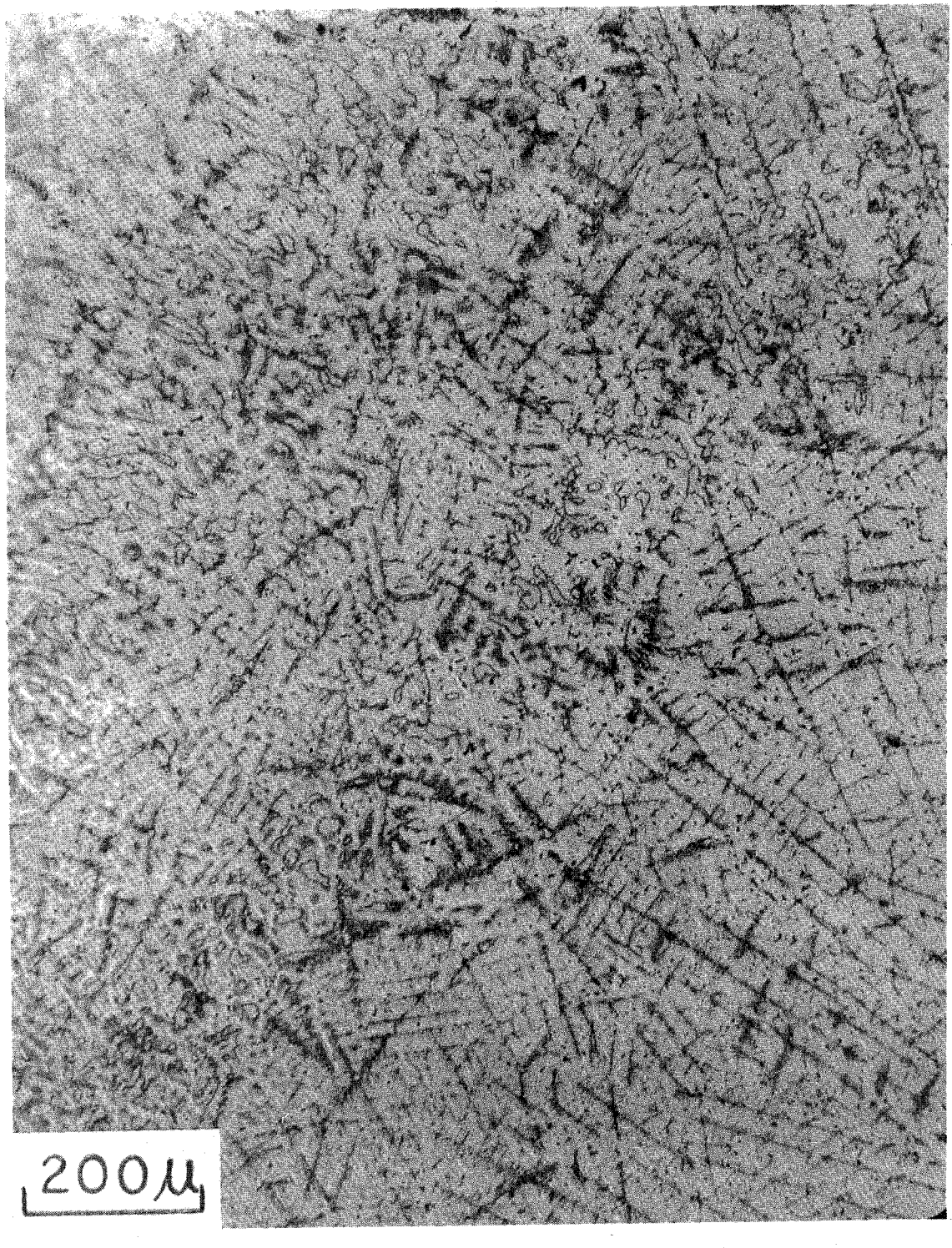

Fig. VI-2

XBB 808-9470

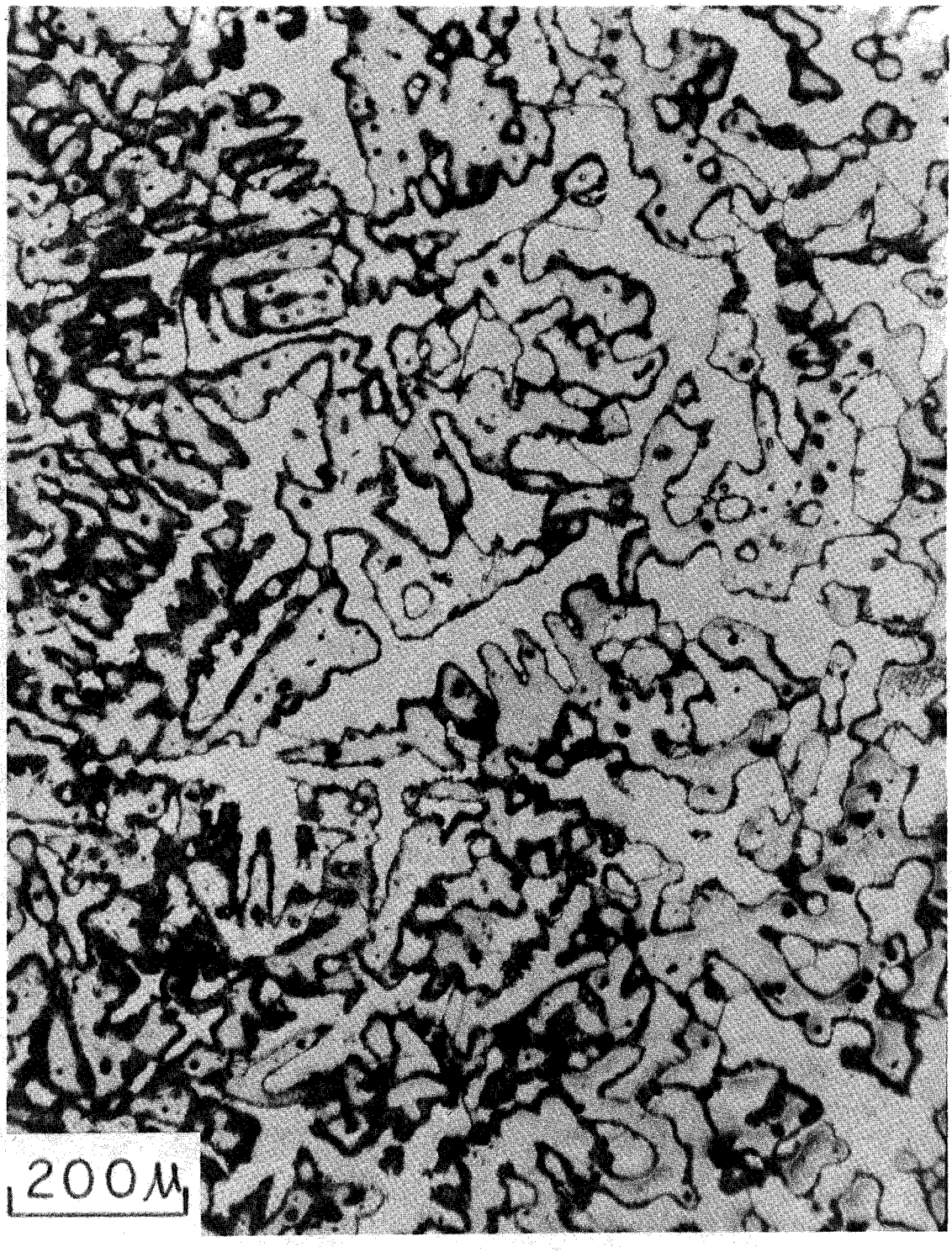

Fig. VI-3 XBB 808-9471

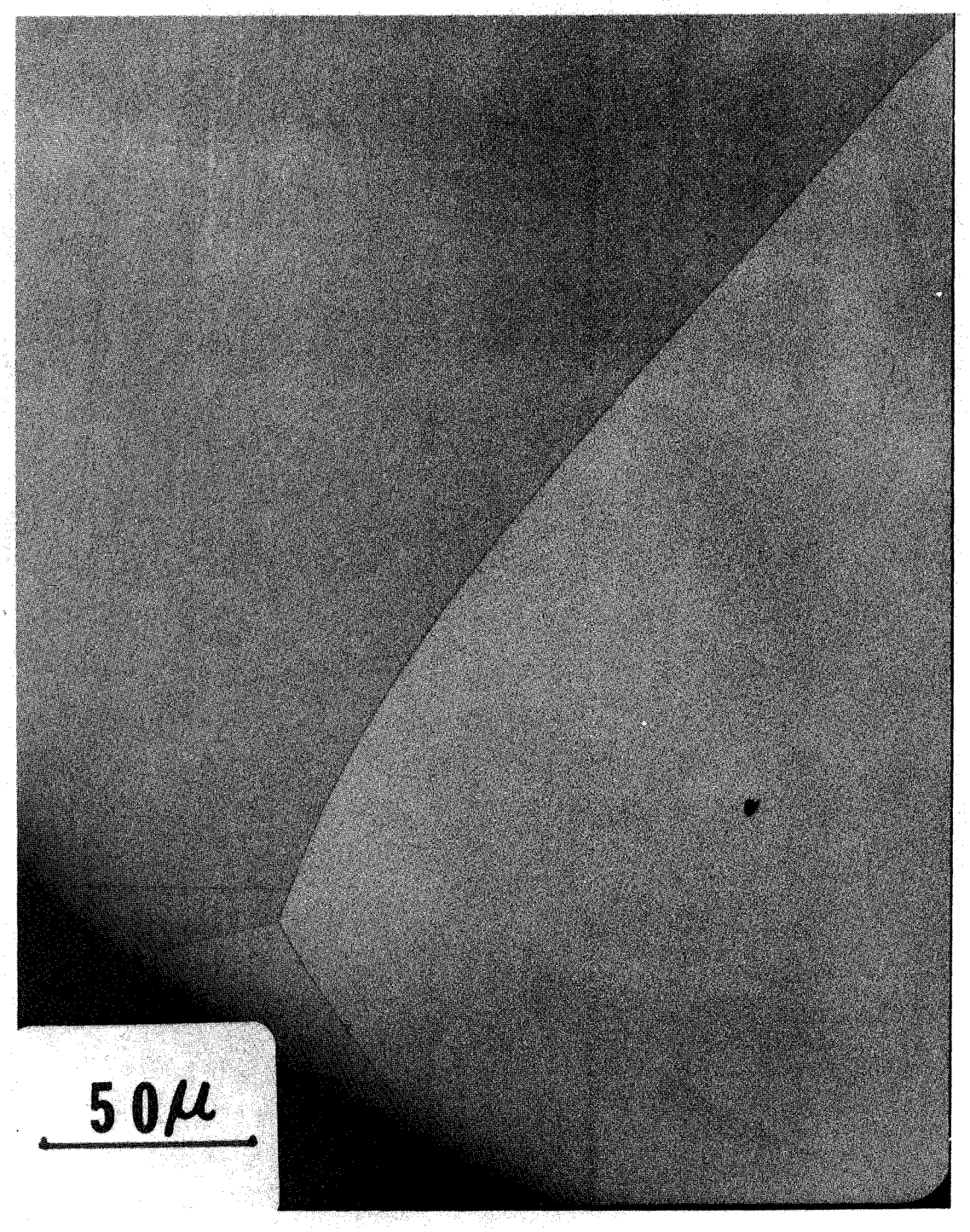

Fig. VI-4 XBB 801-409

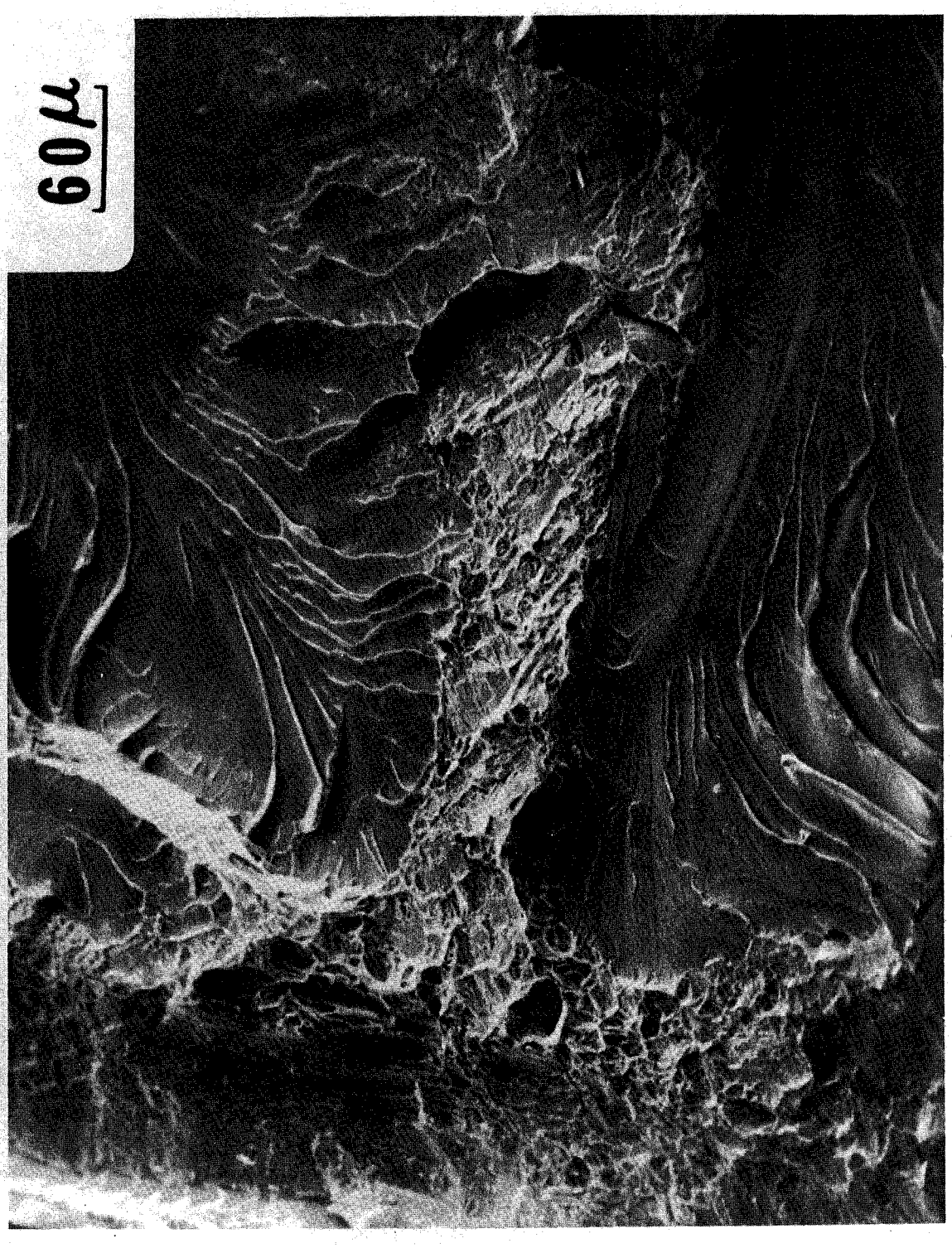

XBB 790-15800

Fig. VI-5

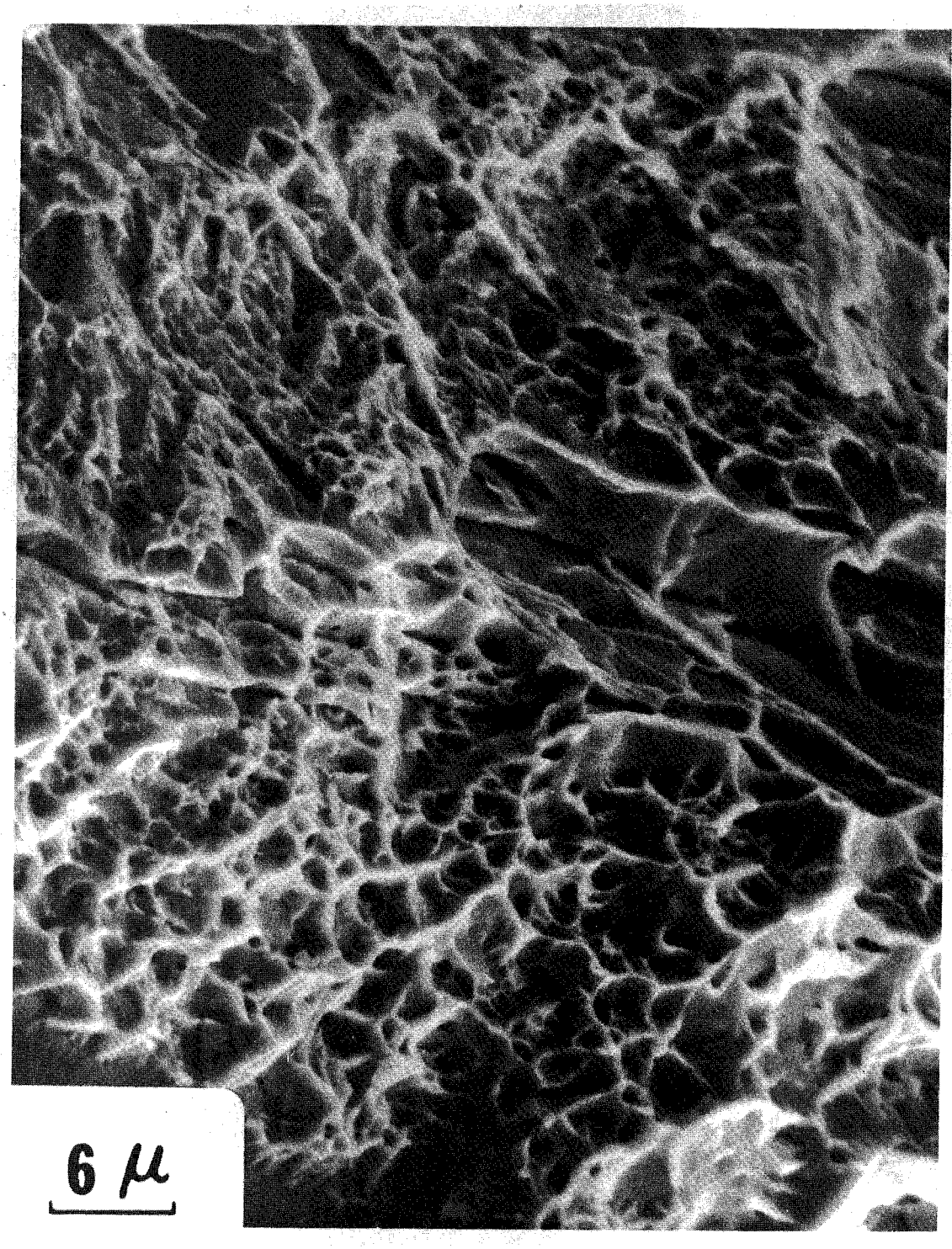

Fig. VI-6 XBB 790-15796

200μ

Fig. VI-7

XBB 808-9469

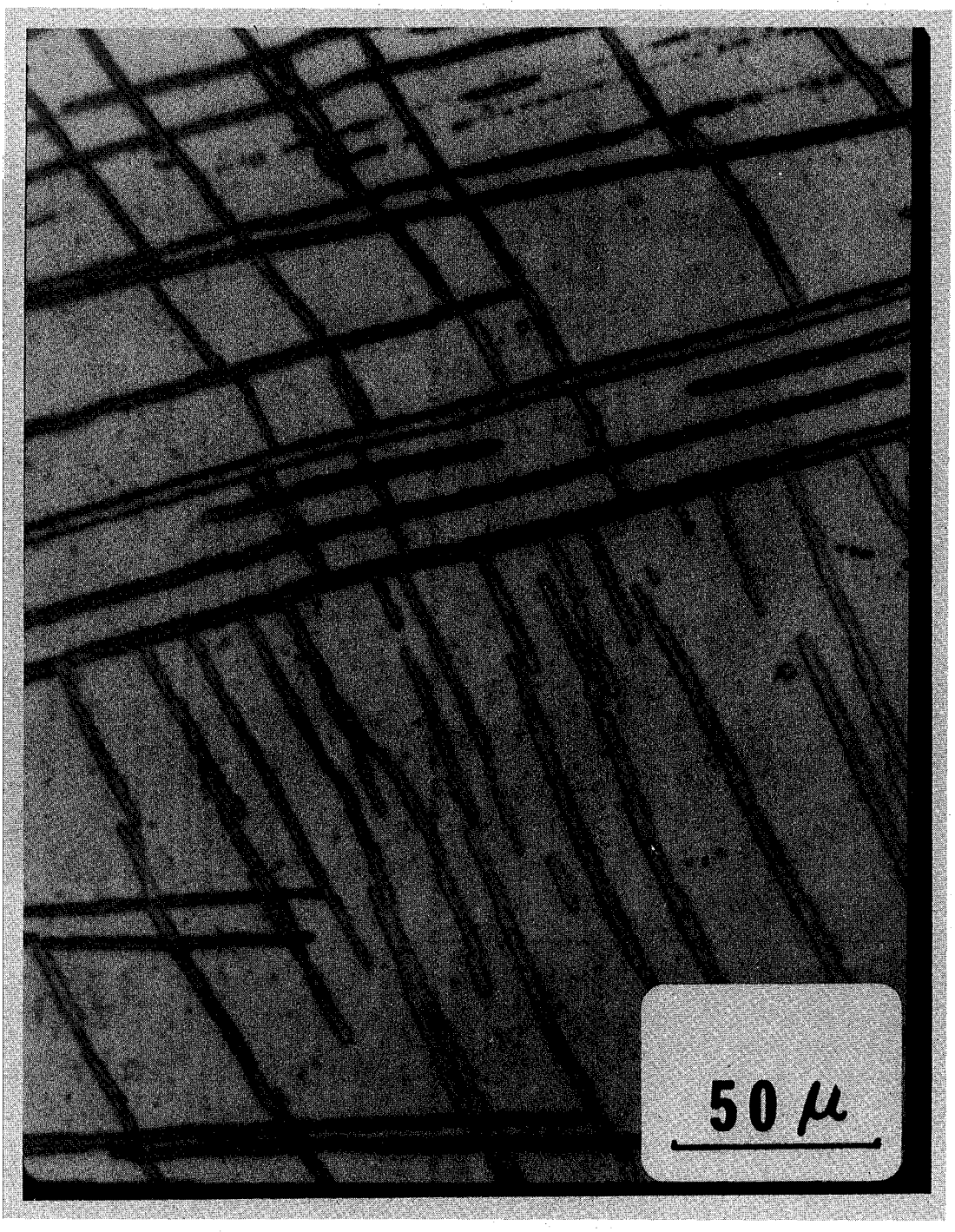

Fig. VI-8

XBB 801-407

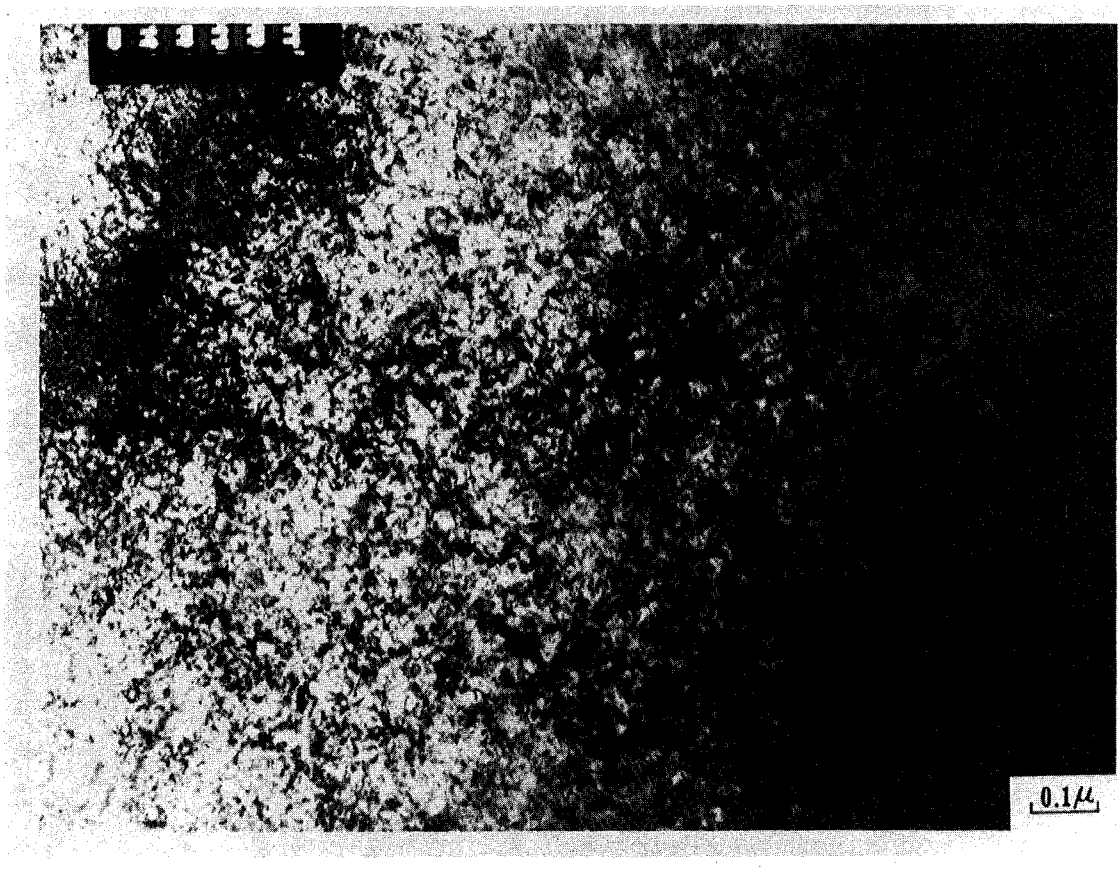

Fig. VI-9 XBB 802-2122

Fig. VI-10

XBB 802-1969

Fig. VI-11

XBB 802-2119

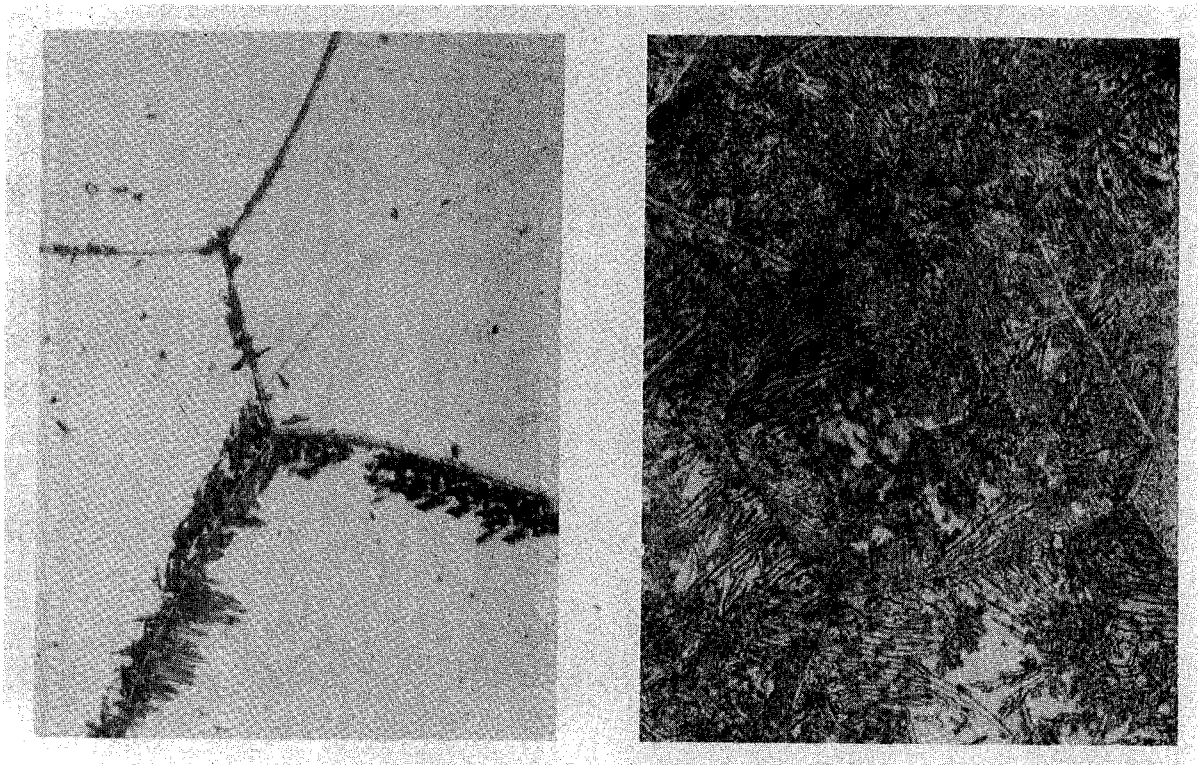

24 HOURS

96 HOURS

V-14.5GA HOMOGENIZATION/A.C.
900°C AGING

Fig. VI-12 XBB 802-1967

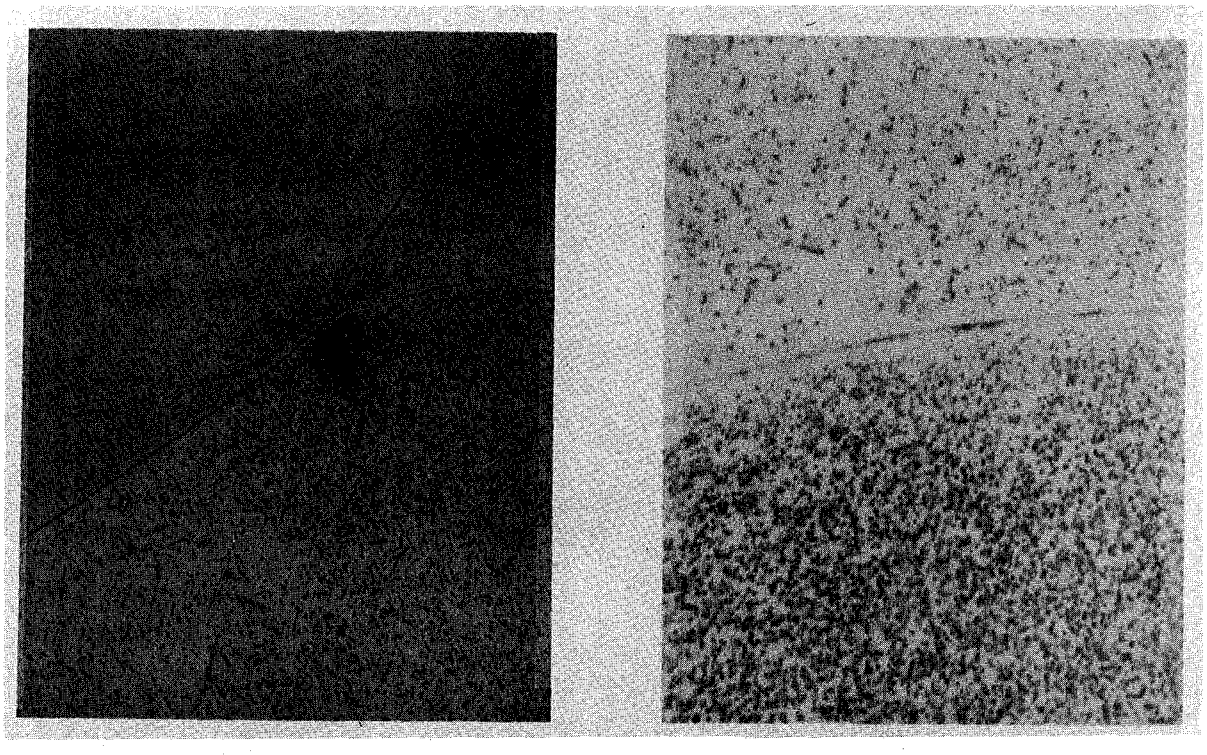

NB-16AL HOMOGENIZATION/W.Q.
750°C AGING
24 HOURS

Fig. VI-13

XBB 802-1068

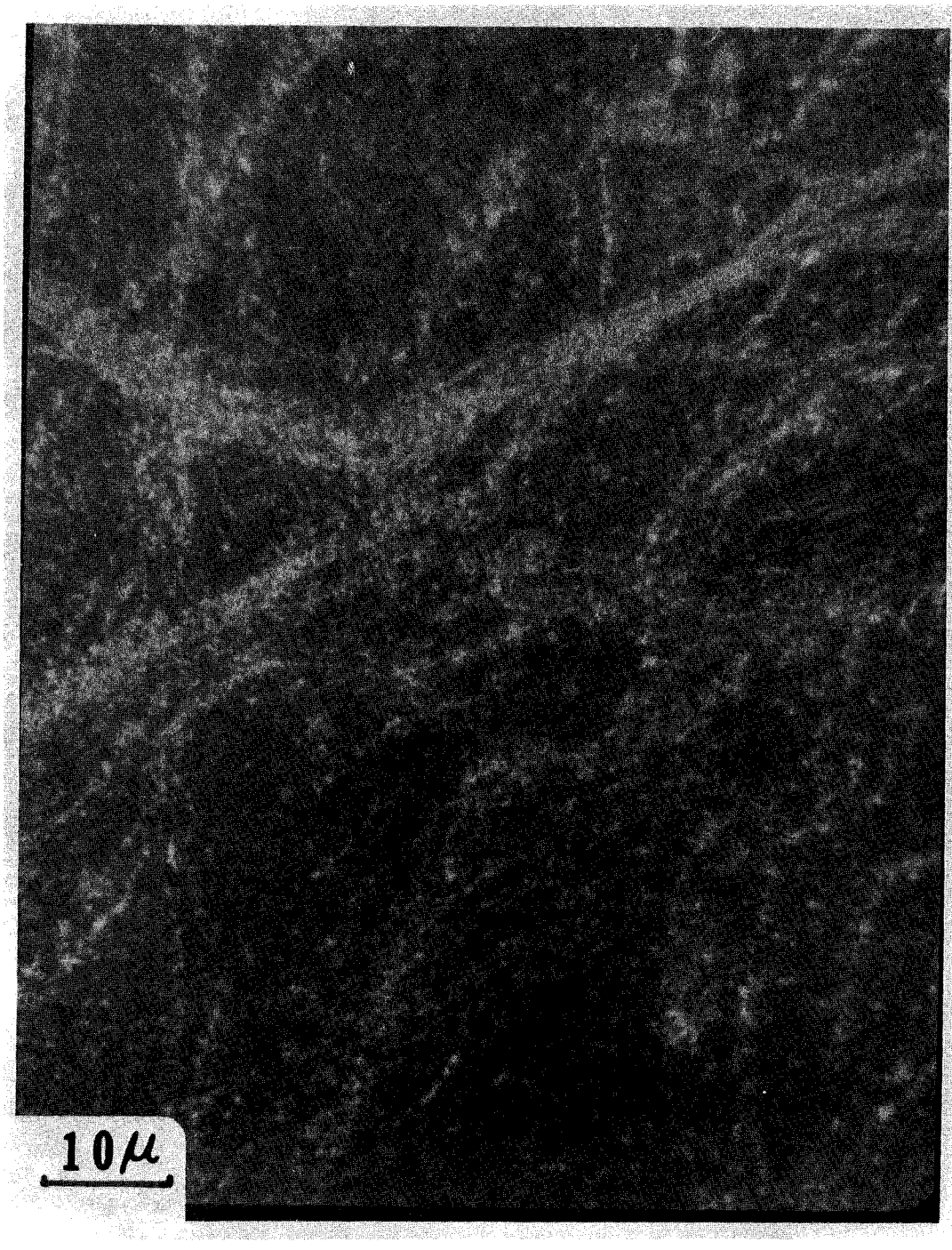
10μ

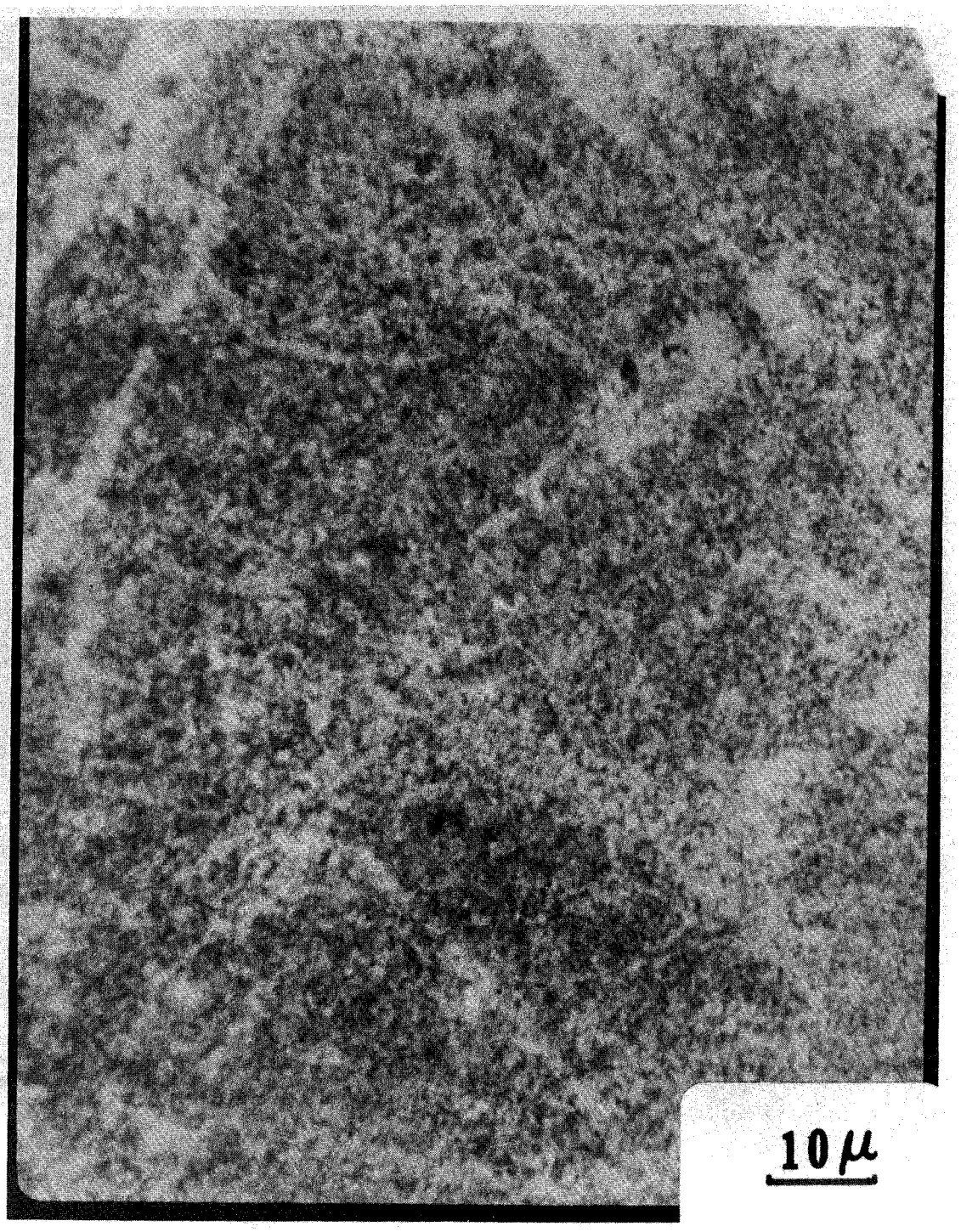

Fig. VI-15 XBB 801-412

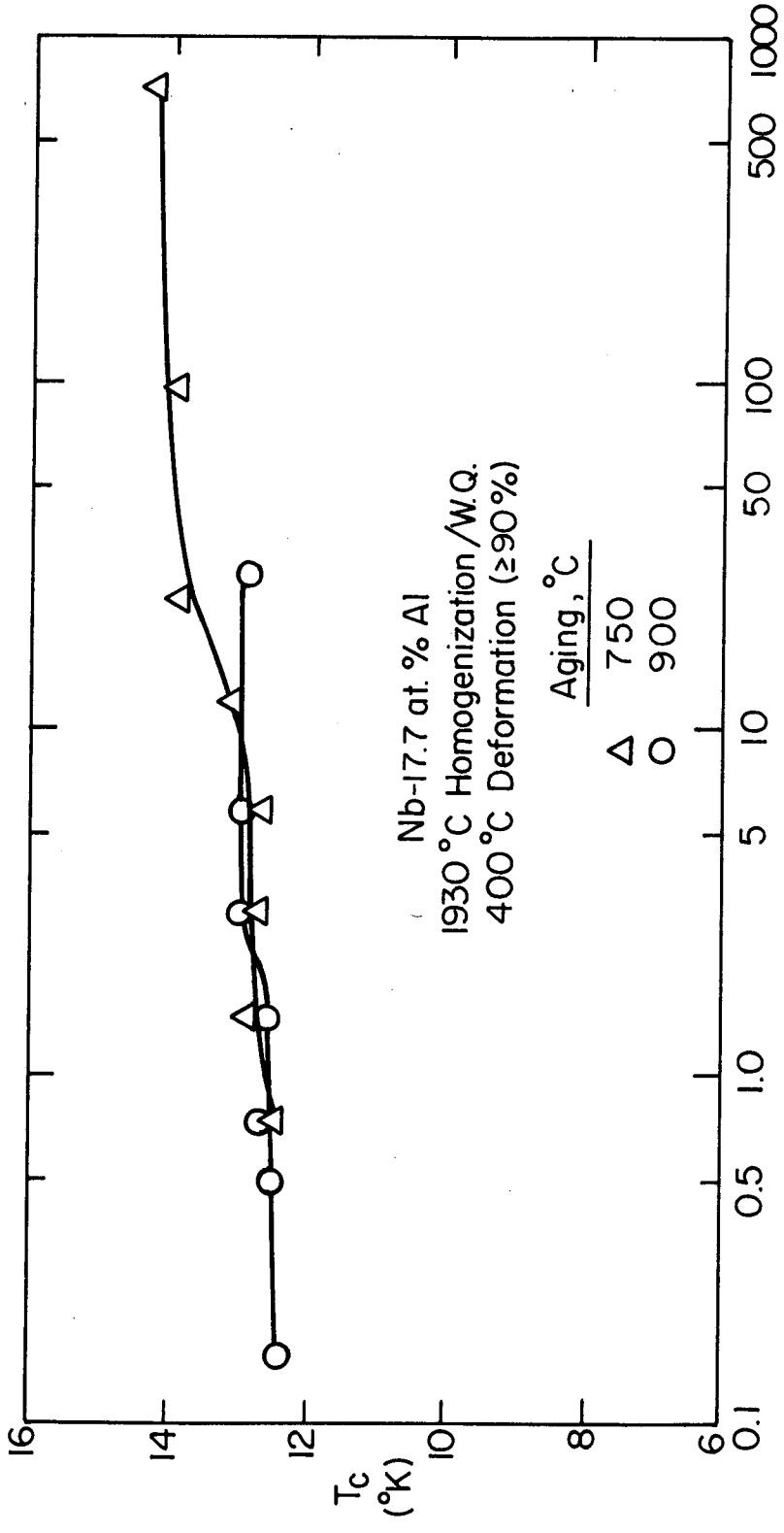

XBL801-4599

Fig. VI-16

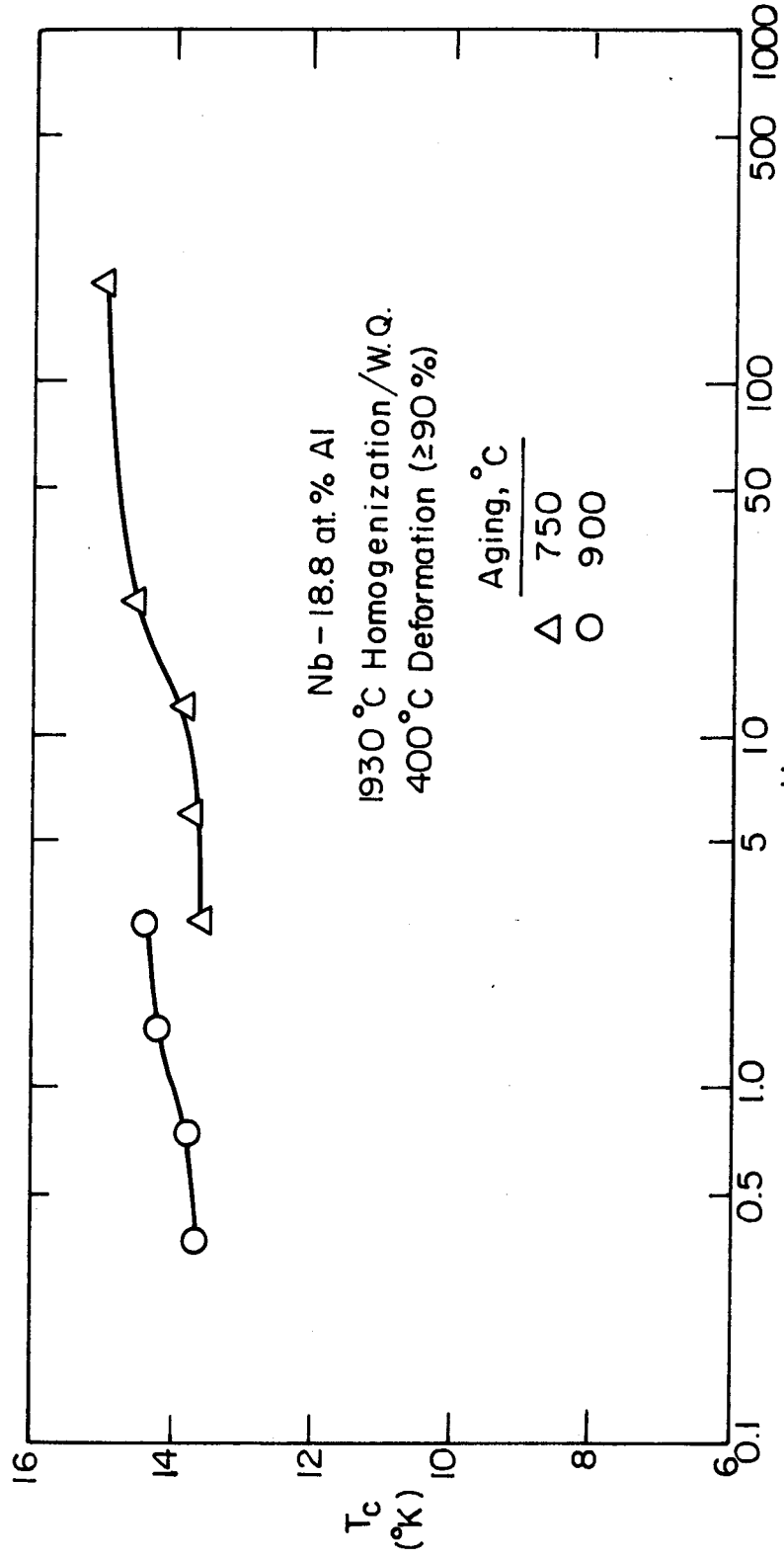

XBL807-5598

Fig. VI-17

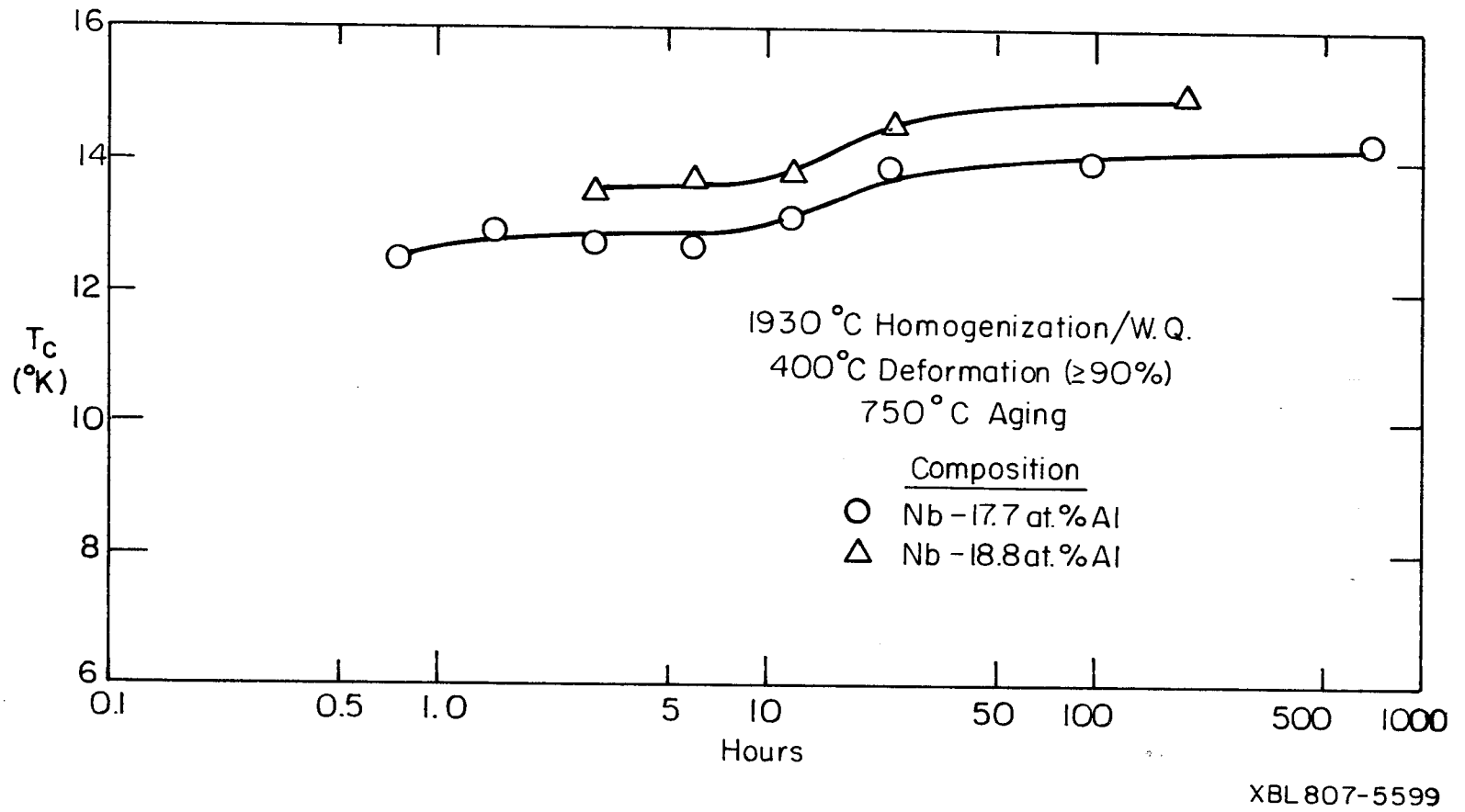
16
14
12
10
8
6
T_c (°K)
0.1
0.5
1.0
5
10
50
100
500
1000
Hours
1930 °C Homogenization/W.Q.
400°C Deformation (≥90%)
750° C Aging
Composition
Nb - 17.7 at.% Al
Nb - 18.8 at.% Al
XBL 807-5599

Fig. VI-18

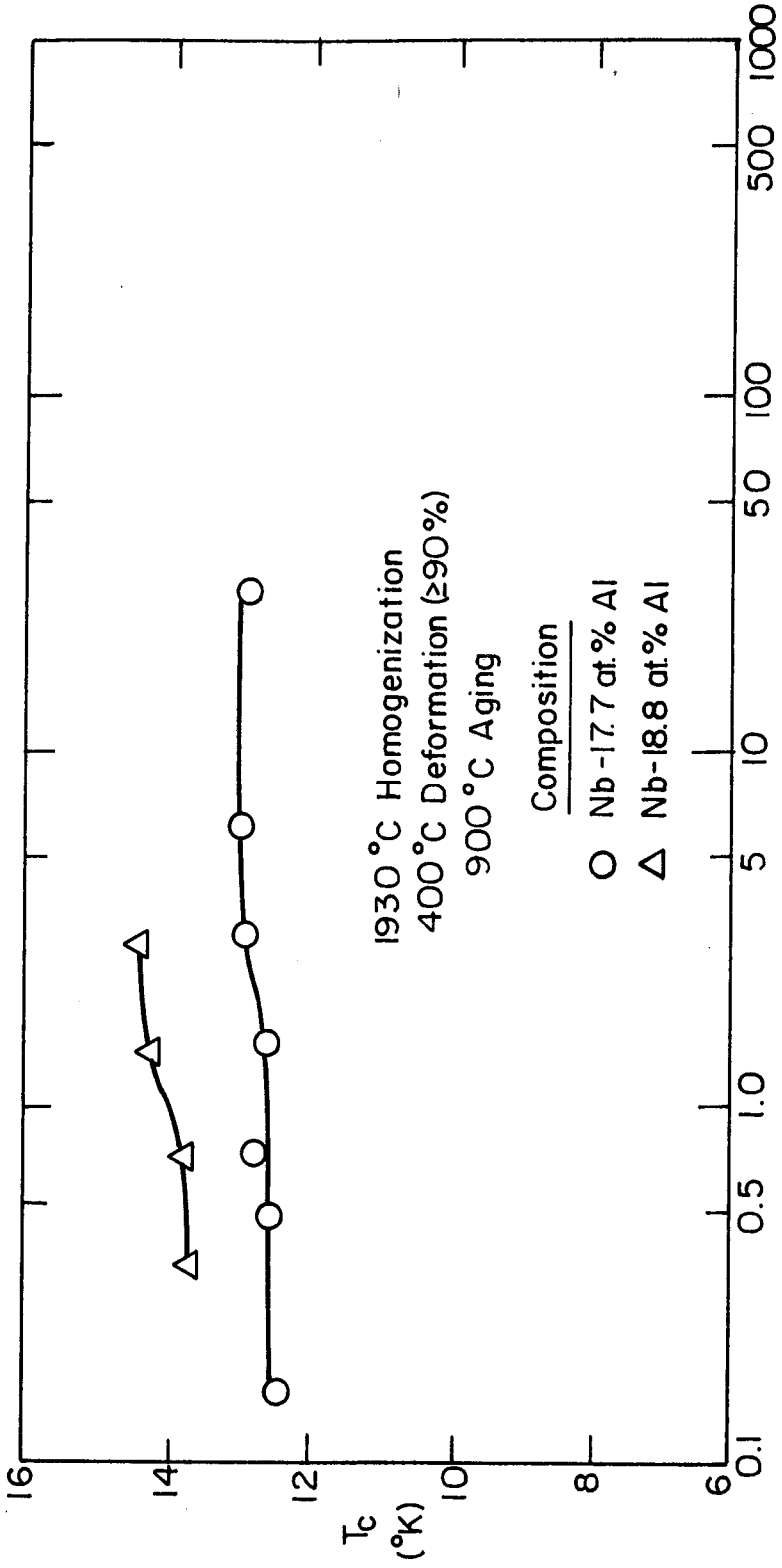

XBL 807-5597

Fig. VI-19

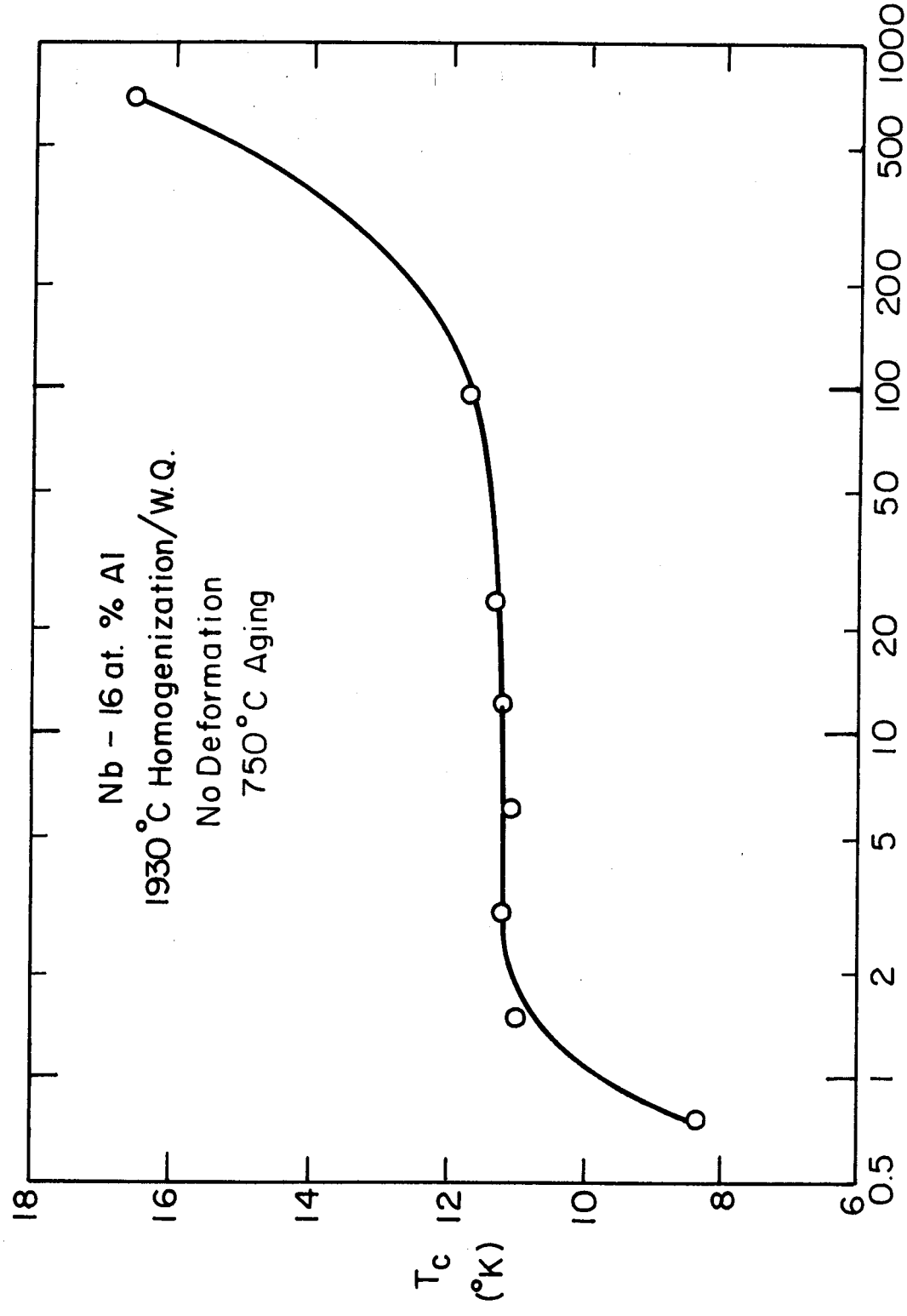

XBL 802-4680

Fig. VI-20

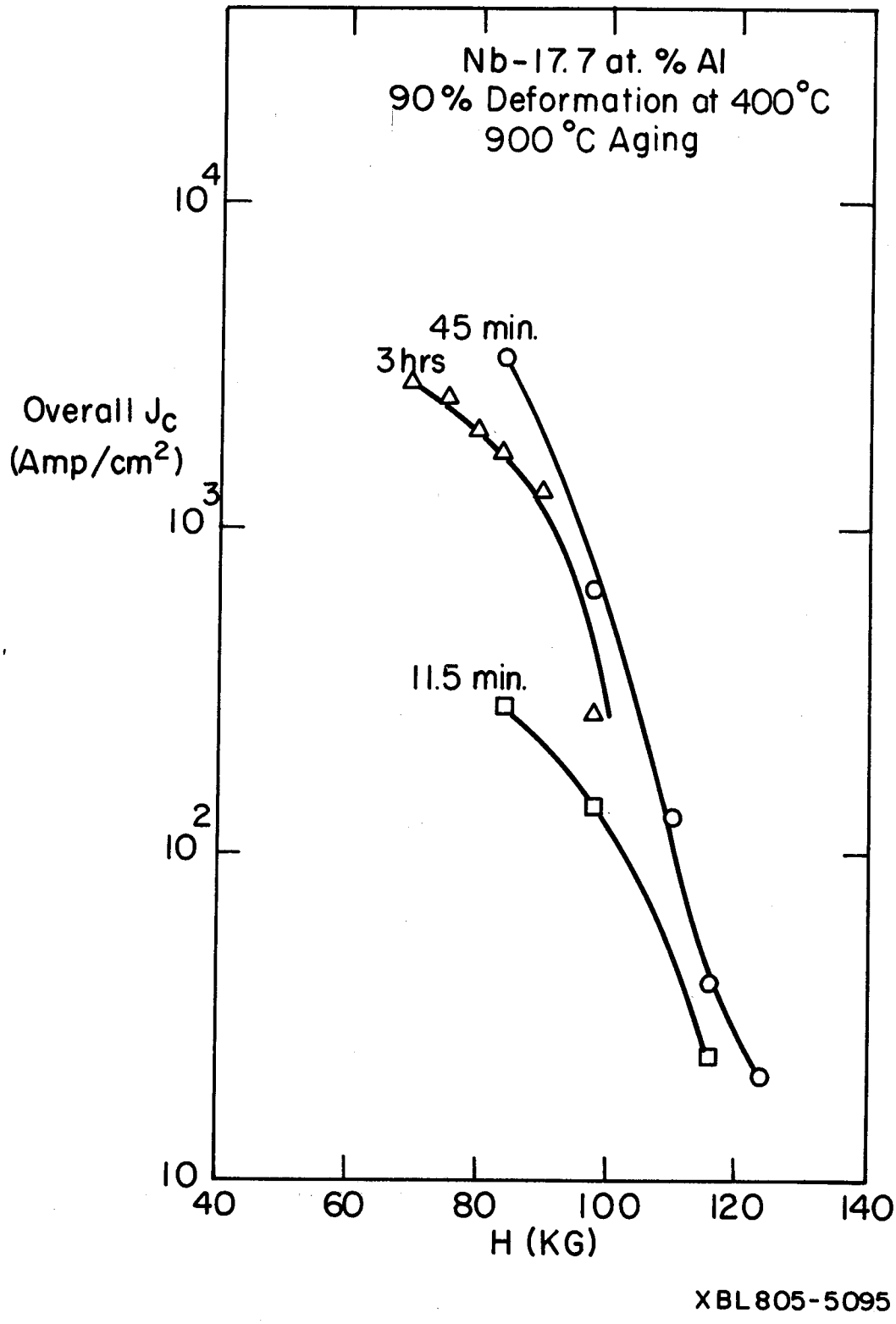
Nb-17.7 at. % Al
90% Deformation at 400°C
900 °C Aging
45 min.
3 hrs
11.5 min.
Overall J_c
(Amp/cm^2)
10^4
10^3
10^2
10
40
60
80
100
120
140
H (KG)
XBL805-5095

Fig. VI-21

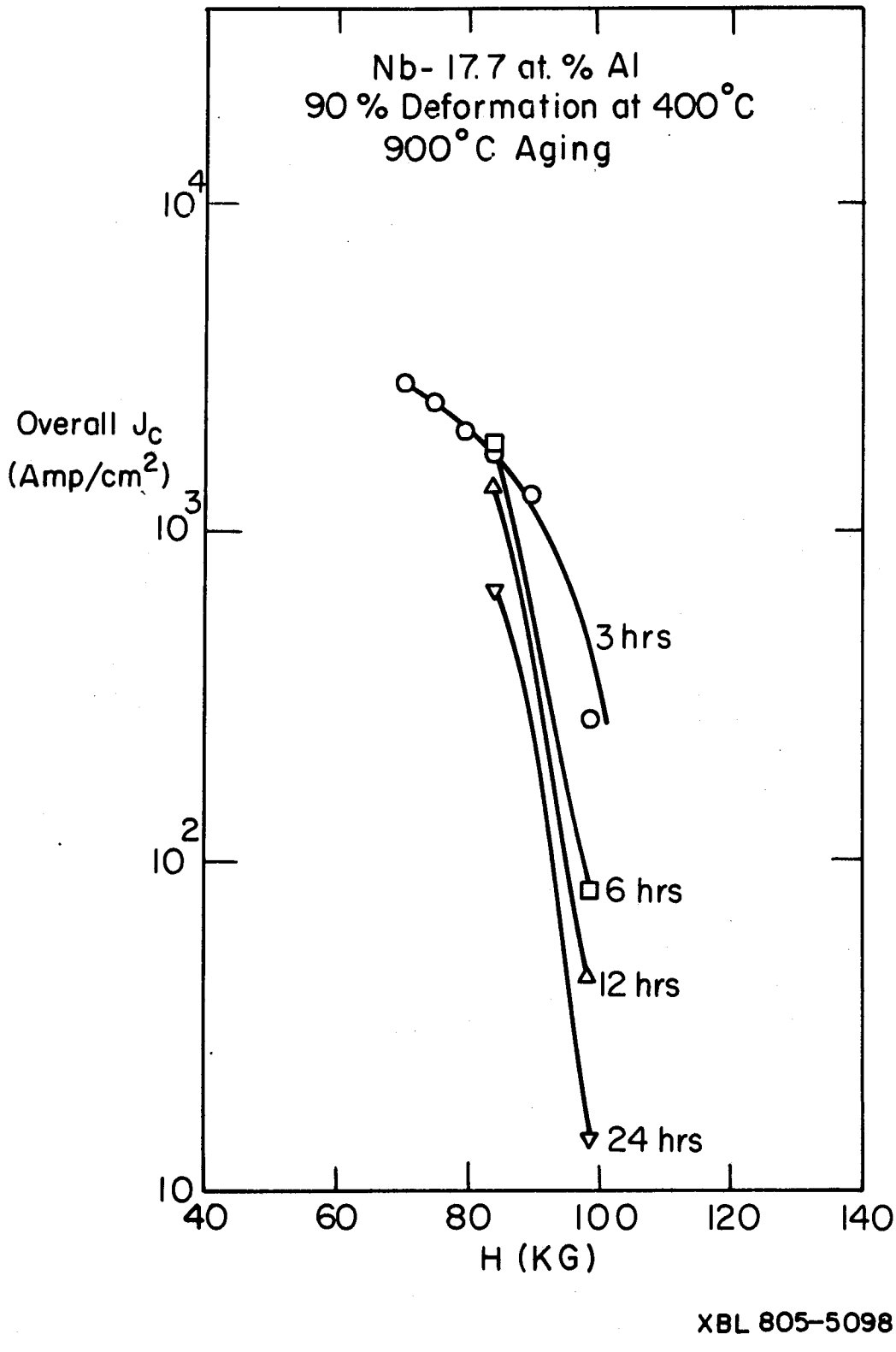

XBL 805-5098

Fig. VI-22

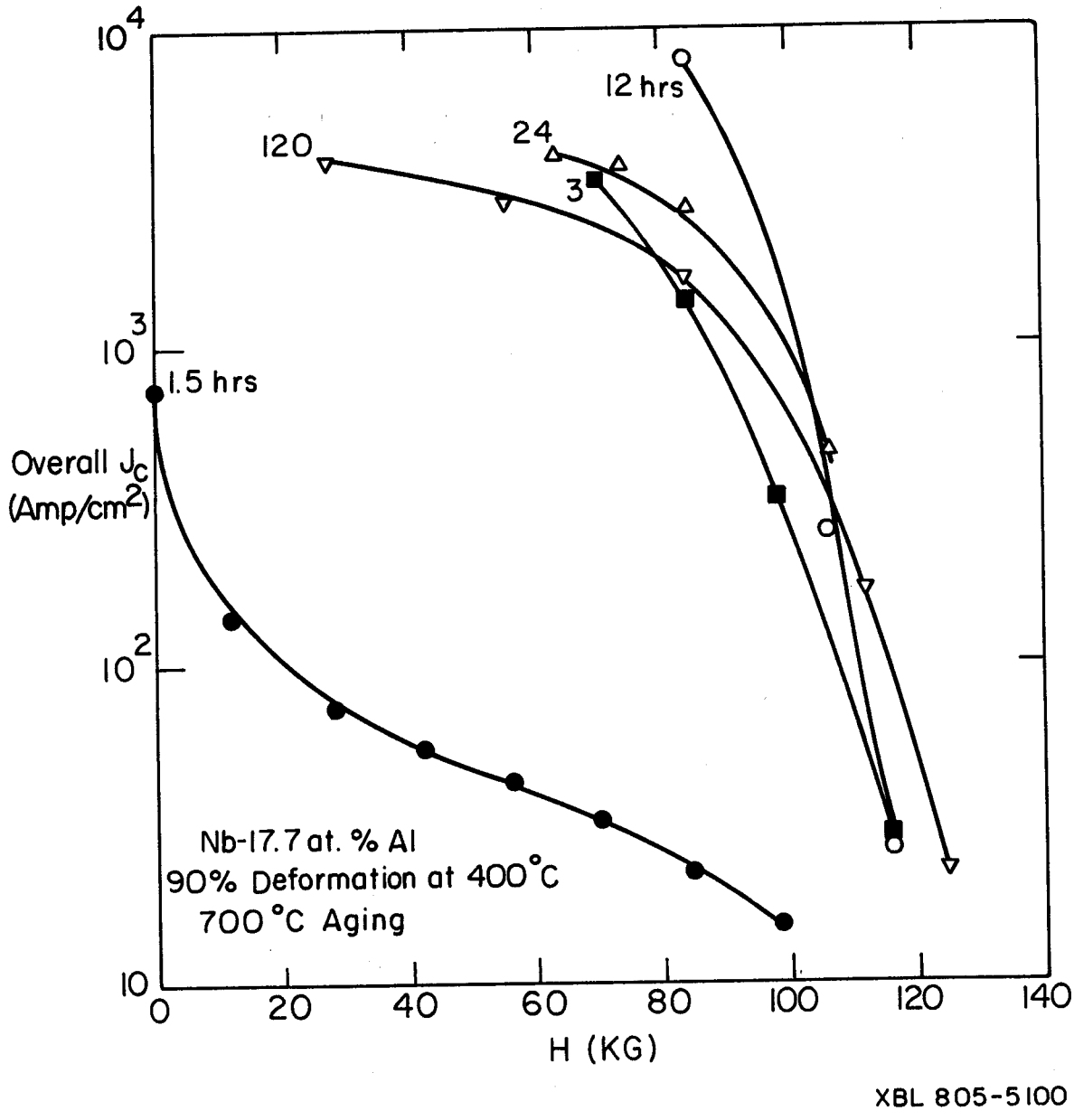
10^4
10^3
10^2
10
12 hrs
24
120
3
1.5 hrs
Overall J_c
(Amp/cm^2)
Nb-17.7 at. % Al
90% Deformation at 400°C
700°C Aging
0
20
40
60
80
100
120
140
H (KG)
XBL 805-5100

Fig. VI-23

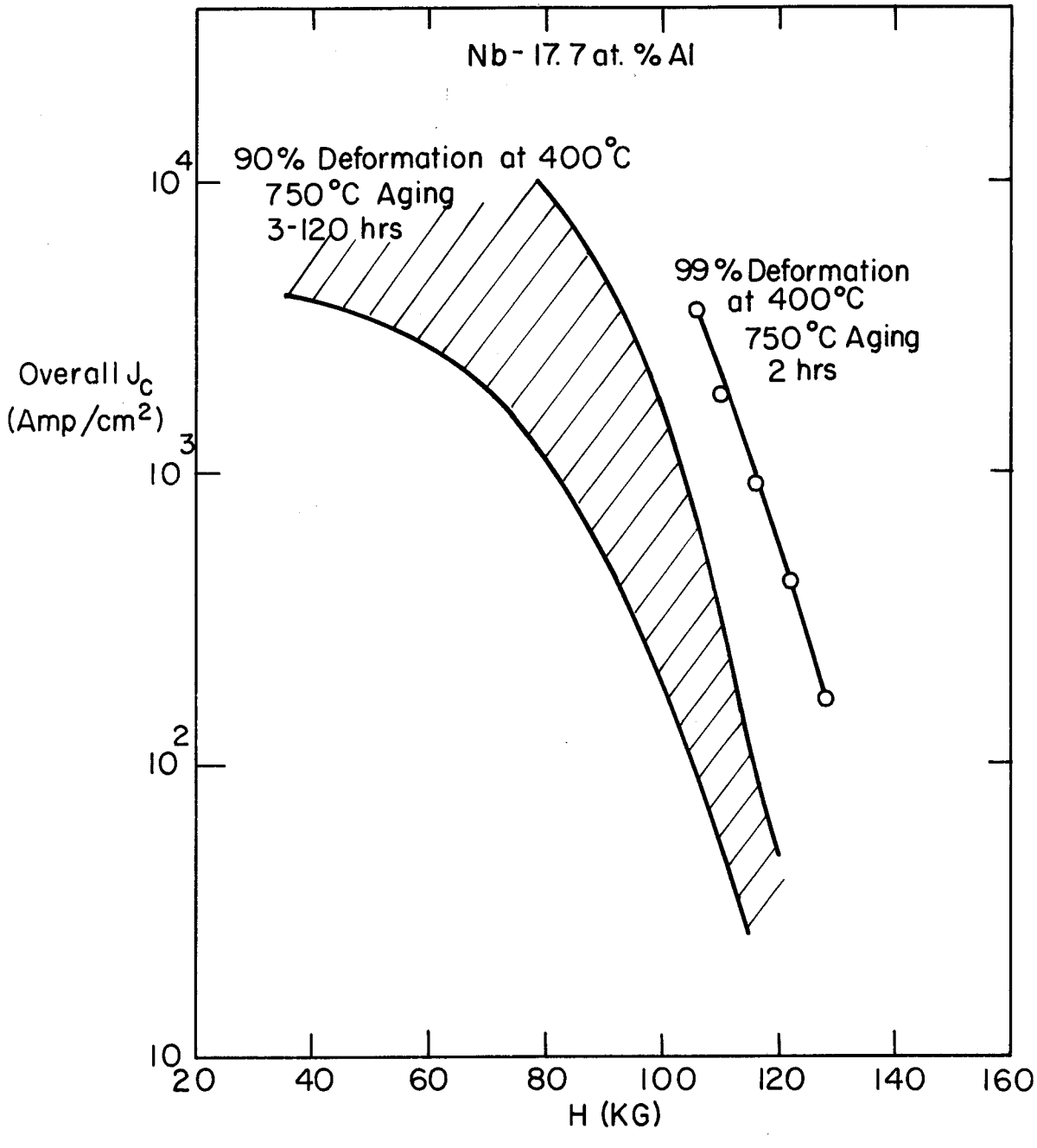

XBL 805-5096

Fig. VI-24

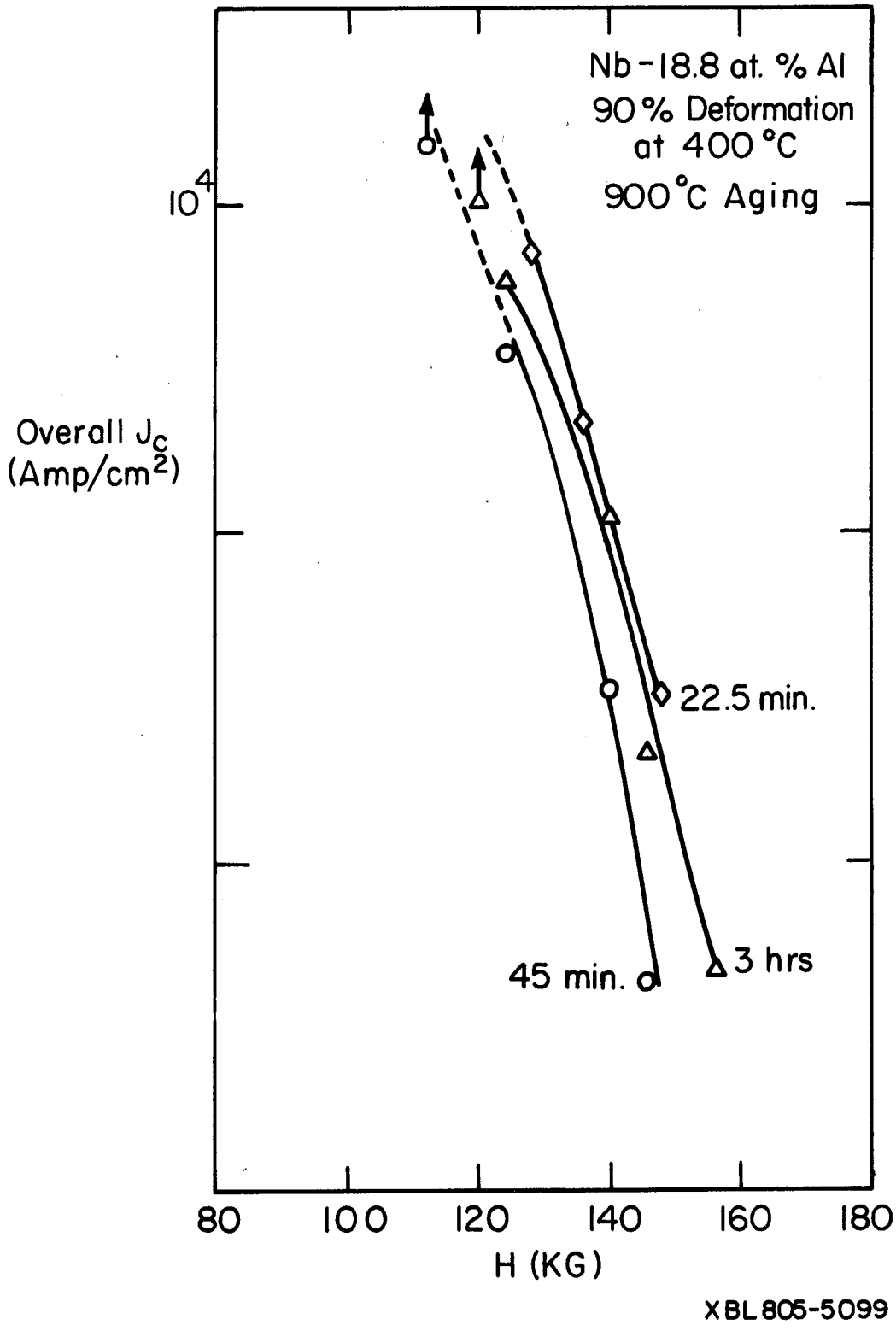
Nb - 18.8 at. % Al
90 % Deformation
at 400 °C
900 °C Aging
10^4
Overall J_c
(Amp/cm^2)
22.5 min.
3 hrs
45 min.
80
100
120
140
160
180
H (KG)
XBL 805-5099

Fig. VI-25

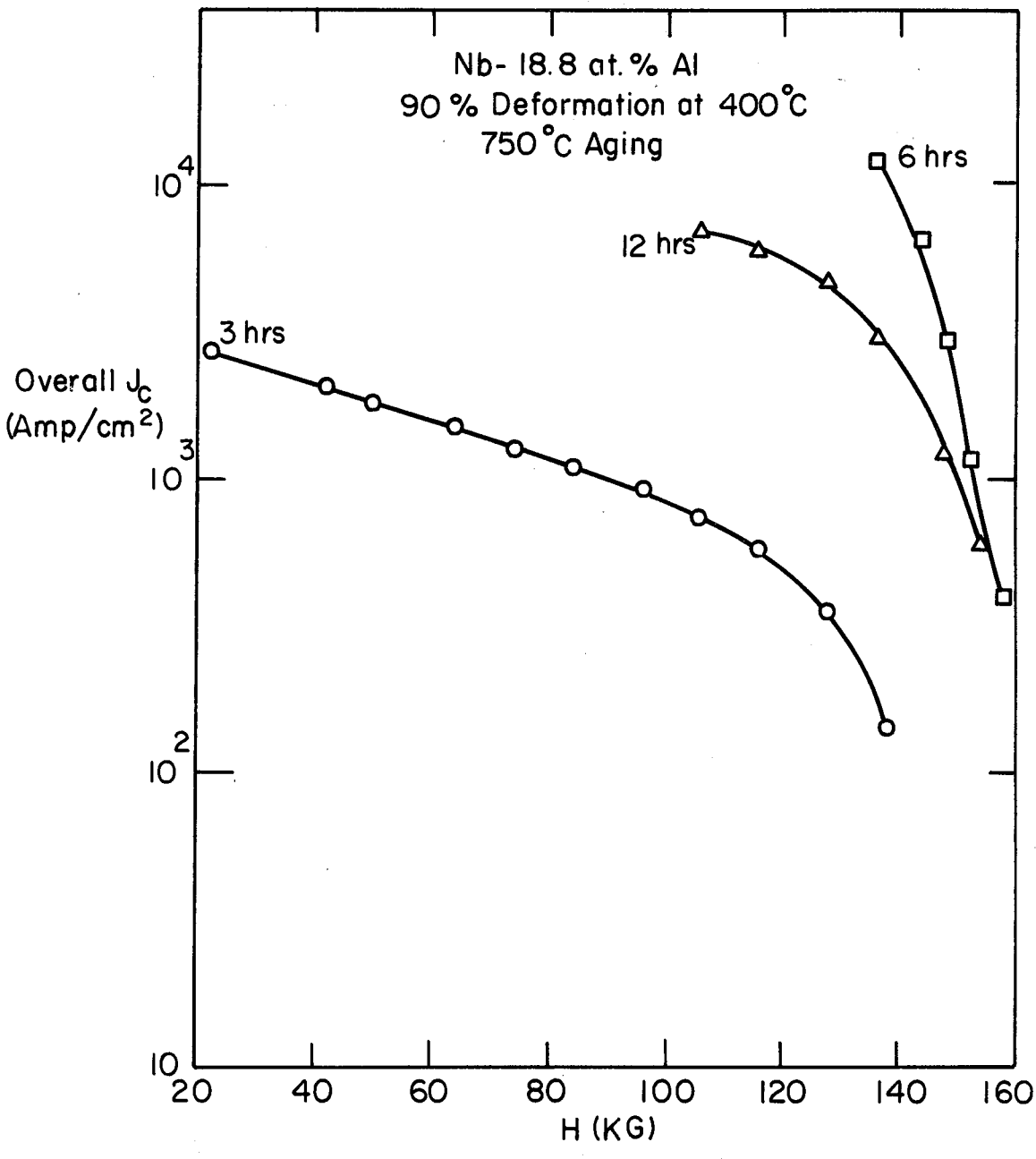
Nb- 18.8 at.% Al
90 % Deformation at 400°C
750°C Aging
6 hrs
12 hrs
3 hrs
Overall J_c
(Amp/cm^2)
10^4
10^3
10^2
10
20
40
60
80
100
120
140
160
H (KG)
XBL805-5097

Fig. VI-26

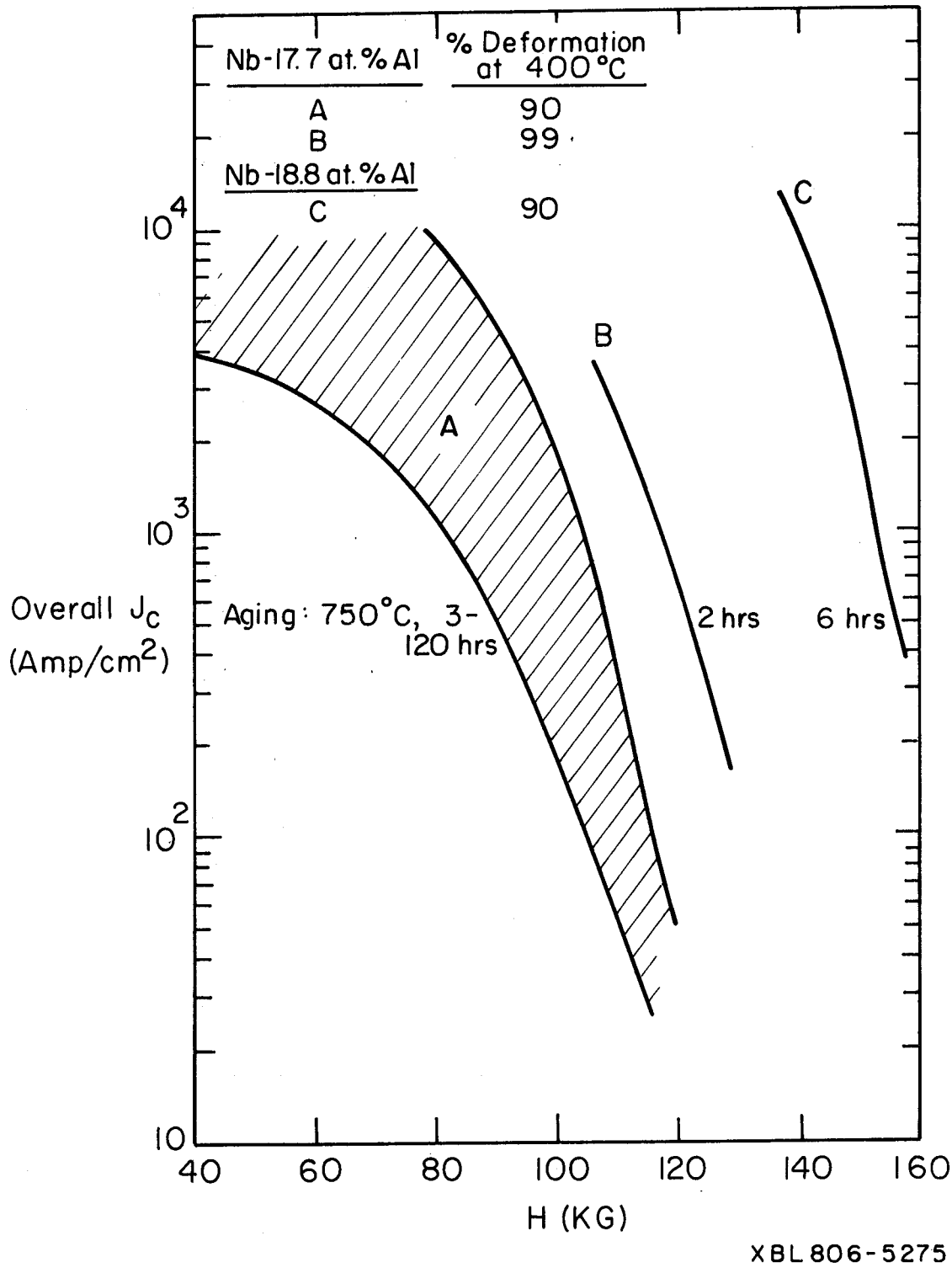
Nb-17.7 at.% Al
% Deformation at 400°C
A
90
B
99
Nb-18.8 at.% Al
C
90
A
B
C
2 hrs
6 hrs
Aging: 750°C, 3-120 hrs
Overall J_c (Amp/cm^2)
10^4
10^3
10^2
10
40
60
80
100
120
140
160
H (KG)
XBL 806-5275

Fig. VI-27

VII. SUMMARY AND CONCLUSIONS

The direct "solid-state" precipitation technique is a monolithic process which is the metallurgically simplest method of wire or tape manufacturing; it involves casting an ingot of the desired composition, homogenizing it, drawing or flat-rolling the material into a wire or tape, and finally aging it to produce the superconducting phase. This monolithic processing procedure is simple and appealing in theory, but its practical implementation faces substantial difficulties: (1) sample preparation, (2) quench cracking, (3) low temperature brittleness, (4) interstitial impurities; (5) non-stoichiometric precipitation, and (6) connectivity of superconducting phases. The solutions of these problems are essential for the success of this solid-state precipitation process.

We have shown the ability to deal with the laboratory-scale samples weighing 30-50 grams. In order to solve the sample preparation problem, we have lowered the Ga content in the V/Ga ingots and the Al content in the Nb/Al ingots. Appropriate temperatures for homogenization and some adequate methods for quenching were used to prevent the quench-cracking problem. The low temperature brittleness problem was solved by deforming the samples at some elevated temperatures: ~400°C for the Nb/Al samples and ~700°C for the V/Ga samples. Cerium element addition in the melt of ingots was found to be very effective in removing oxygen and nitrogen from the V/Ga samples. The last, but most critical point, is whether reasonably good critical transition temperatures and high overall critical current densities can be obtained by this solid-state precipitation approach. Using a non-equilibrium condition, a T_c of 15 K has been obtained in the V-Ga system and 17 K has been achieved in the Nb-Al system.

In order to pass high currents through the tested samples, the superconducting A15 precipitates must form a continuous or semi-continuous network, which has also been established using this solid-state precipitation process. A summary of the best overall critical current densities obtained in this work is presented in Fig. VII-1. In the Nb-Al system, we were able to obtain $J_c \geq 10^4$ A/cm^2 at 140 KG in the 18.8 at.% Al sample, deformed 90% (see curve A). From the comparison between curves D and E, it is believed that a high degree of deformation (≥99%) coupled with an appropriate heat treatment can lead to a high overall J_c in the Nb-Al system. A similar concept should also be applied to the V-Ga system to enhance the $J_c(H)$ values.

Transmission electron microscopy has been used to reveal the microstructure of the tested samples. Microstructures such as grain boundaries are believed to be very important in enhancing the critical current density in A15 systems. Small A15 precipitates not only improve the superconducting characteristics but also enhance the mechanical properties of the final product. The desired microstructure can be obtained by choosing the appropriate prior deformation and the aging treatment. In the Nb-Al system different aging treatments can lead to an A15 grain size from an elongated form, about 5000 Å by 1000 Å with 900°C aging to an equi-axed one of ~300 Å using 750°C aging. Recent TEM data also showed that in the V-Ga system, the A15 grain size can be affected by the prior deformation, from an elongated one of about 1μ by 2000 Å with 75% thickness reduction down to a more equi-axed one around 1000 Å with 90% thickness reduction. A more systematic study of the correlations between the metallurgical microstructure and the corresponding superconducting parameters is necessary.

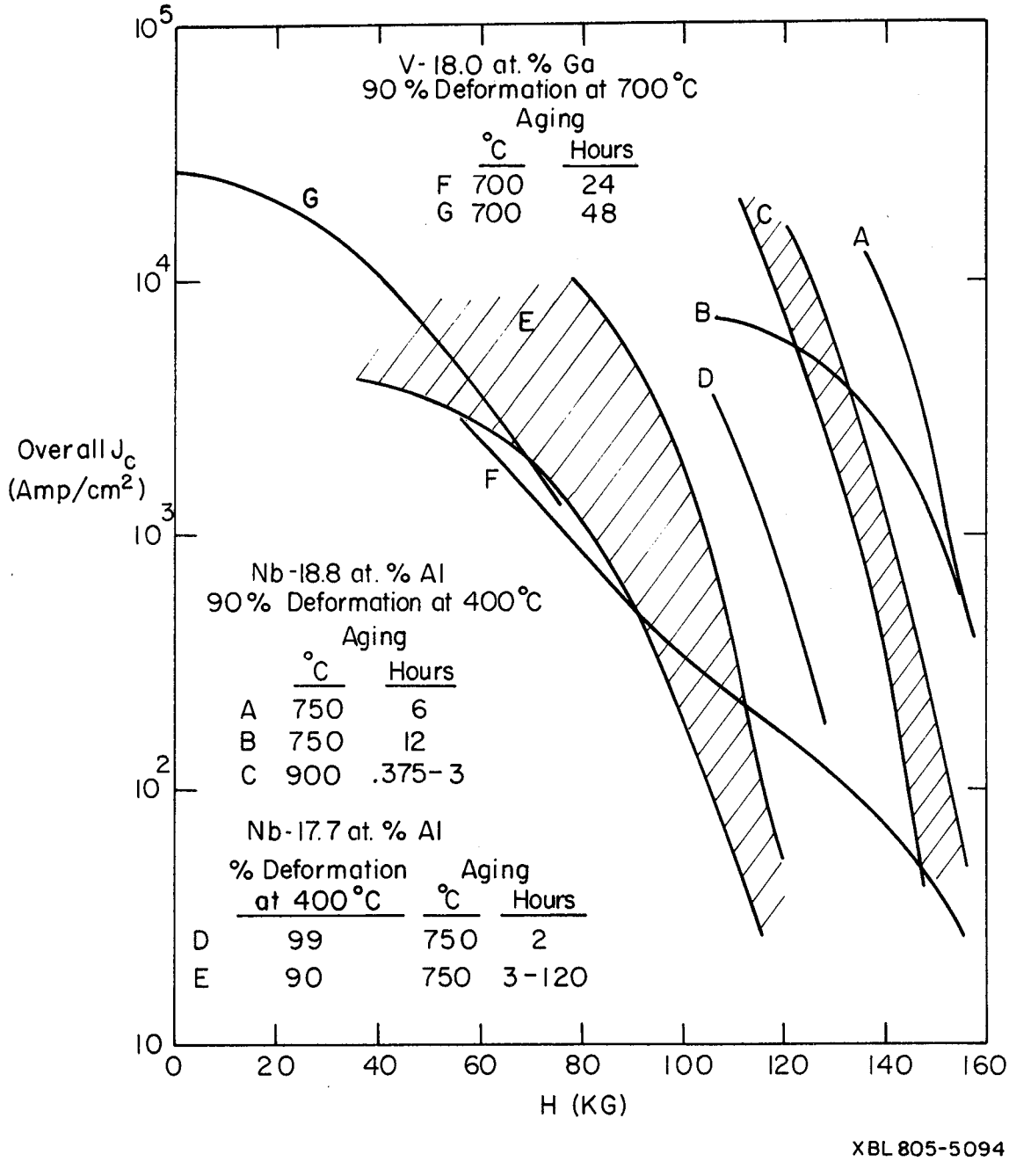

Fig. VII-1

A summary of the best overall critical current densities obtained in this work.